CYTOSKELETAL MODULATION OF PLATELETS AND MEGAKARYOCYTES

by

Matthew C. Smith

A dissertation submitted to the faculty of
The University of Utah
in partial fulfillment of the requirements for the degree of

Doctor of Philosophy

Department of Oncological Sciences

The University of Utah

December 2011

The University of Utah Graduate School

STATEMENT OF DISSERTATION APPROVAL

The dissertation of **Matthew C. Smith**

has been approved by the following supervisory committee members:

Dean Y. Li	, Chair	**8/15/2011** Date Approved
Andrew Weyrich	, Member	**8/15/2011** Date Approved
Jody Rosenblatt	, Member	**8/15/2011** Date Approved
Nikolaus S. Trede	, Member	**8/15/2011** Date Approved
Gerald Spangrude	, Member	**8/15/2011** Date Approved

and by **Donald E. Ayer** , Chair of the Department of **Oncological Sciences**

and by Charles A. Wight, Dean of The Graduate School.

ABSTRACT

Platelets perform a critical role in both physiologic hemostasis and pathologic thrombosis, and the production and activation of platelets involves intricate regulation of cytoskeletal processes within these cells. A greater understanding of these cytoskeletal processes within platelets will offer the ability to manipulate them in hope of mitigating pathologies. In this dissertation I present a continuum of work progressing from the study of neural guidance cues in immune cells to neural guidance cues in platelet cytoskeletal function and finally to cytoskeletal alterations required for platelet production in thrombopoiesis.

This work begins with the finding that, contrary to published reports, Slit2 does not regulate neutrophils directly, but instead acts through Robo4 to blunt endothelial hyper-response to cytokine storm.

These studies led naturally into studies of guidance cues in other hematopoietic lineages, specifically platelets. I present data suggesting that Semaphorin 3E (Sema3E) inhibits all stages of platelet activation. Additionally, Sema3E reversibly inhibits platelet function by inactivating Rap1b, which is required for activation of $\alpha_{IIb}\beta_3$ integrin. In attempts to determine the platelet receptor for Sema3E, using mice with a platelet-specific conditional deletion of the Sema3E receptor PlexinD1, I determined that PlexinD1 is not necessary for the platelet

inhibitory activities of Sema3E. Simultaneously, in an attempt to produce Sema3E protein, I determined that effects originally attributed to Sema3E were in fact a result of Tween-20 contamination from commercially produced Sema3E formulation, thus terminating my studies of Semaphorins in platelets and suggesting the need for another look at the previously published reports of Sema3A in platelets.

The study of cytoskeletal regulation in platelets lent naturally to the study of cytoskeletal functions in thrombopoiesis. Here I show that the proteasome inhibitor bortezomib causes thrombocytopenia by blunting platelet production in mice, consistent with clinical studies in humans. Furthermore, bortezomib prevents the production of proplatelets from megakaryocytes. I demonstrate that bortezomib treatment elevates both RhoA protein levels and RhoA activation in megakaryocytes and that inhibition of RhoA or its downstream kinase ROCK restores proplatelet production. As currently-approved drugs exist that inhibit both RhoA and ROCK, I suggest that these pathways are primary targets for treating bortezomib-induced thrombocytopenia.

TABLE OF CONTENTS

ACKNOWLEDGEMENTS

I would like to thank the many people who contributed to the success of the work described within this dissertation, specifically Members of the Dean Li Laboratory: Dean Li, Nyall London, Aubrey Chan, Weiquan Zhu, Patrick Zimmerman, Chadwick Davis, Dallas Shi, Kirk Thomas, Sutip Navankasattusas; members of the Andy Weyrich and Guy Zimmerman laboratory, including Andy Weyrich, Guy Zimmerman, Hansjorg Schwertz, and Zechariah Franks; and members of the Peter Gross Laboratory, including Peter Gross and Ran Ni. I would also like to thank the many individuals who offered scientific or technical guidance throughout this work, including but not limited to: Frederic Larrieu-Lahargue, Amy Lim, Christopher Gibson, Lise Sorensen Brunhart, Robbie Campbell, Jesse Rowley and Neal Tolley.

CHAPTER 1

EMERGING MECHANISMS OF VASCULAR STABILIZATION

The following chapter is a reprint of a manuscript that Nyall London, Dean Li and I co-authored for the *Journal of Thrombosis and Haemostasis*. It was published in 2009; volume 7 (Supplemental 1), pages 57-60 and has been reprinted with permission from John Wiley and Sons publishing group. Though this review is only peripherally related to the majority of the remainder of this dissertation, the underlying theme of cytoskeletal modulation holds true.

Journal of Thrombosis and Haemostasis, **7** (Suppl. 1): 57–60 DOI: 10.1111/j.1538-7836.2009.03421.x

INVITED REVIEW

Emerging mechanisms of vascular stabilization

N. R. LONDON,*† M. C. P. SMITH*† and D. Y. LI*†‡
**Department of Oncological Sciences; †Program in Molecular Medicine; and ‡Department of Medicine, University of Utah, Salt Lake City, UT, 84112, USA*

To cite this article: London NR, Smith MCP, Li DY. Emerging mechanisms of vascular stabilization. *J Thromb Haemost* 2009; **7** (Suppl. 1): 57–60.

Summary. Neural guidance cues are essential for a growing axon to correctly course through the body and innervate target tissues. Interestingly, the vascular network follows a parallel trajectory along nerves, suggesting that guidance cues important for neural patterning may also be required for proper vascular patterning. However, while an axon arises from one cell, a blood vessel is composed of many endothelial cells. Recent evidence suggests that neural repulsive cues are usurped by multi-cellular blood vessels to ensure vascular stabilization cues. Additional clues into the signaling mechanisms that promote vascular stabilization are emerging from cerebral cavernous malformations, a disease characterized by headache, epilepsy, and stroke. Thus, neurobiology and neurology are providing insights into the concepts of vascular stability.

Keywords: CCM, hemostasis, neurovascular guidance, Robo4, vascular stability.

Mechanisms of neurovascular guidance

The nervous system provides a functional network whereby information can be shared between the brain and the rest of the body. For a proper network to be established, axons must navigate considerable distances to reach their target destination. The growth cone located at the tip of the axon is responsible for coordinating this directed migration [1]. This is achieved through the reaction of the growth cone to positive and negative stimuli, resulting in successful migration to target tissues and proper formation of the neural network.

The vascular system also forms a functional network that can be found throughout the body. This system of tubes permits blood flow, allowing the delivery of nutrients to target tissues. Much of the vascular plexus is formed by angiogenesis, or new blood vessel growth from pre-existing vessels. Interestingly, the vascular network follows a parallel trajectory along nerves, suggesting that guidance mechanisms that are important for neural patterning may also be required for proper vascular patterning. At the leading edge of a sprouting blood vessel is the tip cell, the endothelial analogue to the neural growth cone [2]. Like the growth cone, the tip cell uses filipodial extensions to sense the environment, react to positive and negative stimuli, and navigate the proper path of growth. A key difference, however, is that while the axon arises from one cell, a blood vessel is composed of many endothelial cells requiring orchestrated movements of not only the tip cells, but also the endothelial cells trailing behind the navigating tip cell called stalk cells. Inter-endothelial junctions, such as those formed by vascular endothelial cadherin (VE-cadherin), must be established between endothelial stalk cells to maintain vascular stability, thus further distinguishing the blood vessel from the growing axon.

Correspondence: Dean Y. Li, Department of Medicine, University of Utah, Salt Lake City, UT 84112, USA.
Tel.: 801 585 5505; fax: 801 585 5505.
E-mail: dean.li@hmbg.utah.edu

Slit–Robo as a repulsive neural guidance signaling system

Slits are one family of neural guidance cues known for repulsive activity. This family of ligands is composed of three members, Slit1–3, and are large, secreted extracellular matrix proteins. Slits act through Roundabout (Robo) receptors. In fact, Robo was actually first discovered from a screen for mutations resulting in axon guidance defects in Drosophila [3]. In *robo* mutants, too many axons cross and re-cross the midline, demonstrating that *robo* signaling provides a repulsive cue to prevent misguided axon entry into the midline. Similarly, the growth cones of *slit* mutants enter the midline but never leave [4]. Embryos transheterozygous for *slit* and *robo* showed inappropriate axon crossing of the midline, indicating that Slit and Robo genetically function in the same pathway. Furthermore, two additional Robo family members have been discovered to affect axon guidance in the nervous system.

Robo4 stabilizes the vasculature

A fourth member of the Robo family termed Robo4, or Magic Roundabout, is unique in that its expression is endothelial-specific. Since Robo signaling in the nervous system has been demonstrated to be important in neural guidance, we hypothesized that a vascular specific Robo may be a key mechanism regulating vascular guidance. To investigate whether Robo4 is necessary for vascular guidance *in vivo*, we developed *Robo4*-null ($Robo4^{-/-}$) mice. We anticipated, on the basis of this hypothesis, that removal of Robo4 expression would be lethal

due to extreme defects in vascular guidance. To our surprise, these mice were viable, fertile, and demonstrated no obvious vascular patterning defects in several vascular beds [5]. To understand why Robo4 played no role in vascular guidance *in vivo*, we hypothesized that perhaps Robo4 expression was not found in the endothelial tip cell. Using the retinal vascular bed, we found that Robo4 expression was largely absent from tip cells, but strong expression was found in the stalk cells. This cell-specific expression led us to ask whether the function of Robo4 *in vivo* was that of stalk cells, that is, to strengthen vascular stability.

One aspect of vascular stabilization is the maintenance of essential inter-endothelial junctions to stabilize barrier function. Vascular barrier function can be modeled *in vitro* using a transwell system to assess flux of a reporter across an endothelial monolayer. Using lung endothelial cells isolated from *Robo4*$^{+/+}$ mice, we found that Slit2 could significantly inhibit vascular endothelial growth factor (VEGF) – induced permeability. When this experiment was performed using lung endothelial cells isolated from *Robo4*$^{-/-}$ mice, the effect of Slit2 was lost, demonstrating that Robo4 is necessary for the effect of Slit2. A major effector of VEGF-induced permeability is Src kinase. In fact, Src is necessary for VEGF-induced permeability as the permeability-inducing effect of VEGF is lost in *Src*$^{-/-}$ mice [6]. We found that Slit2 could inhibit VEGF-induced Src activation, demonstrating that Slit impinges upon the Src signaling axis [5]. Next, we assessed whether Slit2 could stabilize the vasculature *in vivo* in the mouse dermis and retina. Using Evans Blue as a tracer for permeability, we found that Slit2 inhibited VEGF-induced permeability in the mouse dermis and retina. Again, the effect of Slit was lost in *Robo4*$^{-/-}$ mice, demonstrating that Robo4 is necessary for the effect of Slit2. Furthermore, Slit3 also inhibited VEGF-induced permeability in the mouse retina through a Robo4-dependent mechanism. This demonstrates that enhancement of the vascular barrier applies to multiple members of the Slit family.

A stabilized phenotype not only applies to the regulation of vascular barrier function, but also to the inhibition of new vascular sprouting and angiogenesis. Pro-angiogenic factors such as VEGF induce angiogenesis through enhancing vascular barrier destabilization, endothelial proliferation, and migration. While Slit2 had no effect on VEGF-induced endothelial cell proliferation, Slit2 did inhibit VEGF-induced endothelial cell migration and tube formation *in vitro*. We next asked whether Slit2 could inhibit neovascularization in a pathologic setting *in vivo*. To answer this question, we turned to oxygen-induced retinopathy (OIR), a mouse model of proliferative diabetic retinopathy. In this model, young mice are placed in a hyper-oxygen environment for several days resulting in excessive vascular pruning. When mice are placed at room oxygen, a perceived oxygen deficit in the mouse retina causes a massive release of VEGF. Using this model, Slit2 did in fact significantly inhibit neovascular tuft formation. Furthermore, when these experiments were repeated in *Robo4*$^{-/-}$ mice, not only was Slit2 ineffective, but *Robo4*$^{-/-}$ mice demonstrated a marked increase in neovascularization as compared to *Robo4*$^{+/+}$ mice. Taken together, these data demonstrate a role for Slit/Robo4 signaling in maintaining vascular stability through maintaining vascular barrier function and inhibiting pathologic neovascularization. Furthermore, these collective data may explain why a repulsive neural cue could translate into a vascular stabilization cue when applied to the multicellular vascular bed.

Emerging mechanisms of maintaining vascular stability

Apart from the Src signaling axis upon which Slit–Robo impinges, recent evidence points to additional intracellular cell signaling systems that are important for maintaining vascular stability. Cerebral cavernous malformations (CCM) are common vascular malformations largely affecting the central nervous system. A frequent finding with these malformations is the presence of hemosiderin, a blood breakdown product. This finding is suggestive of a compromised endothelial barrier, possibly with a concurrent defect in platelet function or coagulation. Indeed, abnormal cell–cell junctions have been observed by ultrastructural analysis [7]. One gene that has been linked to the formation of CCM is osmosensing scaffold for mitogen-activated protein kinase-3 (OSM) also known as CCM2. Recent studies conducted by Whitehead *et al.* [8] have now demonstrated how this intracellular adaptor protein regulates vascular stability.

To understand the functional importance of CCM2 in the vasculature during development, Whitehead *et al.* made mice with an endothelial-specific deletion of CCM2. This mutation resulted in embryonic lethality due to lumenization defects in both the branchial arch artery and the aorta, demonstrating that CCM2 is required for lumen formation *in vivo*. Lumen formation can be modeled *in vitro* by three-dimensional culture. Using this system, endothelial cells form vacuoles that coalesce into tube-like structures. While endothelial cells treated with control siRNA formed a robust tube network, siRNA knockdown of CCM2 caused endothelial cells to form smaller lumens and decreased tube network area. These *in vitro* and *in vivo* data demonstrate that CCM2 plays a necessary role in the generation of vacuoles and the resulting vascular lumen formation.

It has been demonstrated that the cellular cytoskeleton plays a role in lumen formation [9]. To understand whether CCM2 could alter lumen formation through an effect on the cytoskeletal architecture, we performed immunofluorescence on endothelial cells lacking CCM2 expression. Indeed, endothelial cells deficient in CCM2 expression showed a marked increase in stress fiber formation. As stress fiber formation is controlled by Rho, this result was suggestive of overactive Rho signaling. When CCM2 knockdown cells were treated with a Rho inhibitor, the stress fiber phenotype was rescued. Rho signaling has also been demonstrated to play a role in vascular permeability. As previously mentioned, CCMs are characterized by hemosiderin deposits, indicative of vascular leak. Endothelial monolayers deficient in CCM2 expression

demonstrated decreased electrical resistance and increased flux of macromolecules compared to control cells, indicating enhanced permeability *in vitro* [8]. Furthermore, this phenotype was rescued by a Rho inhibitor, further implicating the proper regulation of Rho as a key function of the CCM2 pathway.

While *Ccm2*-null mice are susceptible to severe developmental angiogenic defects, humans that suffer from CCM are heterozygous. We reasoned that perhaps in a clinical setting, physiologic or genetic stressors may precipitate disease pathogenesis in these heterozygous patients. To test this in mice, we injected VEGF into the dermis of $Ccm2^{+/+}$ and $Ccm2^{+/-}$ mice. Using Evans Blue as a tracer for vascular leak, we observed that VEGF induced exaggerated vascular hyperpermeability in $Ccm2^{+/-}$ mice. Next, we tested whether inhibition of Rho could block the exaggerated hyperpermeability. Statins are widely used to treat patients with high blood pressure. In addition to inhibiting cholesterol synthesis, these drugs also inhibit Rho activation. By treating $Ccm2^{+/-}$ mice with simvastatin, we observed a significant reduction in the response of *Ccm2* heterozygous mice to VEGF. These data not only demonstrate the role that CCM2 plays in maintaining correct levels of Rho activity, but also suggest that statins may be used as a therapeutic to treat patients with CCM.

With this recent discovery, the question remains, do any ligand/receptor systems utilize CCM2 as part of a signaling mechanism? Recent data from Kleaveland *et al.* [10] suggest that heart of glass (HEG) participates in CCM signaling. Interestingly, $Heg^{-/-}$ mice demonstrated severely shortened endothelial gaps and junctions between endothelial cells. Additionally, $Heg^{-/-}$; $CCM2^{+/-}$ mice demonstrated many of the same phenotypes as a $CCM2^{-/-}$ mouse such as embryonic lethality and failure to form a lumen in the first branchial arch artery. These results show that HEG and CCM2 interact genetically. Furthermore, HEG binds to CCM1 and it is known that CCM1 binds to CCM2 [11]. Thus, input from HEG could be important for modulating the CCM2 pathway.

Questions remain

As neurobiology has informed vascular biology, so now both fields can be translated into hemostasis and thrombosis. The nexus of the Slit/Robo signaling pathways and the mechanisms behind the pathogenesis of CCMs lies in the stabilization and destabilization of cytoskeletal structures within the cell. Cytoskeletal changes in platelets are reminiscent of those involved in axon guidance and endothelial cell migration in the developing vasculature. Similarities among these cells beg the question as to whether cytoskeletal rearrangements of platelets, such as those needed for spreading, granule release and aggregation, are regulated by the same mechanisms that direct axon guidance and vascular development. The idea that molecules once thought to be primarily involved in directing axon growth are also involved in the development and function of other tissues is a rapidly emerging field [5,12]. Each of the four classes of molecules originally thought to function primarily in axon guidance (Slits, Netrins, Semaphorins and Ephrins) has been implicated in vascular and cardiac development and more recently in immune system function [12,13].

Though there have been no reports implicating a role for Slit/Robo or CCM signaling pathway in platelets, it is known that platelet function is dependent on the same cytoskeletal modulators that control these two signaling pathways. Additionally, two neural guidance cues (Semaphorins and Ephrins) have been reported to function in platelets by altering cytoskeletal remodeling in a manner similar to their respective function in neurons [14]. The question remains, which of these vascular stability mechanisms will also prove critical in the cytoskeletal stability of platelets and thus be the next target of anti or pro thrombotic drug therapy?

In this review, we have highlighted how a repulsive neural cue can translate into a vascular stabilization cue when applied to the multi-cellular vascular bed. Furthermore, it seems clear that angiogenesis, permeability and endothelial activation during inflammation are controlled by similar mechanisms including regulation of VE-cadherin function by Src [15]. The relationship between endothelial instability/stability and activation/quiescence is another emerging issue in the field of vascular biology. Is there a relationship between the concept of endothelial tip cells/vascular instability and endothelial activation? Will factors that stabilize the vasculature also inhibit endothelial activation? These signaling mechanisms may be the coalescence of vascular biology, immunology and thrombosis.

Acknowledgments

This work was funded by grants from the National Institutes of Health, Ruth L. Kirschstein National Research Service Award (N.R.L.); T-32 Hematology Training Grant (M.C.P.S); NHLBI, American Heart Association, Juvenile Diabetes Research Foundation, HA and Edna Benning Foundation, and the Burroughs Wellcome Foundation (D.Y.L.).

Disclosure of Conflict of Interests

N.R.L., M.C.P.S, and D.Y.L. are employed by the University of Utah, which has filed intellectual property surrounding the therapeutic uses of targeting Robo4 and CCM2 with the intent to license this body of intellectual property for commercialization.

References

1 Huber AB, Kolodkin AL, Ginty DD, Cloutier JF. Signaling at the growth cone: ligand-receptor complexes and the control of axon growth and guidance. *Annu Rev Neurosci* 2003; **26**: 509–63.

2 Gerhardt H, Golding M, Fruttiger M, Ruhrberg C, Lundkvist A, Abramsson A, Jeltsch M, Mitchell C, Alitalo K, Shima D, Betsholtz C. VEGF guides angiogenic sprouting utilizing endothelial tip cell filopodia. *J Cell Biol* 2003; **161**: 1163–77.

3 Seeger M, Tear G, Ferres-Marco D, Goodman CS. Mutations affecting growth cone guidance in Drosophila: genes necessary for guidance toward or away from the midline. *Neuron* 1993; **10**: 409–26.

4 Kidd T, Bland KS, Goodman CS. Slit is the midline repellent for the robo receptor in Drosophila. *Cell* 1999; **96**: 785–94.

5 Jones CA, London NR, Chen H, Park KW, Sauvaget D, Stockton RA, Wythe JD, Suh W, Larrieu-Lahargue F, Mukouyama YS, Lindblom P, Seth P, Frias A, Nishiya N, Ginsberg MH, Gerhardt H, Zhang K, Li DY. Robo4 stabilizes the vascular network by inhibiting pathologic angiogenesis and endothelial hyperpermeability. *Nat Med* 2008; **14**: 448–53.

6 Eliceiri BP, Paul R, Schwartzberg PL, Hood JD, Leng J, Cheresh DA. Selective requirement for Src kinases during VEGF-induced angiogenesis and vascular permeability. *Mol Cell* 1999; **4**: 915–24.

7 Clatterbuck RE, Eberhart CG, Crain BJ, Rigamonti D. Ultrastructural and immunocytochemical evidence that an incompetent blood-brain barrier is related to the pathophysiology of cavernous malformations. *J Neurol Neurosurg Psychiatry* 2001; **71**: 188–92.

8 Whitehead KJ, Chan AC, Navankasattusas S, Wonshill K, London NR, Jing L, Mayo AH, Drakos SG, Marchuk DA, Davis GE, Li DY. The *Cerebral Cavernous Malformation* signaling pathway promotes vascular integrity via Rho GTPases. *Nat Med* 2009; **15**: 177–84.

9 Bayless KJ, Davis GE. Microtubule depolymerization rapidly collapses capillary tube networks in vitro and angiogenic vessels in vivo through the small GTPase Rho. *J Biol Chem* 2004; **279**: 11686–95.

10 Kleaveland B, Zheng X, Liu JJ, Blum Y, Tung JJ, Zou Z, Chen M, Guo L, Lu MM, Zhou D, Kitajewski J, Affolter M, Ginsberg MH, Kahn ML. Regulation of cardiovascular development and integrity by the heart of glass-cerebral cavernous malformation pathway. *Nat Med* 2009; **15**: 169–76.

11 Zawistowski JS, Stalheim L, Uhlik MT, Abell AN, Ancrile BB, Johnson GL, Marchuk DA. CCM1 and CCM2 protein interactions in cell signaling: implications for cerebral cavernous malformations pathogenesis. *Hum Mol Genet* 2005; **14**: 2521–31.

12 Wilson BD, Ii M, Park KW, Suli A, Sorensen LK, Larrieu-Lahargue F, Urness LD, Suh W, Asai J, Kock GA, Thorne T, Silver M, Thomas KR, Chien CB, Losordo DW, Li DY. Netrins promote developmental and therapeutic angiogenesis. *Science* 2006; **313**: 640–4.

13 Suzuki K, Okuno T, Yamamoto M, Pasterkamp RJ, Takegahara N, Takamatsu H, Kitao T, Takagi J, Rennert PD, Kolodkin AL, Kumanogoh A, Kikutani H. Semaphorin 7A initiates T-cell-mediated inflammatory responses through alpha1beta1 integrin. *Nature* 2007; **446**: 680–4.

14 Kashiwagi H, Shiraga M, Kato H, Kamae T, Yamamoto N, Tadokoro S, Kurata Y, Tomiyama Y, Kanakura Y. Negative regulation of platelet function by a secreted cell repulsive protein, semaphorin 3A. *Blood* 2005; **106**: 913–21.

15 Gavard J. Breaking the VE-cadherin bonds. *FEBS Lett* 2009; **583**: 1–6.

CHAPTER 2

TARGETING ROBO4-DEPENDENT SLIT SIGNALING TO SURVIVE THE CYTOKINE STORM IN SEPSIS AND INFLUENZA

The following chapter is a reprint of a manuscript published in *Science Translational Medicine*. It was published March 17, 2010, volume 2 (23). In addition to myself, the other authors were Nyall London, Weiquan Zhu, Fernando Bozza, Dan Greif, Lise Sorensen, Luming Chen, Yuuki Kaminoh, Aubrey Chan, Samuel Passi, Craig Day, Dale Barnard, Guy Zimmerman, Mark Krasnow, and Dean Li. This manuscript has been reprinted with permission from The American Association for the Advancement of Science. I participated in the design, execution, interpretation of data, and preparation of the manuscript, primarily in the cell biology pertaining to Slit's effect on neutrophil migration and function.

RESEARCH ARTICLE

SEPSIS

Targeting Robo4-Dependent Slit Signaling to Survive the Cytokine Storm in Sepsis and Influenza

Nyall R. London,[1,2,3]* Weiquan Zhu,[1,2,3]* Fernando A. Bozza,[4] Matthew C. P. Smith,[1,2,3] Daniel M. Greif,[5,6] Lise K. Sorensen,[1,2,3] Luming Chen,[1,2,3] Yuuki Kaminoh,[1,2,3] Aubrey C. Chan,[1,2,3] Samuel F. Passi,[1,2,3] Craig W. Day,[7] Dale L. Barnard,[7] Guy A. Zimmerman,[2] Mark A. Krasnow,[5] Dean Y. Li[1,2,3]†

(Published 17 March 2010; Volume 2 Issue 23 23ra19)

The innate immune system provides a first line of defense against invading pathogens by releasing multiple inflammatory cytokines, such as interleukin-1β and tumor necrosis factor–α, which directly combat the infectious agent and recruit additional immune responses. This exuberant cytokine release paradoxically injures the host by triggering leakage from capillaries, tissue edema, organ failure, and shock. Current medical therapies target individual pathogens with antimicrobial agents or directly either blunt or boost the host's immune system. We explored a third approach: activating with the soluble ligand Slit an endothelium-specific, Robo4-dependent signaling pathway that strengthens the vascular barrier, diminishing deleterious aspects of the host's response to the pathogen-induced cytokine storm. This approach reduced vascular permeability in the lung and other organs and increased survival in animal models of bacterial endotoxin exposure, polymicrobial sepsis, and H5N1 influenza. Thus, enhancing the resilience of the host vascular system to the host's innate immune response may provide a therapeutic strategy for treating multiple infectious agents.

INTRODUCTION

The devastating consequences of influenza epidemics, the poor medical outcome after sepsis, and the emergence of new infectious pandemic and biowarfare threats have kindled interest in the development of broad-spectrum strategies that can be rapidly implemented by public health and military defense agencies (*1*, *2*). There are now two main ways to address these infectious threats. The first is to target specific pathogens with antimicrobials. With this approach, time is required to identify the specific pathogen once a pandemic has emerged. In addition, pathogens often mutate, developing resistance to antibiotics and antiviral agents (*3*, *4*). The recent emergence of a pandemic influenza strain highlights these limitations (*5*).

A second approach is to modulate the host's innate immune system (*6*). Innate immunity provides the host with immediate protection against a broad and unforeseen spectrum of pathogens. When activated by endotoxin [lipopolysaccharide (LPS)] or other microbial components, this system, which is composed of neutrophils, monocytes, macrophages, Langerhans cells, dendritic cells, and natural killer cells, releases multiple cytokines with broad antibacterial and antiviral properties as well as regulatory effects on subsequent adaptive immune responses. The marked and abrupt release of multiple cytokines by the immune system, often referred to as hypercytokinemia or cytokine storm, itself has disruptive effects on the host's physiology. In many infections, components of the resulting cytokine-induced secondary inflammatory injury can be more toxic than the invading microbes themselves (*7*). Inflammatory cytokines, such as tumor necrosis factor (TNF) and interleukin-1β (IL-1β), destabilize endothelial cell-cell interactions and cripple vascular barrier function, resulting in capillary leakage, tissue edema, organ failure, and death (*5*, *8*, *9*). These phenomena occur in septic shock, acute lung injury, and acute respiratory distress syndrome—all common endpoints in patients exposed to serious infections (for example, the 1918 influenza pandemic). The prominent role of cytokines in these pathologies has led to the testing of agents that reduce cytokine signaling as possible therapeutics (*10*). This clinical strategy has, however, been disappointing, often resulting in increased mortality (*11*–*13*). The converse strategy of boosting the immune system with infusion of inflammatory cytokines has also been advocated, but its clinical use has been limited because of undesirable outcomes (*6*). For example, delivery of ILs to treat melanoma precipitates aseptic vasogenic shock in patients (*14*). Thus, for survival of the infected patient or animal, a balance must be struck between a protective innate immune response that eliminates the pathogen and an excessive immune response that injures the host.

Here, we have explored a third approach: maximizing the host's endogenous ability to overcome infectious challenge by limiting the disruptive effects of proinflammatory mediators on the vasculature. By augmenting the resilience of the host's vascular system to cytokines, we sought to enable the body to endure an excessive innate immune response. We identified the Slit-induced signaling pathway as a modulator of vascular stability that can strengthen endothelial cell-cell interactions. Activation of this pathway is effective in reducing capillary leak, multiorgan edema, and death in multiple animal models of infections, including H5N1 influenza.

[1]Department of Oncological Sciences, University of Utah, Salt Lake City, UT 84112, USA. [2]Department of Medicine, University of Utah, Salt Lake City, UT 84112, USA. [3]Program in Molecular Medicine, University of Utah, Salt Lake City, UT 84112, USA. [4]Intensive Care Unit, Instituto de Pesquisa Clínica Evandro Chagas, and Laboratório de Imunofarmacologia, Fundação Oswaldo Cruz, Rio de Janeiro 21045-900, Brazil. [5]Department of Biochemistry and Howard Hughes Medical Institute, Stanford University School of Medicine, Stanford, CA 94305, USA. [6]Department of Medicine, Division of Cardiovascular Medicine, Stanford University School of Medicine, Stanford, CA 94305, USA. [7]Institute for Antiviral Research, Utah State University, Logan, UT 84322, USA.

*These authors contributed equally to this work.

†To whom correspondence should be addressed. E-mail: dean.li@u2m2.utah.edu

7

RESULTS

Slit regulates vascular endothelial cadherin localization

Because the vascular system is exposed to ischemic, infectious, and inflammatory stresses, the endothelium is continuously challenged by angiogenic factors, inflammatory mediators, and permeability agents. All of these molecules disrupt the endothelial barrier of the mature vascular system and contribute to the classic findings of calor (heat), dolor (pain), rubor (redness), and tumor (swelling) on inflammation. Members of the Slit family of neurovascular guidance cues inhibit vascular endothelial growth factor (VEGF)–induced vascular hyperpermeability in a process dependent on the endothelial-specific receptor Robo4 (*15*). This inhibition of VEGF signaling by Slit protein is mediated through the small intracellular guanosine triphosphatase, Arf6 (*16*). Because Robo4 messenger RNA concentrations increase in response to a diverse repertoire of angiogenic (*15*, *17*, *18*) and inflammatory exposures, we hypothesized that Robo4 may be part of a vascular stability signaling program. We tested this hypothesis by examining whether Robo4-dependent Slit signaling reduces the endothelial hyperpermeability induced by endotoxin (LPS), TNF-α, and IL-1β, all important mediators of inflammation (*19*). To study barrier function in vitro, we assessed the ability of a human endothelial cell monolayer to act as a barrier to diffusion of a horseradish peroxidase reporter. We used the N-terminal fragment (Slit2N), which is the active fragment of Slit that is released by proteolytic cleavage (*20*). Slit2N at 10 nM substantially reduced LPS-induced, TNF-α–induced, and IL-1β–induced permeability (Fig. 1A) but did not significantly affect basal permeability (fig. S1A). Furthermore, the inhibitory effect of Slit2N was lost in cells exposed to small interfering RNA (siRNA) directed against Robo4 but not in those exposed to control scrambled siRNA (Fig. 1B and fig. S1B).

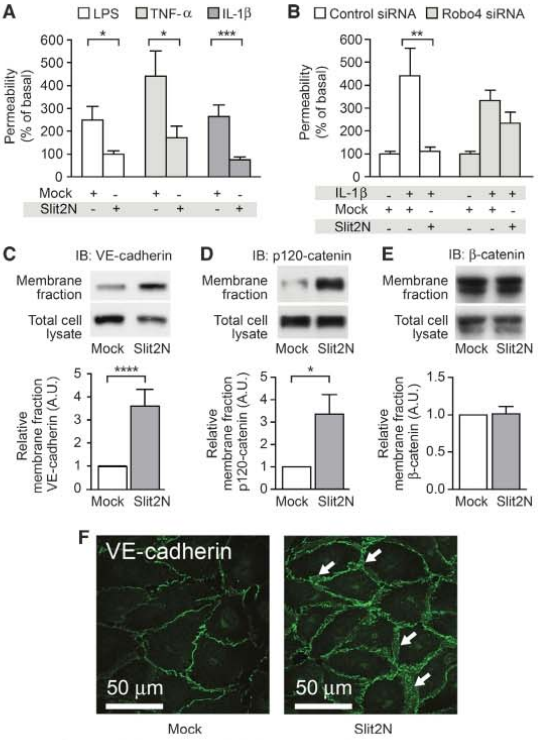

Fig. 1. Slit2N stabilizes the endothelium in vitro by enhancing VE-cadherin localization at the cell surface. (**A**) In vitro permeability was measured in HMVEC-lung cells stimulated with LPS, TNF-α, or IL-1β in the presence of Mock (see Materials and Methods) or Slit2N. (**B**) Robo4 or control siRNA knockdown-treated HMVEC-lung cells were stimulated with IL-1β in the presence of Mock or Slit2N to assess permeability in vitro. (**C** to **E**) HMVEC-lung cells were treated with Mock or Slit2N and subjected to membrane fractionation and subsequent immunoblotting for VE-cadherin (C), p120-catenin (D), or β-catenin (E). (**F**) HMVEC-lung cells were stimulated with Mock or Slit2N and subjected to immunofluorescence for VE-cadherin (green). White arrows, areas of enhanced VE-cadherin cell surface localization. For all experiments, $n \geq 3$, and error bars represent SEM. $^{*}P < 0.05$, $^{**}P < 0.01$, $^{***}P < 0.005$, $^{****}P < 0.001$.

Because Robo4-dependent Slit2N signaling tempers the effects of such a range of angiogenic and inflammatory cytokines (Fig. 1A), we tested whether this pathway promotes vascular stability by directly enhancing the molecular machinery responsible for cell-cell interactions. In the endothelium, critical intercellular interactions are mediated by the adherens junction protein vascular endothelial cadherin (VE-cadherin) (*21*, *22*). When we treated human microvascular lung endothelial (HMVEC-lung) cells with Slit2N, VE-cadherin abundance was significantly increased at the cell surface junctions (Fig. 1, C and F, and fig. S1C). VE-cadherin presence on the cell surface is regulated by the association of p120-catenin with VE-cadherin, an association that inhibits VE-cadherin internalization from the cell surface and promotes vascular stability (*23*, *24*). Slit2N also increased the cell surface abundance of p120-catenin (Fig. 1D) but had no effect on β-catenin (Fig. 1E).

Next, we determined whether Slit2N affected VE-cadherin at the cell surface after exposure to IL-1β. IL-1β reduced VE-cadherin at the cell surface, and Slit2N negated this effect (Fig. 2A). IL-1β stimulation decreased p120-catenin at the cell surface, and Slit2N reversed this effect (Fig. 2A). IL-1β induced dissociation of VE-cadherin from p120-catenin and internalization of VE-cadherin (Fig. 2, B and C). Slit2N restored the association of VE-cadherin and p120-catenin and blocked internalization of VE-cadherin (Fig. 2, B and C). VE-cadherin internalization experiments were performed in the presence of primaquine to prevent endocytic recycling (*25*). In the absence of primaquine, we were unable to detect IL-1β–induced VE-cadherin internalization (fig. S1D). It has been proposed that phosphorylation of VE-cadherin at Tyr^{658} disrupts its binding to p120-catenin and results in the endocytosis of VE-cadherin (*23*). Our experiments indicate that Slit2N stabilized the interaction between VE-cadherin and p120-catenin by inhibiting IL-1β–induced phosphorylation of VE-cadherin at Tyr^{658} (fig. S1E).

Next, we investigated whether the effect of Slit2N on VE-cadherin localization is necessary for its ability to enhance vascular stability. Because VE-cadherin siRNA had a potent disruptive effect on the endothelial monolayer at baseline (fig. S1, F and G), we used an antibody to VE-cadherin to block the effect of Slit2N on permeability in vitro. Slit2N inhibited IL-1β–induced permeability in vitro in the presence of a nonspecific immunoglobulin G (IgG); however, the effect of Slit2N was lost in the presence of an antibody to VE-cadherin (Fig. 2D). Together, these data suggest that Slit2N preserves the association of p120-catenin with VE-cadherin in the face of IL-1β stimulation and thereby promotes vascular integrity by reducing cytokine-induced VE-cadherin endocytosis.

Slit enhances vascular stability in vivo

To examine whether Slit reduces permeability under conditions of cytokine storm in vivo, we used a bacterial endotoxin model of pulmonary inflammation. In this model, LPS is administered to the lungs of mice through intratracheal instillation, simulating a Gram-negative infection (*26*). LPS administration triggers a massive inflammatory reaction and release of cytokines, resulting in a large increase in alveolar capillary permeability. Using Evans blue albumin (EBA) as a tracer, we found that Slit2N significantly reduced vascular leak in the lungs of LPS-treated *Robo4*$^{+/+}$ mice (Fig. 3A). The effect of Slit2N was lost in *Robo4*-null (*Robo4*$^{AP/AP}$) mice, showing that Robo4 is necessary for the effect of Slit2N in vivo (Fig. 3A). This result also indicates that this activity is endothelial-specific, as Robo4 is only detected in the endothelium (*17*, *18*). LPS instillation in the lung also induces accumulation of protein exudates and leukocytes in the alveolar space, inflammatory responses that can be quantified in bronchoalveolar lavage fluid (BALF) (*26*). Slit2N reduced protein exudate, a key marker of acute lung injury and indicator of vascular barrier disruption (*10*), and inflammatory cell accumulation in the BALF of *Robo4*$^{+/+}$ mice in a dose-dependent manner (Fig. 3, B to D, and fig. S2, A and B). The Slit2N-induced inhibition of protein and leukocyte accumulation in BALF was lost in *Robo4*$^{AP/AP}$ mice, indicating again that Slit2N acts directly on the vasculature to decrease protein exudates and inflammatory cell accumulation in the alveoli (Fig. 3, B to D). Finally, histological examination of the lung confirmed that Slit2N acts in a Robo4-dependent manner by reducing LPS-induced lung inflammation in *Robo4*$^{+/+}$ but not *Robo4*$^{AP/AP}$ mice (Fig. 3E and fig. S2C). Because neutrophils are a predominant cell type in bacterial pneumonia and LPS challenge models (*26*), we tested whether Slit2N had a direct effect on neutrophil migration. Primary human polymorphonuclear leukocytes (hPMNs) did not respond to Slit2N, consistent with the fact that they do not express Robo receptors (fig. S3, A and B).

One might anticipate that the loss of Robo4 would make mice more sensitive to LPS exposure, but in initial studies, we did not detect enhanced sensitivity in the lungs of *Robo4*$^{AP/AP}$ mice relative to *Robo4*$^{+/+}$ mice (Fig. 3, B to D). We reasoned that if the amount of LPS administered was too large, it could cause such severe damage that any difference between the two genotypes would be masked. Thus, we lowered the dose of LPS used to challenge the mice and, under these conditions, found that *Robo4*$^{AP/AP}$ mice exhibited signifi-

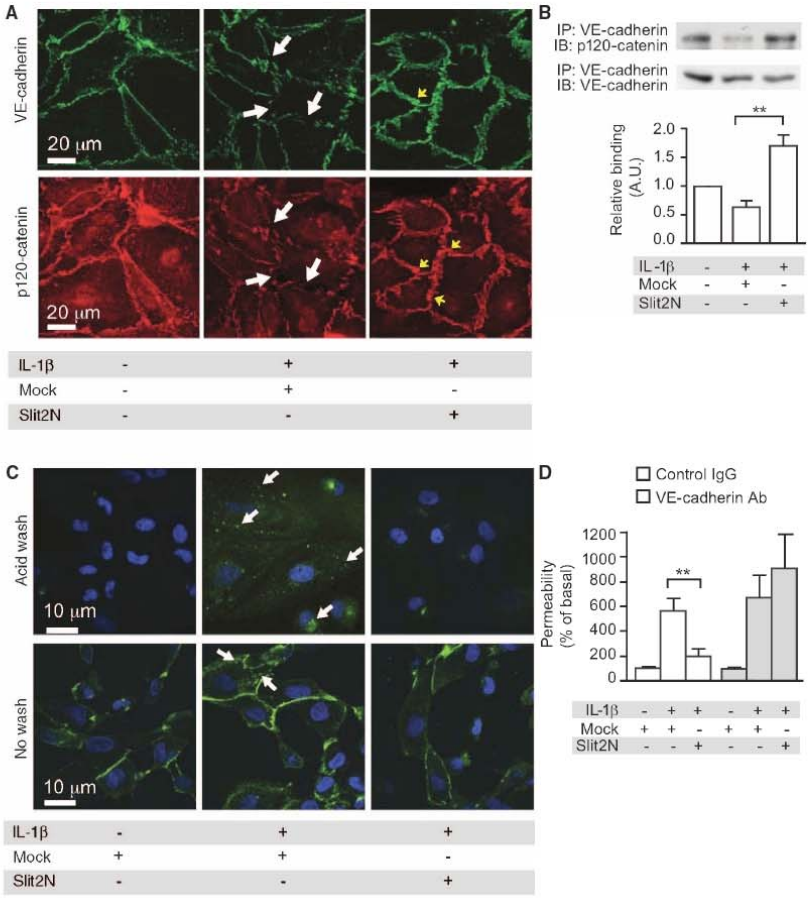

Fig. 2. Slit2N enhances a VE-cadherin–p120-catenin interaction in vitro. (**A**) HMVEC-lung cells were stimulated with IL-1β in the presence of Mock or Slit2N and immunostained for VE-cadherin and p120-catenin. White arrows, cell surface areas lacking VE-cadherin or p120-catenin in Mock-treated cells; yellow arrows, areas of enhanced cell surface localization of VE-cadherin or p120-catenin in Slit2N-treated cells. (**B**) HMVEC-lung cells were stimulated with IL-1β in the presence of Mock or Slit2N. Lysates were subjected to immunoprecipitation for VE-cadherin followed by immunoblot for p120-catenin and VE-cadherin. (**C**) HMVEC-lung cells were labeled with an antibody to VE-cadherin and stimulated with IL-1β in the presence of Mock or Slit2N. Cells were acid-washed to strip the surface-bound VE-cadherin (top row). VE-cadherin internalization (green) was assessed. White arrows, areas of internalization. (**D**) In vitro permeability was measured in the presence of a control IgG or VE-cadherin antibody (Ab). For all experiments, $n \geq 3$, and error bars represent SEM. $^{**}P < 0.01$.

cantly higher protein concentrations in BALF than did littermate *Robo4*$^{+/+}$ mice (Fig. 3F). This increased sensitivity of *Robo4*$^{AP/AP}$ mice to LPS suggests that endogenous Robo4-dependent Slit signaling normally dampens the effects of cytokines on the vasculature. Consistent with this suggestion, Slit2 protein is expressed throughout the lung and in close proximity to the endothelium (fig. S4).

To determine whether Slit acts via a VE-cadherin–dependent mechanism in vivo, we blocked VE-cadherin with a specific antibody that prevents homophilic interactions between VE-cadherin expressed on adjacent endothelial cells (*27*). Slit2N reduced protein exudates and inflammatory cell infiltration in the presence of a control IgG antibody but not in the presence of a VE-cadherin–blocking antibody (Fig. 3, G to I). Thus, as in our cell culture experiments, our in vivo experimental results support the idea that Slit2N promotes VE-cadherin expression at the cell surface, which blunts cytokine-mediated endothelial hyperpermeability.

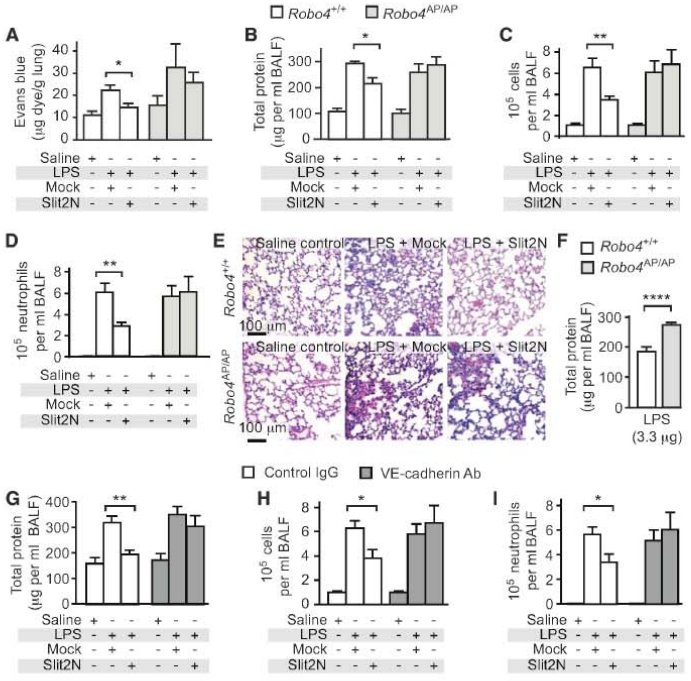

Fig. 3. Slit2N inhibits LPS-induced permeability, protein exudates, and cell infiltrates in vivo. (**A**) *Robo4*$^{+/+}$ and *Robo4*$^{AP/AP}$ mice were given an intravenous injection of Mock or Slit2N followed by intratracheal instillation of LPS (10 μg). Mice later received an intravenous injection of EBA, and EBA accumulation in the lungs was used to assess vascular permeability ($n \geq 4$). (**B** to **D**) Twenty-four hours after LPS administration, bronchoalveolar lavages were obtained and assessed for protein content (B), total inflammatory cell accumulation (C), or neutrophil accumulation (saline value is too low to be visible) (D) ($n \geq 5$). (**E**) H&E staining was performed on lung sections from mice exposed to LPS in the presence of Mock or Slit2N. (**F**) Protein exudates measured in mice treated with 3.3 μg of LPS ($n = 5$). (**G** to **I**) Mice were given an intravenous injection of Mock or Slit2N with control or VE-cadherin–blocking antibody followed by intratracheal instillation of LPS. Bronchoalveolar lavages were obtained and assessed for protein content (G), total inflammatory cell accumulation (H), or neutrophil accumulation (I) ($n \geq 5$). Error bars represent SEM. *$P < 0.05$, **$P < 0.01$, ****$P < 0.001$.

Enhancing vascular stability during polymicrobial sepsis

To evaluate whether Slit2N can reduce mortality in the setting of systemic vascular instability, and whether the effect of Slit2N is limited to the lung, we used a model of polymicrobial sepsis known as cecal ligation and puncture (CLP) (*28*). Slit2N significantly reduced vascular permeability in the kidney and spleen (Fig. 4, A and B) and improved the survival of mice exposed to CLP-induced sepsis from 33 to ~80% (Fig. 4C). Under the conditions of these experiments, CLP did not cause significant damage to the lung (fig. S5, A to C). Because a hyperinflammatory response contributes to the pathogenesis of sepsis, we also tested whether Slit2N could affect cytokine and chemokine concentrations in the plasma of septic mice (*19*). Slit2N did not alter plasma concentrations of a panel of cytokines and chemokines, demonstrating that the therapeutic effect of Slit2N is not secondary to a reduction in inflammatory cytokine and chemokines (Fig. 4, D and E). The effect of Slit2N on mortality after CLP treatment was lost in *Robo4*$^{AP/AP}$ mice (Fig. 4F), hence Robo4 is necessary for this activity of Slit2N. Additionally, the loss of Robo4 did not alter cytokine receptor levels, nor does Slit2N inhibit cytokine receptor activation or induce Robo4 expression in endothelial cells (fig. S6, A and B). Together, these data demonstrate that Slit can enhance survival by specifically enhancing vascular stability during the systemic inflammatory response triggered by sepsis.

Stabilizing the vasculature reduces mortality after H5N1 infection

LPS instillation and CLP mimic the vascular instability and dysregulated inflammation induced by bacterial pathogens. To determine whether a therapeutic strategy of vascular stabilization can be productively applied to viral infections, we examined the effects of Robo4-dependent Slit2N treatment in a model of H5N1 influenza. Pandemic influenzas such as avian flu (H5N1) provide extreme examples of infection-induced lung injury characterized by large increases in cytokine concentrations and excessive inflammation (*29*–*31*). Slit2N significantly inhibited endothelial hyperpermeability in the lung 3 days after H5N1 infection of mice (Fig. 5A) and also reduced mortality (Fig. 5B). The lung pathology in Slit2N-treated mice was less severe than it was in mock-treated mice (Fig. 5C). To exclude the possibility that Slit2N has direct antiviral activity, we measured lung viral titers and found that Slit2N did not alter viral load (Fig. 5D); further, Slit2N did not significantly reduce the amount of inflammatory cytokine released in the lung after H5N1 infection (Fig. 5, E and F). These results are consistent with our LPS and CLP studies and indicate that limiting the vascular response to hypercytokinemia is sufficient to reduce mortality and morbidity in animal models of serious infection.

DISCUSSION

Pandemic influenza and bacterial sepsis are infections that have sizable mortality rates and substantially affect public health (*32*). New ways to address these constantly evolving biological threats are needed (*33*). Here, using rodent models of infection, we have demonstrated that cytokine storm and capillary leakage contribute to the poor outcome of endotoxin-induced acute lung injury, polymicrobial sepsis, and pandemic influenza. We further show that administration of the exogenous ligand Slit2N strengthens the endothelial barrier and blunts vascular leak in response to cytokine storm (Fig. 6). Exogenously applied Slit2N stabilizes cell surface VE-cadherin, a primary molecular determinant of intact barrier function in the endothelium, and this strengthened barrier can protect mice from the lethal effects of sepsis or influenza infection. Furthermore, in genetically modified mice lacking Robo4, Slit2N cannot prevent vascular leakage in infection or sepsis, indicating that Robo4 is a critical mediator of Slit-promoted vascular stability.

We and others have long assumed that Robo4 played an essential role in development based on a number of observations, including the role of Slit-Robo signaling in neuronal guidance (*34*) and the lethality of mutations in genes of this signaling pathway (*35*–*37*). Yet, unexpectedly, mice homozygous for null mutations of *Robo4* are viable (*15*). Similarly, in a detailed characterization of lung development, we could find no structural differences between *Robo4*$^{AP/AP}$ (null) mice and their wild-type sibling controls (figs. S7 and S8).

Our results suggest an alternative function for Robo4: This receptor may be important for modulating the vascular response to inflammatory cytokines but not for development. As with other pathways that maintain adult homeostasis, including many involved in the immune response, one cannot a priori expect that these pathways are also essential for development. Genetic alterations in these pathways might only manifest after exposure to physiologic or environmental stress (*38*).

In our experiments, we tested one way that signaling via Robo4 could modulate critical host inflammatory responses. Because Slit2 affects migration of dimethyl sulfoxide (DMSO)–treated HL-60 cells, a promyelocytic leukemia cell line often used as a surrogate for primary neutrophils (*39*), we asked whether Slit2 inhibits migration of neutrophils, which could account for the reduced numbers of inflammatory cells in the lungs of LPS-treated mice (*40*). Although in our hands Slit2 also inhibited migration of DMSO-treated HL-60 cells, we found no evidence that primary hPMNs respond to Slit2N, nor do they express Robo receptors (fig. S3, A and B).

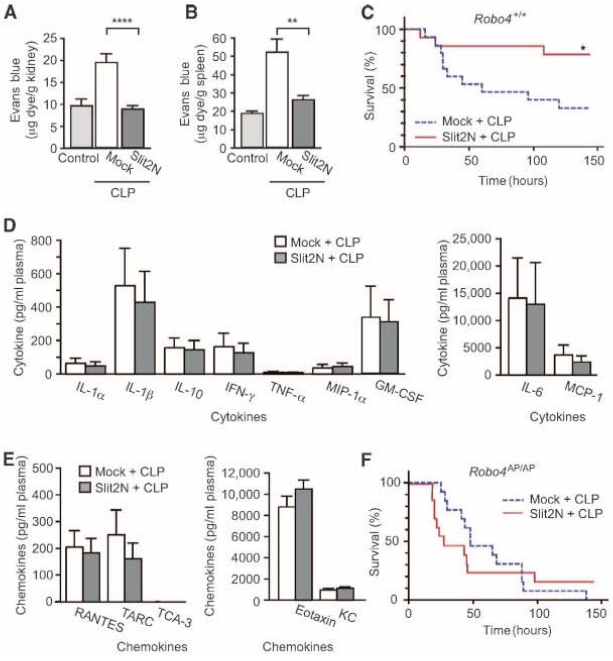

Fig. 4. Slit2N reduces permeability and mortality in a CLP model of sepsis. (**A** and **B**) Mice were subjected to CLP or sham operation and then given an intravenous injection of EBA. EBA accumulation was measured in the kidney (A) or spleen (B) to assess vascular permeability ($n = 5$). (**C**) *Robo4*$^{+/+}$ mice were subjected to CLP and treated with Mock or Slit2N, and survival was assessed (Mock-treated, $n = 15$; Slit2N-treated, $n = 14$). (**D** and **E**) Cytokine (D) and chemokine (E) concentrations in the serum of Mock- or Slit2N-treated CLP mice ($n = 6$). (**F**) *Robo4*$^{AP/AP}$ mice were subjected to CLP and treated with Mock or Slit2N, and survival was assessed (Mock-treated, $n = 13$; Slit2N-treated, $n = 13$). Error bars represent SEM. $^{*}P < 0.05$, $^{**}P < 0.01$, $^{****}P < 0.001$.

Rather, our data demonstrate that Robo4 is required for the effect of Slit2N on VE-cadherin–mediated vascular barrier function. Similarly, expression of either Robo4 or Robo1 is necessary and sufficient to make cells sensitive to Slit (*15*, *16*, *18*, *39*, *41*). The simplest interpretation of these data would be that Slit2 acts as a direct ligand for Robo4. This may not be the case, however. Others have postulated that co-receptors such as syndecans are required for the function of Robo receptors in neural guidance (*42*–*45*). Western blot and immunoprecipitation studies in the presence of non-denaturing detergents (0.5% NP-40) reveal specific binding of Slit2 to Robo4 (*18*), but the use of harsher conditions using ionic denaturing detergents (1% Triton X-100–0.5% deoxycholate) fails to preserve this interaction (*46*). To reconcile this variable and detergent-dependent binding between Slit2 and cell surface Robo4, the absence of strong interaction between Slit and Robo4 in an in vitro Biacore assay (*46*), and the strong signaling and functional response of Robo4 to Slit, Sheldon *et al.* (*42*) and Suchting *et al.* (*46*) propose that Robo4 and Robo1 receptors form a heterodimeric complex in human vein endothelial cells and show that the Robo1 and Robo4 receptors bind to one another. Consistent with their model, we find that knockdown of either Robo4 or Robo1 abrogates the ability of Slit to inhibit migration of human vein endothelial cells (fig. S9). Further investigation of the roles of Robo1 and syndecans as co-receptors for Robo4 is needed.

The endothelial cell monolayer provides a critical semipermeable barrier between the blood and tissue that regulates the passage of nutrients, fluid, and leukocytes into the interstitial space (*47*). The integrity of this barrier is determined by homophilic interactions between the cell surface adherens junction protein VE-cadherin on adjacent endothelial cells (*48*). In states of active angiogenesis or acute inflammation, cytokines induce rapid endocytosis of VE-cadherin, disrupting the transcellular homophilic binding of VE-cadherins, deconstructing paracellular adherens junctions, and resulting

in hyperpermeability (*21*, *49*–*51*). Our study suggests that the destabilizing effects of angiogenic and inflammatory cytokines are opposed by extracellular cues that promote vascular stability. Although two stabilizing regulators of the vascular barrier, Tie2-dependent angiopoietin signaling and Robo4-dependent Slit signaling, use different immediate downstream signaling cascades, both ultimately blunt cytokine-mediated endocytosis of cell surface VE-cadherin (*15*, *16*, *52*). Thus, the strength of the endothelial barrier may be a product of a constant tug-of-war between opposing stabilizing and destabilizing signals that control VE-cadherin trafficking, allowing the vascular system the necessary plasticity to respond to changing physiologic needs.

The innate immune system provides the first line of defense of the body against pathogens and must be rapid, broad-spectrum, and toxic to the offending pathogen. There is a fine line between overwhelming the invaders and inflicting severe collateral damage to the host. Boosting the innate immune system with cytokines increases the risk of vasogenic shock, yet efforts to reduce secondary damage by suppressing the innate immune response with glucocorticoids can worsen the outcomes from severe infection. Thus, pharmacologic modulation of the innate immune response has a narrow therapeutic window.

The specific cytokines elaborated and their temporal secretion profile may differ for each pathogen. Nevertheless, the cumulative effects of hypercytokinemia on vascular leakage and noncardiogenic shock are common among severe infections characterized by septic shock (*29*, *30*, *53*). Our data suggest that an alternative approach to combating these infections is to strengthen the vascular barrier. The pharmacologic promotion of vascular stability was sufficient to mute the vascular hyperpermeability induced by multiple different cytokines and the subsequent mortality in rodent models of severe bacterial and viral infections. Enhancing stability offers practical advantages over a more complicated approach aimed at blocking each individual cytokine contributing to cytokine storm. The practical success of targeting the vascular response to cytokines may require a careful characterization of the temporal sequence involving infection, hypercytokinemia, vascular leakage, organ failure, and eventual death (*9*, *29*, *30*, *54*). A likely limitation is that this therapeutic approach may need to be used before the vascular damage is too grave to repair. Even so, targeting the host and not the pathogen offers a stratagem that could offer sufficient flexibility to successfully combat ever-changing biologic threats from drug-resistant, mutating, and emerging infectious agents (*55*).

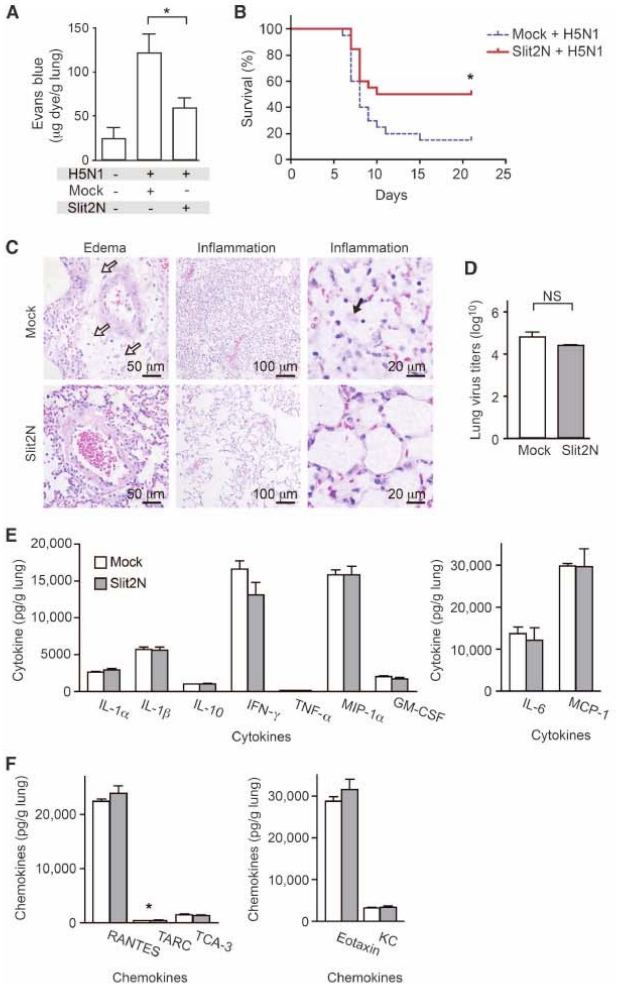

Fig. 5. Slit2N reduces mortality in models of H5N1 infection. (**A**) BALB/c mice were infected intranasally with H5N1 virus. Mice were given an intravenous injection of EBA, and EBA accumulation was measured in the lungs to assess vascular permeability (n = 5). (**B**) Mouse survival after H5N1 infection (Mock-treated, n = 20; Slit2N-treated, n = 20). (**C**) H&E staining was performed on lung sections from H5N1-infected mice 6 days after infection. White arrows in the top left panel show accumulation of edema fluid around a pulmonary arteriole. The top middle panel demonstrates exuberant alveolar inflammation. The black arrow in the top right panel shows the presence of foamy macrophages. (**D**) H5N1 viral titers were measured 6 days after infection (n = 3 groups of pooled mice). (**E** and **F**) Cytokine (E) or chemokine (F) concentrations measured in lung homogenates 6 days after infection (n = 3 groups of pooled mice). *P < 0.05. NS, not significant.

MATERIALS AND METHODS

Preparation of recombinant Slit2N

293T cells plated onto poly-L-lysine (Sigma)–coated dishes were transiently transfected with empty vector pSecTagB or pSecTagB::hSlit2N. For each 15-cm dish of cells, 60 μg of DNA and 100 μl of Lipofectamine (Invitrogen) in serum-free Opti-MEM were used. Slit2N protein was salt-extracted as described (*15*). Using this protocol, we obtained Slit2N concentrations of 0.5 to 1.5 mg/ml. We performed the same salt extraction procedure on cells transfected with empty vector pSecTagB. This preparation is referred to as Mock and was used as a control for Slit2N in all experiments. In vitro studies were conducted with 10 nM Slit2N.

In vitro permeability assay

In vitro permeability testing was performed as described (*15*) with LPS (100 ng/ml; serotype 0111:B4; Sigma) for 3 hours, TNF-α (10 ng/ml; R&D Systems) for 6 hours, or IL-1β (10 ng/ml; R&D Systems) for 2 hours. As indicated, this was repeated in the presence of control rabbit IgG (25 μg/ml; Jackson ImmunoResearch) or antibody to human VE-cadherin (25 μg/ml; RDI Fitzgerald). Basal permeability for unstimulated monolayers was set at 100%. Data are presented as mean ± SEM of at least three independent experiments performed in triplicate.

Robo4 siRNA knockdown

huRobo4 siRNA duplex (Hs_Robo4_1_HP; Qiagen) or equimolar All-Stars Negative Control siRNA (Qiagen) transfection complexes were formed according to standard protocol and added to the upper chamber of Transwell filters. Twenty-four hours later, cells were transfected a second time with huRobo4 or control siRNA. After an additional 24 hours, in vitro permeability was assessed as described. Data are presented as mean ± SEM of at least three independent experiments performed in triplicate. Successful knockdown of Robo4 protein expression was confirmed by Western blot with antibodies against Robo4 (N-17) or β-tubulin (Santa Cruz Biotechnology).

Subcellular fractionation

HMVEC-lung cells were treated with Slit2N or Mock in 0.1% fetal bovine serum (FBS) EBM-2 for 1.5 hours. Cells were then washed twice with ice-cold phosphate-buffered saline (PBS) containing Ca^{2+}-Mg^{2+} and once with HLB buffer [10 mM tris-HCl (pH 7.4), 5 mM KCl, and 1 mM $MgCl_2$] and collected in HLB buffer supplemented with protease inhibitors (Roche), phosphatase inhibitors (Sigma), and 1 mM dithiothreitol (DTT). Cells were then homogenized in a Dounce homogenizer (20 strokes). The homogenate was centrifuged at 400*g* for 10 min at 4°C to pellet cell debris. The resulting supernatant was centrifuged again at 16,000*g* for 30 min at 4°C. The pellet was washed once with HLB and resuspended in radioimmunoprecipitation assay (RIPA) buffer for 30 min at 4°C. The resuspended pellet was centrifuged (16,000*g* for 15 min at 4°C), and the resulting supernatant was saved as a soluble membrane fraction. To obtain the total cell lysate, we saved an aliquot before Dounce homogenization. RIPA buffer was added to this aliquot and centrifuged at 13,000*g* for 10 min at 4°C. The supernatant was saved and used as total cell lysate. Antibodies to VE-cadherin were obtained from Cell Signaling, and p120-catenin and β-catenin were from BD Biosciences. Densitometry was performed on at least three independent experiments and data are presented as mean ± SEM.

Immunofluorescence

Immunofluorescence was performed as described (*15*). Cells were pretreated with Slit2N or Mock for 30 min followed by stimulation with IL-1β (10 ng/ml) for 3 hours. Primary antibodies to VE-cadherin (BD Biosciences) or p120-catenin (Santa Cruz Biotechnology) were applied at 4°C overnight. Images are representative of three independent experiments.

Immunoprecipitation

HMVEC-lung cells (Lonza) were treated with Slit2N or Mock in 0.1% FBS EBM-2 for 30 min. Cells were then stimulated with IL-1β (10 ng/ml) for 10 min. HMVEC-lung cells were then washed with ice-cold PBS and lysed with ice-cold lysis buffer [10 mM tris-HCl (pH 7.4), 50 mM NaCl, 1% NP-40, and 10% glycerol] supplemented with protease inhibitors, phosphatase inhibitors, and 1 mM DTT. Cell lysates were incubated on ice for 30 min and centrifuged at 13,000*g* for 15 min to pellet cell debris. Protein concentrations were determined by BCA assay (Pierce), and 0.5 mg of lysate was incubated with 8 μg of VE-cadherin antibody (Cell Signaling) and protein A/G–Sepharose (Santa Cruz Biotechnology) for 1 hour at 4°C. Complexes were washed three times with lysis buffer. The immunoprecipitates were subjected to Western blot analysis using a 95% fraction of the immunoprecipitate for the p120-catenin blots and the remaining 5% fraction for the VE-cadherin blots (Fig. 2B). Densitometry was performed on three independent experiments, and data as a ratio of immunoprecipitated p120-catenin to loaded VE-cadherin are presented as mean ± SEM.

Internalization assay

VE-cadherin internalization was performed as described (*24*). In brief, HMVEC-lung cells were seeded onto chamber slides and cultured for 72 hours. The media were then removed, and the cells were labeled for 30 min at 4°C with an antibody to VE-cadherin (clone BV6; RDI Fitzgerald). Cells were then pretreated with Slit2N or Mock for 30 min. Excess antibody was removed by washing twice on ice with ice-cold media. Chamber slides were moved to 37°C and incubated for 1 hour with IL-1β (10 ng/ml) and 0.6 mM primaquine in the presence of 10 nM Slit2N or Mock. Cells were acid-washed to strip the surface-bound VE-cadherin. Monolayers were washed, fixed, and permeabilized. Internalized VE-cadherin antibody was detected with Alexa 488–conjugated donkey antibody to mouse IgG (Molecular Probes). Images are representative of four independent experiments.

Animals

The Institutional Animal Care and Use Committee at the University of Utah or at Utah State University approved the following animal protocols. *Robo4*$^{AP/AP}$ mice have been described (*15*).

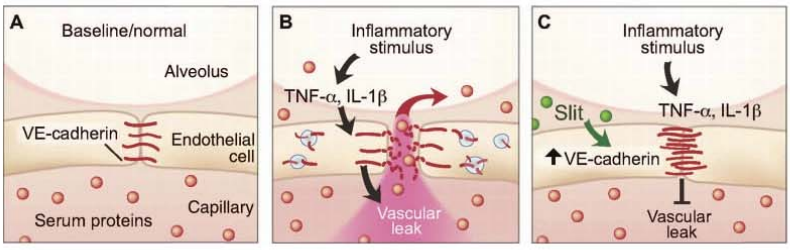

Fig. 6. Slit reduces vascular leak caused by multiple inflammatory stimuli through enhancing VE-cadherin at the cell surface. (**A**) Under normal conditions, alveolar capillaries are semipermeable. (**B**) Inflammatory stimuli cause a large release of cytokines, leading to internalization of VE-cadherin and disruption of barrier function. This results in vascular leak and accumulation of protein-rich edema fluid in the alveolar space. (**C**) Slit enhances vascular barrier function against multiple cytokines by enhancing VE-cadherin at the cell surface.

LPS-induced acute lung injury

Eight- to 12-week-old C57BL/6 mice were injected intravenously with saline alone or 3.5 μg of Slit2N or Mock in saline. Alternatively, the intravenous injection also contained 20 μg of control IgG or 20 μg of VE-cadherin–blocking antibody (clone BV13; eBiosciences). Animals were anesthetized with Avertin before surgical exposure of the trachea. LPS (10 μg; serotype 0111:B4) in 100 μl of saline or saline alone was administered intratracheally. Twenty-four hours later, the trachea was reexposed and catheterized. BALF was obtained by injection of saline (1 ml) followed by aspiration repeated three times. BALF was centrifuged at 300*g* for 5 min to recover inflammatory cells. The pellet was treated with ACK buffer for 3 min to remove red blood cells. Cells were centrifuged at 300*g* for 5 min and resuspended in 1 ml of PBS containing 1% FBS. Cell counts were then determined by hemocytometer. Neutrophil counts were determined by cell differential counts. A white blood cell differential was achieved by staining an aliquot of cells followed by microscopic examination to determine the percentage of the cell population that were neutrophils. BALF protein was assessed by protein assay (Bio-Rad). Data are presented as SEM of at least five mice per condition.

CLP sepsis model

Seven- to 11-week-old male C57BL/6 mice were given an intraperitoneal injection of 5 μg of Slit2N or Mock. One hour later, mice were anesthetized with isoflurane, and CLP was performed as described (*56*). Mice continued to receive an intraperitoneal injection of 5 μg of Slit2N or Mock once a day. Mice in the sham operation group were subjected to identical procedures, except that ligation and puncture of the cecum were omitted. Survival rate of mice subjected to CLP was determined for 6 days, with $n = 14$ for Slit2N treatment and $n = 15$ for Mock treatment for *Robo4*$^{+/+}$ mice. For *Robo4*$^{AP/AP}$ mice, $n = 13$ for Slit2N treatment and $n = 13$ for Mock treatment.

H5N1 infection

Female, 18 to 20 g, BALB/c mice (Charles River Laboratories) were anesthetized and infected with H5N1 virus (Influenza A, Duck/MN/1525/81) intranasally. Mice were given an intravenous injection of 1.56 μg of Slit2N or Mock daily for 5 days. Survival rate of mice subjected to H5N1 lung infection was determined for 21 days with 20 mice per condition.

Evans blue permeability

Vascular permeability in the lung was assessed with EBA as described (*57*). Five hours after intratracheal instillation of LPS, 4 hours after CLP, and 3 days after H5N1 infection, mice were given an intravenous injection of EBA (20 mg/kg). EBA was allowed to circulate for 1 hour, and mice were deeply anesthetized and perfused with saline plus 5 mM EDTA. Lungs were excised, weighed, and homogenized in 2 ml of PBS. Formamide (4 ml; Invitrogen) was added, and the samples were incubated overnight at 60°C to extract Evans blue dye. The samples were then centrifuged, and supernatants were analyzed by spectrophotometry at both 620 and 740 nm. CLP-treated mice were perfused, and their kidneys and spleen were removed, weighed, and placed in formamide for 48 hours at 60°C. The absorbances were normalized as described (*57*) and converted to microgram Evans blue dye per gram wet weight of lungs, kidneys, or spleen, respectively. Data are presented as SEM of at least four mice per condition.

Histology

Twenty-four hours after LPS exposure or CLP, mice were killed by CO_2 asphyxiation. Chest cavities were opened, and lungs were inflated with $ZnSO_4$-buffered 10% formalin. Formalin-fixed tissues were processed routinely, embedded in paraffin, sectioned at 6 μm, and stained with hematoxylin and eosin (H&E). Histologic quantification was modified from methods described (*58*). For H5N1 samples, 6 days after infection, the right lobes of the lungs from two animals were harvested and fixed in 10% neutral-buffered formalin. Formalin-fixed tissues were processed routinely, embedded in paraffin, sectioned at 5 μm, stained with H&E, and evaluated for microscopic lesions by a board-certified veterinary pathologist.

Lung immunofluorescence

Adult *Robo4*$^{+/AP}$ mice were killed by CO_2 asphyxiation. Chest cavities were opened, and lungs were inflated with optimum cutting temperature (OCT) embedding compound and frozen quickly in OCT on dry ice. Lung sections were stained for alkaline phosphatase activity, denoting areas of Robo4 expression as described (*15*). Sections were then stained with primary antibodies against Slit2 (E-20; Santa Cruz Biotechnology) or CD31 (BD Pharmingen) followed by fluorescent secondary antibody staining.

Cytokine or chemokine array

Six hours after CLP, mice were heavily anesthetized. Whole blood was drawn into acid-citrate-dextrose solution (ACD) (~1:9 volume) from the carotid artery. Plasma was isolated by centrifugation of blood at 4000*g* for 10 min. Plasma was analyzed by Quansys Biosciences to quantify cytokine and chemokine levels. Data are presented as mean ± SEM of six mice per condition. For H5N1 samples, 6 days after infection, clarified mouse lung homogenates were prepared and inflammatory cytokine and chemokine profiles were determined with mouse cytokine and chemokine arrays (Quansys Biosciences). Data are presented as mean ± SEM of three groups of pooled mice.

Lung virus titer determination

These assays were performed as described (*59*).

Lung development

Embryos were dissected, fixed, and rehydrated as described (*60*). Lungs were serially immunostained with primary antibody to platelet endothelial cell adhesion molecule (clone MEC 13.3; BD Pharmingen) and primary antibody to E-cadherin (clone ECCD-2; Zymed) with a variation of the described method (*60*).

Neutrophil migration

HL-60 cells were grown under standard conditions with RPMI 1640 supplemented with 10% FBS and 1% penicillin–streptomycin. Cells induced with 1.2% DMSO were obtained by seeding HL-60 cells at 3×10^6 per milliliter in growth media and culturing for 4 to 6 days (*61*). Human PMNs were isolated from healthy adult donor whole blood with ACD using techniques previously described (*62*). The leukocyte chemoattractant *N*-formyl-Met-Leu-Phe (*f*MLP) (10 μM), along with Slit2 or Mock, was placed in the lower wells of a 48-well chemotaxis chamber (Neuroprobe). A fibronectin-coated (overnight at 4°C) polycarbonate membrane (5 μm; Neuroprobe) was placed between the chemoattractant and the cells. HL-60 cells induced with DMSO or hPMNs (50 μl, 50,000 cells) were added to the upper wells. After incubating at 37°C for 2 hours, cells on the top surface of the filter were removed and cells that had migrated through the filter onto the undersurface were fixed and stained using Diff-Quik stain set (Dade Behring). Migrated cells in five

high-power fields were counted and migration was expressed as the percent of cells migrated relative to cells migrated toward *f*MLP in the absence of Slit2 or Mock. Data are presented as SEM of at least three independent experiments.

Quantitative polymerase chain reaction

For hPMN studies, RNA was isolated using Trizol (Invitrogen) and quantitative polymerase chain reaction was performed with TaqMan assays (Applied Biosystems) for human *GAPDH* and *ROBO1* to *ROBO4*.

Endothelial cell migration

Equimolar huRobo1 siRNA (Hs_Robo1_11_HP; Qiagen), huRobo4 siRNA (Hs_Robo4_1_HP), or AllStars Negative Control siRNA transfection complexes were formed according to standard protocol and added to human umbilical vein endothelial cells (Lonza). Companion dishes were prepared to assess knockdown of gene expression. Forty-eight hours later, cells were serum-starved, and 30,000 cells were seeded per fibronectin-coated 6.5-mm Transwell filters with an 8-μm pore size (Costar). Cells were allowed to migrate to 2 nM VEGF in the presence of 10 nM Slit2N or Mock for 20 hours. Filters were removed, migrated cells were counterstained, and eight high-power fields per filter were counted. Relative migration over unstimulated was determined, and data are presented as mean ± SEM of at least three independent experiments performed in at least triplicate.

Statistical analysis

The Student's *t* test, log rank test, or analysis of variance with post hoc tests, where appropriate, was used to assess statistical significance. A P value of <0.05 was considered statistically significant.

SUPPLEMENTARY MATERIAL

www.sciencetranslationalmedicine.org/cgi/content/full/2/23/23ra19/DC1
Fig. S1. Slit2N stabilizes VE-cadherin at the cell surface.
Fig. S2. Slit2N inhibits LPS-induced cell infiltrates in a dose-dependent manner.
Fig. S3. Slit does not reduce migration of primary human PMNs.
Fig. S4. Slit2 protein is expressed throughout the lung in close proximity to the endothelium.
Fig. S5. Significant lung injury is absent during CLP.
Fig. S6. Loss of *Robo4* does not significantly change cytokine receptor expression in vivo.
Fig. S7. Loss of Robo4 does not affect patterning of the vascular endothelium in the early developing lung.
Fig. S8. Loss of Robo4 does not affect patterning of the vascular endothelium in the developing lung.
Fig. S9. Robo1 and Robo4 are necessary for Slit2N-mediated inhibition of VEGF-induced HUVEC migration.

REFERENCES AND NOTES

1. M. L. Perdue, D. E. Swayne, Public health risk from avian influenza viruses. *Avian Dis.* **49**, 317–327 (2005).
2. P. Bossi, D. Garin, A. Guihot, F. Gay, J. M. Crance, T. Debord, B. Autran, F. Bricaire, Bioterrorism: Management of major biological agents. *Cell. Mol. Life Sci.* **63**, 2196–2212 (2006).
3. J. C. De Jong, G. F. Rimmelzwaan, R. A. Fouchier, A. D. Osterhaus, Influenza virus: A master of metamorphosis. *J. Infect.* **40**, 218–228 (2000).
4. S. S. Morse, R. L. Garwin, P. J. Olsiewski, Public health. Next flu pandemic: What to do until the vaccine arrives? *Science* **314**, 929 (2006).
5. Y. C. Hsieh, T. Z. Wu, D. P. Liu, P. L. Shao, L. Y. Chang, C. Y. Lu, C. Y. Lee, F. Y. Huang, L. M. Huang, Influenza pandemics: Past, present and future. *J. Formos. Med. Assoc.* **105**, 1–6 (2006).
6. C. J. Hackett, Innate immune activation as a broad-spectrum biodefense strategy: Prospects and research challenges. *J. Allergy Clin. Immunol.* **112**, 686–694 (2003).
7. C. Nathan, Points of control in inflammation. *Nature* **420**, 846–852 (2002).
8. W. C. Aird, The role of the endothelium in severe sepsis and multiple organ dysfunction syndrome. *Blood* **101**, 3765–3777 (2003).
9. D. M. Morens, A. S. Fauci, Dengue and hemorrhagic fever: A potential threat to public health in the United States. *JAMA* **299**, 214–216 (2008).
10. L. B. Ware, M. A. Matthay, The acute respiratory distress syndrome. *N. Engl. J. Med.* **342**, 1334–1349 (2000).
11. E. Abraham, P. F. Laterre, J. Garbino, S. Pingleton, T. Butler, T. Dugernier, B. Margolis, K. Kudsk, W. Zimmerli, P. Anderson, M. Reynaert, D. Lew, W. Lesslauer, S. Passe, P. Cooper, A. Burdeska, M. Modi, A. Leighton, M. Salgo, P. Van der Auwera; Lenercept Study Group, Lenercept (p55 tumor necrosis factor receptor fusion protein) in severe sepsis and early septic shock: A randomized, double-blind, placebo-controlled, multicenter phase III trial with 1,342 patients. *Crit. Care Med.* **29**, 503–510 (2001).
12. N. F. Crum, E. R. Lederman, M. R. Wallace, Infections associated with tumor necrosis factor-α antagonists. *Medicine* **84**, 291–302 (2005).
13. L. Cronin, D. J. Cook, J. Carlet, D. K. Heyland, D. King, M. A. Lansang, C. J. Fisher Jr., Corticosteroid treatment for sepsis: A critical appraisal and meta-analysis of the literature. *Crit. Care Med.* **23**, 1430–1439 (1995).
14. M. B. Atkins, M. T. Lotze, J. P. Dutcher, R. I. Fisher, G. Weiss, K. Margolin, J. Abrams, M. Sznol, D. Parkinson, M. Hawkins, C. Paradise, L. Kunkel, S. A. Rosenberg, High-dose recombinant interleukin 2 therapy for patients with metastatic melanoma: Analysis of 270 patients treated between 1985 and 1993. *J. Clin. Oncol.* **17**, 2105–2116 (1999).
15. C. A. Jones, N. R. London, H. Chen, K. W. Park, D. Sauvaget, R. A. Stockton, J. D. Wythe, W. Suh, F. Larrieu-Lahargue, Y. S. Mukouyama, P. Lindblom, P. Seth, A. Frias, N. Nishiya, M. H. Ginsberg, H. Gerhardt, K. Zhang, D. Y. Li, Robo4 stabilizes the vascular network by inhibiting pathologic angiogenesis and endothelial hyperpermeability. *Nat. Med.* **14**, 448–453 (2008).
16. C. A. Jones, N. Nishiya, N. R. London, W. Zhu, L. K. Sorensen, A. C. Chan, C. J. Lim, H. Chen, Q. Zhang, P. G. Schultz, A. M. Hayallah, K. R. Thomas, M. Famulok, K. Zhang, M. H. Ginsberg, D. Y. Li, Slit2–Robo4 signalling promotes vascular stability by blocking Arf6 activity. *Nat. Cell Biol.* **11**, 1325–1331 (2009).
17. L. Huminiecki, M. Gorn, S. Suchting, R. Poulsom, R. Bicknell, Magic roundabout is a new member of the roundabout receptor family that is endothelial specific and expressed at sites of active angiogenesis. *Genomics* **79**, 547–552 (2002).
18. K. W. Park, C. M. Morrison, L. K. Sorensen, C. A. Jones, Y. Rao, C. B. Chien, J. Y. Wu, L. D. Urness, D. Y. Li, Robo4 is a vascular-specific receptor that inhibits endothelial migration. *Dev. Biol.* **261**, 251–267 (2003).
19. C. A. Dinarello, Proinflammatory and anti-inflammatory cytokines as mediators in the pathogenesis of septic shock. *Chest* **112**, 321S–329S (1997).
20. A. Chédotal, Slits and their receptors. *Adv. Exp. Med. Biol.* **621**, 65–80 (2007).
21. E. Dejana, F. Orsenigo, M. G. Lampugnani, The role of adherens junctions and VE-cadherin in the control of vascular permeability. *J. Cell Sci.* **121**, 2115–2122 (2008).
22. D. Vestweber, VE-cadherin: The major endothelial adhesion molecule controlling cellular junctions and blood vessel formation. *Arterioscler. Thromb. Vasc. Biol.* **28**, 223–232 (2008).
23. M. D. Potter, S. Barbero, D. A. Cheresh, Tyrosine phosphorylation of VE-cadherin prevents binding of p120- and β-catenin and maintains the cellular mesenchymal state. *J. Biol. Chem.* **280**, 31906–31912 (2005).
24. K. Xiao, J. Garner, K. M. Buckley, P. A. Vincent, C. M. Chiasson, E. Dejana, V. Faundez, A. P. Kowalczyk, p120-catenin regulates clathrin-dependent endocytosis of VE-cadherin. *Mol. Biol. Cell* **16**, 5141–5151 (2005).
25. A. Gampel, L. Moss, M. C. Jones, V. Brunton, J. C. Norman, H. Mellor, VEGF regulates the mobilization of VEGFR2/KDR from an intracellular endothelial storage compartment. *Blood* **108**, 2624–2631 (2006).
26. G. Matute-Bello, C. W. Frevert, T. R. Martin, Animal models of acute lung injury. *Am. J. Physiol. Lung Cell. Mol. Physiol.* **295**, L379–L399 (2008).
27. M. Corada, F. Liao, M. Lindgren, M. G. Lampugnani, F. Breviario, R. Frank, W. A. Muller, D. J. Hicklin, P. Bohlen, E. Dejana, Monoclonal antibodies directed to different regions of vascular endothelial cadherin extracellular domain affect adhesion and clustering of the protein and modulate endothelial permeability. *Blood* **97**, 1679–1684 (2001).
28. W. J. Hubbard, M. Choudhry, M. G. Schwacha, J. D. Kerby, L. W. Rue III, K. I. Bland, I. H. Chaudry, Cecal ligation and puncture. *Shock* **24**, 52–57 (2005).
29. M. D. de Jong, C. P. Simmons, T. T. Thanh, V. M. Hien, G. J. Smith, T. N. Chau, D. M. Hoang, N. V. Chau, T. H. Khanh, V. C. Dong, P. T. Qui, B. V. Cam, Q. Ha do, Y. Guan, J. S. Peiris, N. T. Chinh, T. T. Hien, J. Farrar, Fatal outcome of human influenza A (H5N1) is associated with high viral load and hypercytokinemia. *Nat. Med.* **12**, 1203–1207 (2006).
30. D. Kobasa, S. M. Jones, K. Shinya, J. C. Kash, J. Copps, H. Ebihara, H. Ebihara, Y. Hatta, J. H. Kim, P. Halfmann, M. Hatta, F. Feldmann, J. B. Alimonti, L. Fernando, Y. Li, M. G. Katze, H. Feldmann, Y. Kawaoka, Aberrant innate immune response in lethal infection of macaques with the 1918 influenza virus. *Nature* **445**, 319–323 (2007).
31. Writing Committee of the Second World Health Organization Consultation on Clinical Aspects of Human Infection with Avian Influenza A (H5N1) Virus; A. N. Abdel-Ghafar, T. Chotpitayasunondh, Z. Gao, F. G. Hayden, D. H. Nguyen, M. D. de Jong, A. Naghdaliyev, J. S. Peiris, N. Shindo, S. Soeroso, T. M. Uyeki, Update on avian influenza A (H5N1) virus infection in humans. *N. Engl. J. Med.* **358**, 261–273 (2008).

32. K. A. Sepkowitz, Forever unprepared—The predictable unpredictability of pathogens. *N. Engl. J. Med.* **361**, 120–121 (2009).
33. S. P. Layne, A. S. Monto, J. K. Taubenberger, Pandemic influenza: An inconvenient mutation. *Science* **323**, 1560–1561 (2009).
34. M. Seeger, G. Tear, D. Ferres-Marco, C. S. Goodman, Mutations affecting growth cone guidance in *Drosophila*: Genes necessary for guidance toward or away from the midline. *Neuron* **10**, 409–426 (1993).
35. J. Xian, K. J. Clark, R. Fordham, R. Pannell, T. H. Rabbitts, P. H. Rabbitts, Inadequate lung development and bronchial hyperplasia in mice with a targeted deletion in the *Dutt1/Robo1* gene. *Proc. Natl. Acad. Sci. U.S.A.* **98**, 15062–15066 (2001).
36. U. Grieshammer, M. Le, A. S. Plump, F. Wang, M. Tessier-Lavigne, G. R. Martin, SLIT2-mediated ROBO2 signaling restricts kidney induction to a single site. *Dev. Cell* **6**, 709–717 (2004).
37. C. Sabatier, A. S. Plump, M. Le, K. Brose, A. Tamada, F. Murakami, E. Y. Leem, M. Tessier-Lavigne, The divergent Robo family protein Rig-1/Robo3 is a negative regulator of Slit responsiveness required for midline crossing by commissural axons. *Cell* **117**, 157–169 (2004).
38. S. T. Qureshi, R. Medzhitov, Toll-like receptors and their role in experimental models of microbial infection. *Genes Immun.* **4**, 87–94 (2003).
39. J. Y. Wu, L. Feng, H. T. Park, N. Havlioglu, L. Wen, H. Tang, K. B. Bacon, Z. Jiang, X. Zhang, Y. Rao, The neuronal repellent Slit inhibits leukocyte chemotaxis induced by chemotactic factors. *Nature* **410**, 948–952 (2001).
40. S. H. Mei, S. D. McCarter, Y. Deng, C. H. Parker, W. C. Liles, D. J. Stewart, Prevention of LPS-induced acute lung injury in mice by mesenchymal stem cells overexpressing angiopoietin 1. *PLoS Med.* **4**, e269 (2007).
41. P. Seth, Y. Lin, J. Hanai, V. Shivalingappa, M. P. Duyao, V. P. Sukhatme, Magic roundabout, a tumor endothelial marker: Expression and signaling. *Biochem. Biophys. Res. Commun.* **332**, 533–541 (2005).
42. H. Sheldon, M. Andre, J. A. Legg, P. Heal, J. M. Herbert, R. Sainson, A. S. Sharma, J. K. Kitajewski, V. L. Heath, R. Bicknell, Active involvement of Robo1 and Robo4 in filopodia formation and endothelial cell motility mediated via WASP and other actin nucleation-promoting factors. *FASEB J.* **23**, 513–522 (2009).
43. H. Hu, Cell-surface heparan sulfate is involved in the repulsive guidance activities of Slit2 protein. *Nat. Neurosci.* **4**, 695–701 (2001).
44. E. Hohenester, S. Hussain, J. A. Howitt, Interaction of the guidance molecule Slit with cellular receptors. *Biochem. Soc. Trans.* **34**, 418–421 (2006).
45. P. Steigemann, A. Molitor, S. Fellert, H. Jäckle, G. Vorbrüggen, Heparan sulfate proteoglycan syndecan promotes axonal and myotube guidance by Slit/Robo signaling. *Curr. Biol.* **14**, 225–230 (2004).
46. S. Suchting, P. Heal, K. Tahtis, L. M. Stewart, R. Bicknell, Soluble Robo4 receptor inhibits in vivo angiogenesis and endothelial cell migration. *FASEB J.* **19**, 121–123 (2005).
47. D. Vestweber, M. Winderlich, G. Cagna, A. F. Nottebaum, Cell adhesion dynamics at endothelial junctions: VE-cadherin as a major player. *Trends Cell Biol.* **19**, 8–15 (2009).
48. Y. Wallez, P. Huber, Endothelial adherens and tight junctions in vascular homeostasis, inflammation and angiogenesis. *Biochim. Biophys. Acta* **1778**, 794–809 (2008).
49. J. Gavard, J. S. Gutkind, VEGF controls endothelial-cell permeability by promoting the β-arrestin-dependent endocytosis of VE-cadherin. *Nat. Cell Biol.* **8**, 1223–1234 (2006).
50. A. M. Ferreira, C. J. McNeil, K. M. Stallaert, K. A. Rogers, M. Sandig, Interleukin-1β reduces transcellular monocyte diapedesis and compromises endothelial adherens junction integrity. *Microcirculation* **12**, 563–579 (2005).
51. D. J. Angelini, S. W. Hyun, D. N. Grigoryev, P. Garg, P. Gong, I. S. Singh, A. Passaniti, J. D. Hasday, S. E. Goldblum, TNF-α increases tyrosine phosphorylation of vascular endothelial cadherin and opens the paracellular pathway through fyn activation in human lung endothelia. *Am. J. Physiol. Lung Cell. Mol. Physiol.* **291**, L1232–L1245 (2006).
52. J. Gavard, V. Patel, J. S. Gutkind, Angiopoietin-1 prevents VEGF-induced endothelial permeability by sequestering Src through mDia. *Dev. Cell* **14**, 25–36 (2008).
53. P. Villa, G. Sartor, M. Angelini, M. Sironi, M. Conni, P. Gnocchi, A. M. Isetta, G. Grau, W. Buurman, L. J. van Tits, Pattern of cytokines and pharmacomodulation in sepsis induced by cecal ligation and puncture compared with that induced by endotoxin. *Clin. Diagn. Lab. Immunol.* **2**, 549–553 (1995).
54. N. Coltel, V. Combes, N. H. Hunt, G. E. Grau, Cerebral malaria—A neurovascular pathology with many riddles still to be solved. *Curr. Neurovasc. Res.* **1**, 91–110 (2004).
55. N. R. London, K. J. Whitehead, D.Y. Li, Endogenous endothelial cell signaling systems maintain vascular stability. *Angiogenesis* **12**, 149–158 (2009).
56. R. N. Gomes, R. T. Figueiredo, F. A. Bozza, P. Pacheco, R. T. Amâncio, A. P. Laranjeira, H. C. Castro-Faria-Neto, P. T. Bozza, M. T. Bozza, Increased susceptibility to septic and endotoxic shock in monocyte chemoattractant protein 1/cc chemokine ligand 2-deficient mice correlates with reduced interleukin 10 and enhanced macrophage migration inhibitory factor production. *Shock* **26**, 457–463 (2006).
57. J. Moitra, S. Sammani, J. G. Garcia, Re-evaluation of Evans Blue dye as a marker of albumin clearance in murine models of acute lung injury. *Transl. Res.* **150**, 253–265 (2007).
58. N. Gupta, X. Su, B. Popov, J. W. Lee, V. Serikov, M. A. Matthay, Intrapulmonary delivery of bone marrow-derived mesenchymal stem cells improves survival and attenuates endotoxin-induced acute lung injury in mice. *J. Immunol.* **179**, 1855–1863 (2007).
59. R. W. Sidwell, K. W. Bailey, M. H. Wong, D. L. Barnard, D. F. Smee, In vitro and in vivo influenza virus-inhibitory effects of viramidine. *Antiviral Res.* **68**, 10–17 (2005).
60. R. J. Metzger, O. D. Klein, G. R. Martin, M. A. Krasnow, The branching programme of mouse lung development. *Nature* **453**, 745–750 (2008).
61. S. J. Collins, F. W. Ruscetti, R. E. Gallagher, R. C. Gallo, Terminal differentiation of human promyelocytic leukemia cells induced by dimethyl sulfoxide and other polar compounds. *Proc. Natl. Acad. Sci. U.S.A.* **75**, 2458–2462 (1978).
62. G. A. Zimmerman, T. M. McIntyre, S. M. Prescott, Thrombin stimulates the adherence of neutrophils to human endothelial cells in vitro. *J. Clin. Invest.* **76**, 2235–2246 (1985).

63. Acknowledgments: We thank D. Lim for graphical assistance and K. Thomas, M. Sanguinetti, A. Welm, C. Murtaugh, S. Odelberg, and S. Stanley for critical reading of this manuscript.
Funding: National Heart, Lung, and Blood Institute (NHLBI); National Institute of Allergy and Infectious Diseases (NIAID); Rocky Mountain Regional Center of Excellence in Biodefense and Emerging Infectious Disease; Juvenile Diabetes Research Foundation; HA and Edna Benning Foundation; American Asthma Foundation; National Center for Research Resources Public Health Services research grant UL1-RR025764; and Department of Defense. D.Y.L. is a Burroughs Wellcome Foundation Clinical Scientist in Translational Research and an Established Investigator of the American Heart Association. N.R.L., M.C.P.S., and A.C.C. were supported, respectively, by the Ruth L. Kirschstein National Research Service Award, T-32 Hematology Training Grant, and training grant T32-GM007464. This work was also supported by NIAID contract NO1-AI-15435 (C.W.D. and D.L.B.); a NIH Merit Award 5R37 HL44525-20 (G.A.Z.); and the Sarnoff Cardiovascular Research Foundation Scholar Award, NIH-NHLBI (K08), and the Pulmonary Hypertension Association (D.M.G.). F.A.B. is a research scholar supported by Conselho Nacional de Desenvolvimento Cientifico e Tecnológico (CNPq, Brazil).
Author contributions: N.R.L., W.Z., and D.Y.L. were responsible for project conceptualization, experimental design, and data analysis. N.R.L., G.A.Z., and D.Y.L. were responsible for manuscript preparation. N.R.L., W.Z., and F.A.B. were responsible for performing all experiments or coordinating experimental design and work of others. M.C.P.S., D.M.G., L.K.S., L.C., Y.K., A.C.C., and S.F.P. performed necessary experiments for the manuscript or in response to reviewers. C.W.D., D.L.B., G.A.Z, and M.A.K. provided important expertise, reagents, technical personnel and advice.
Competing interests: N.R.L., W.Z., M.C.P.S., L.K.S., L.C., Y.K., S.F.P., G.A.Z., and D.Y.L. are or were previously employed by the University of Utah, which has filed intellectual property surrounding the therapeutic uses of targeting Robo4 and with the intent to license this body of intellectual property for commercialization. The University of Utah has licensed Robo4 technology to Navigen, a biotechnology company owned in part by the University of Utah Research Foundation. N.R.L. and W.Z. are paid consultants for Navigen, and D.Y.L. is a founder of and is on the Board of Directors of Navigen.

Submitted 25 November 2009
Accepted 26 February 2010
Published 17 March 2010
10.1126/scitranslmed.3000678

Citation: N. R. London, W. Zhu, F. A. Bozza, M. C. P. Smith, D. M. Greif, L. K. Sorensen, L. Chen, Y. Kaminoh, A. C. Chan, S. F. Passi, C. W. Day, D. L. Barnard, G. A. Zimmerman, M. A. Krasnow, D. Y. Li, Targeting Robo4-dependent slit signaling to survive the cytokine storm in sepsis and influenza. *Sci. Transl. Med.* **2**, 23ra19 (2010).

www.sciencetranslationalmedicine.org/cgi/content/full/2/23/23ra19/DC1

Supplementary Materials for

Targeting Robo4-Dependent Slit Signaling to Survive the Cytokine Storm in Sepsis and Influenza

Nyall R. London, Weiquan Zhu, Fernando A. Bozza, Matthew C. P. Smith, Daniel M. Greif, Lise K. Sorensen, Luming Chen, Yuuki Kaminoh, Aubrey C. Chan, Samuel F. Passi, Craig W. Day, Dale L. Barnard, Guy A. Zimmerman, Mark A. Krasnow, Dean Y. Li*

*To whom correspondence should be addressed. E-mail: dean.li@u2m2.utah.edu

Published 17 March 2010, *Sci. Transl. Med.* **2**, 23ra19 (2010)
DOI: 10.1126/scitranslmed.3000678

This PDF file includes:

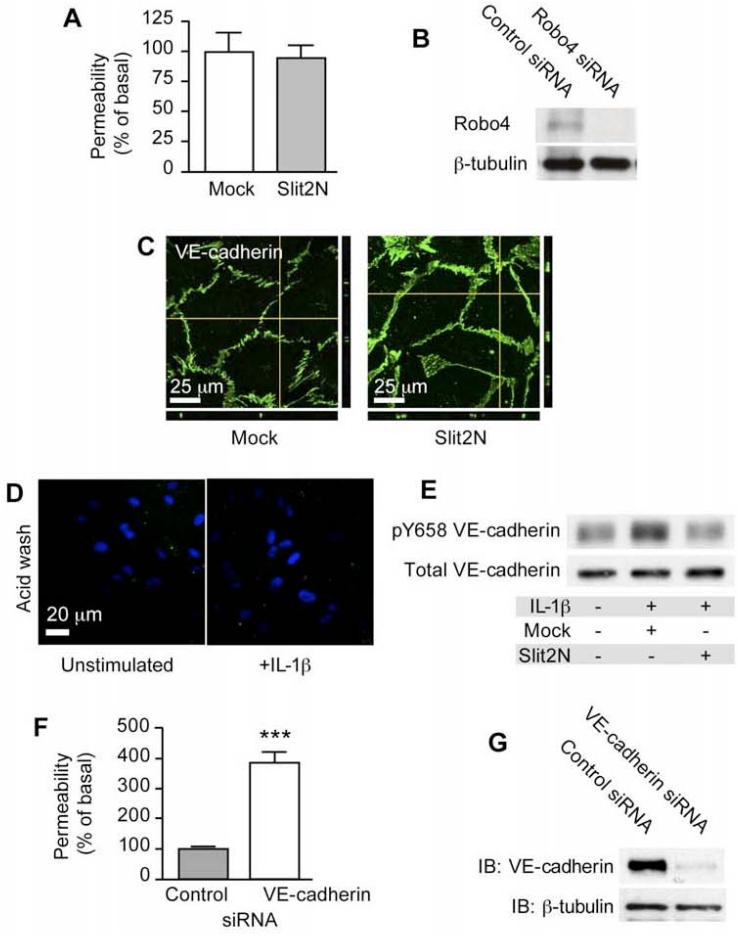

Fig. S1. Slit2N stabilizes VE-cadherin at the cell surface. (**A**) HMVEC-lung were treated with Mock or Slit2N and basal permeability was assessed. (**B**) Robo4 or control siRNA knockdown HMVEC-lung were assessed for Robo4 expression by immunoblot. (**C**) Confocal images of the Z-axis are shown below and to the side as indicated by yellow lines. Enhanced junctional thickness is observed in Slit2N treated cells. (**D**) In the absence of primaquine, detection of IL-1β-induced VE-cadherin internalization is compromised. **(E)** HMVEC-lung were exposed to IL-1β in the presence or absence of Mock or Slit2N followed by immunoblot using a phosphorylation specific antibody against VE-cadherin Y658. (**F**) HMVEC-lung were subjected to control or VE-cadherin siRNA knockdown and barrier function assessed by *in vitro* permeability. (**G**) Western blot analysis confirmed knockdown of VE-cadherin expression. ***P<0.005.

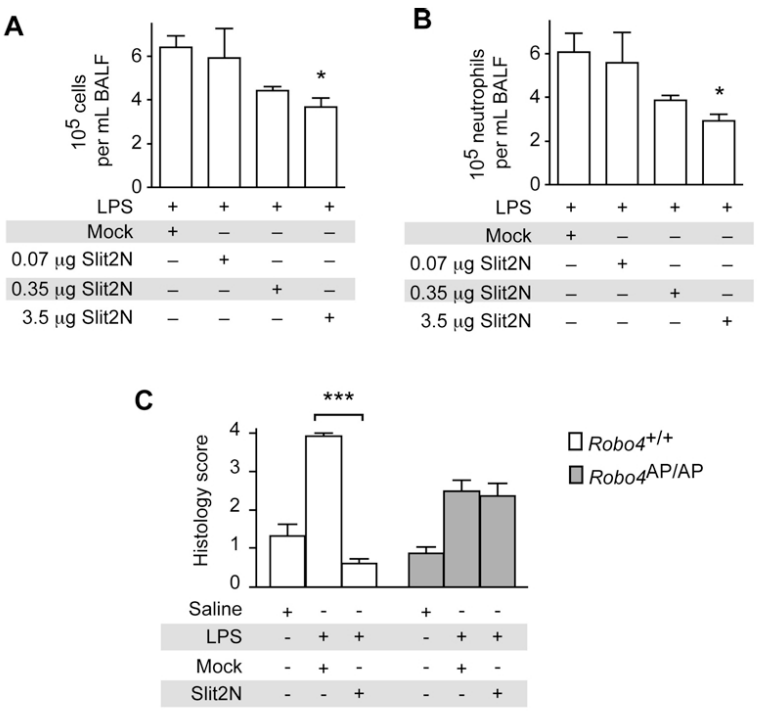

Fig. S2. Slit2N inhibits LPS-induced cell infiltrates in a dose-dependent manner. (**A-B**) Mice were subjected to LPS-induced ALI in the presence of increasing levels of Slit2N. Cell infiltrate and neutrophil counts are shown. N≥4, * P<0.05. (**C**) *Robo4*$^{+/+}$ and *Robo4*$^{AP/AP}$ mice were subjected to LPS-induced ALI in the presence of Mock or Slit2N. Lung sections from these mice were stained for H&E and quantitative histology to assess the degree of lung injury was performed by blinded investigators. N=3, *** P<0.005.

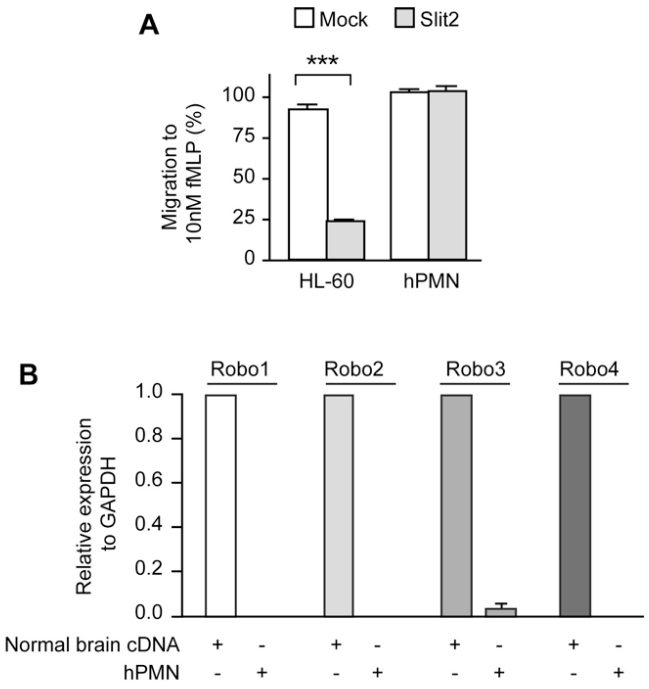

Fig. S3. Slit does not reduce migration of primary human PMNs. (**A**) Cells were subjected to migration to the leukocyte chemoattractant fMLP in the presence of Mock or Slit2. (**B**) RNA was isolated from hPMNs and subjected to quantitative PCR. Brain cDNA was used as a positive control. N=3, *** P<0.005, error bars represent s.e.m.

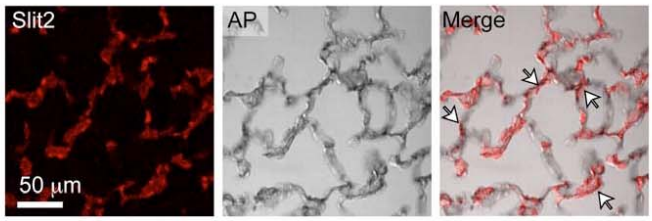

Fig. S4. Slit2 protein is expressed throughout the lung in close proximity to the endothelium. Slit2 (red) co-localizes with Robo4 alkaline phosphatase (AP) expression (black) indicated by white arrows.

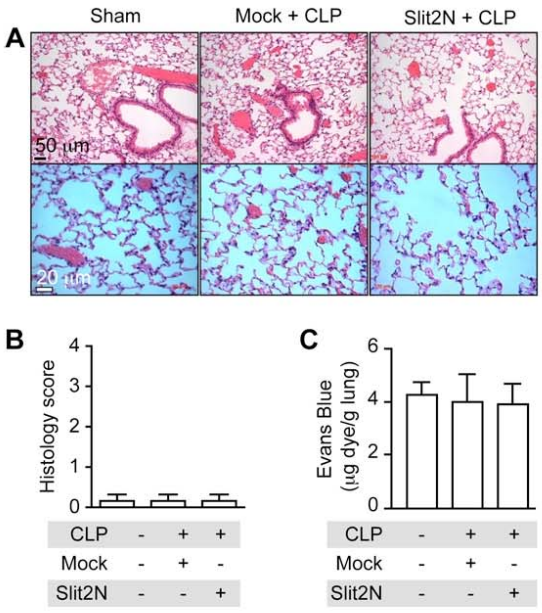

Fig. S5. Significant lung injury is absent during CLP. (**A-C**) Mice were subjected to CLP and treated with Mock or Slit2N. Lung sections were stained with H&E (**A**) and quantitative histology to assess the degree of lung injury performed (**B**) N=3. (**C**) Permeability in the lungs of mice was assessed using Evans Blue Albumin. N=5.

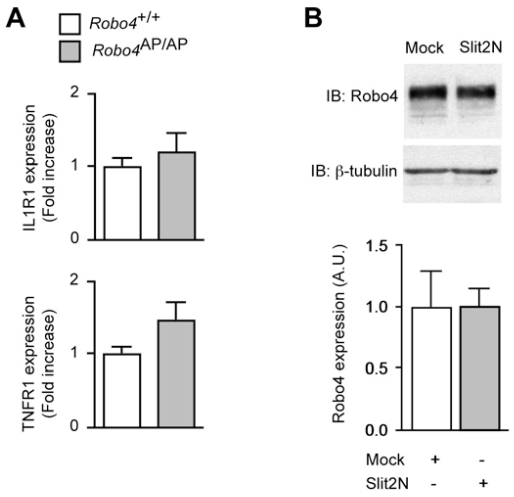

Fig. S6. Loss of *Robo4* does not significantly change cytokine receptor expression *in vivo.* (**A**) RNA from *Robo4*$^{+/+}$ or *Robo4*$^{AP/AP}$ mice was isolated and subjected to qPCR for IL1R1 or TNFR1. N=9 per genotype. (**B**) HMVEC-lung were exposed to Mock or Slit2N treatment and subjected to Western Blot analysis. Densitometric analysis is presented below representative blots.

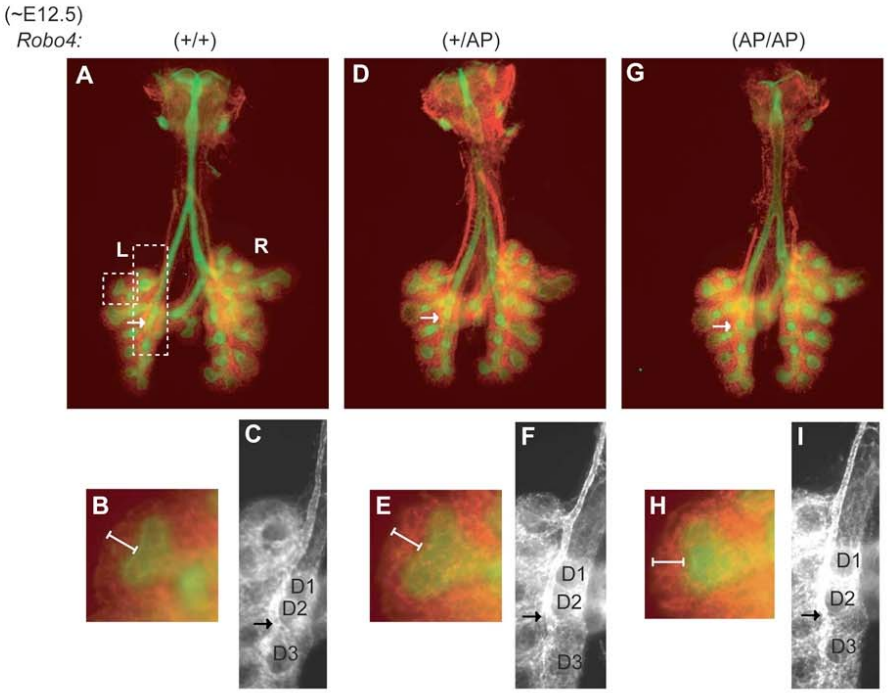

Fig. S7. Loss of Robo4 does not affect patterning of the vascular endothelium in the early developing lung. **A-C, D-F** and **G-I** show $Robo4^{+/+}$, $Robo4^{+/AP}$ and $Robo4^{AP/AP}$ ~E12.5 lungs, respectively, stained for epithelium (E-cadherin, green) and vasculature (CD31, red). Arrows indicate the distal extent of the left pulmonary artery EC tube. **B**, **E**, and **H** are magnified views of the distal branches of the first left lateral secondary airway branch with the white crossbar denoting the thickness of the CD31+ plexus compartment extending linearly outward from the vertex of the distal branches. **C, F**, and **I** show magnified views of the distal left pulmonary artery EC tube regions stained with an antibody directed against CD31. The locations of the first, second and third left dorsal secondary airway buds are denoted by D1, D2 and D3.

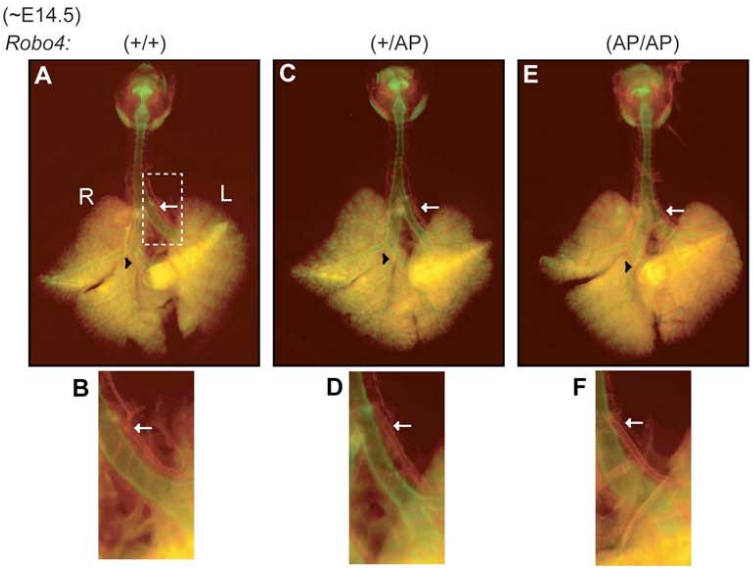

Fig. S8. Loss of Robo4 does not affect patterning of the vascular endothelium in the developing lung. **A-B, C-D** and **E-F** show *Robo4*$^{+/+}$, *Robo4*$^{+/AP}$ and *Robo4*$^{AP/AP}$ ~E14.5 lungs, respectively, stained for lung epithelium (E-cadherin, green) and vascular development (CD31, red). Arrows denote the left pulmonary artery located lateral to the left primary bronchus. The black arrowheads in **A, C,** and **E** mark the branch of the right pulmonary artery supplying the right accessory lobe and located posterior to the right secondary airway branch to the accessory lobe.

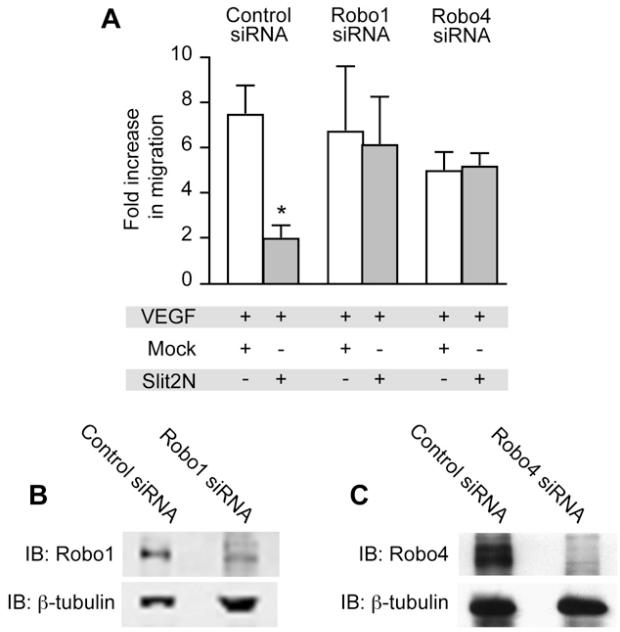

Fig. S9. Robo1 and Robo4 are necessary for Slit2N-mediated inhibition of VEGF-induced HUVEC migration. (**A**) Human umbilical vein endothelial cells were subjected to control, Robo1, or Robo4 siRNA and migrated to VEGF in the presence of Mock or Slit2N. N=3, * $P<0.05$. Western blot analysis confirmed knockdown of Robo1 (**B**) or Robo4 (**C**) expression.

CHAPTER 3

SEMAPHORIN EFFECTS ON PLATELET FUNCTION ARE CAUSED BY DETERGENT CONTAMINATION

Summary

The following chapter pertains to work not intended for publication. Within this chapter I describe the effects of the neural guidance cue, Semaphorin 3E (Sema3E), and its ability to reversibly inhibit platelet function both *in vitro* and *in vivo*. This chapter also details a contamination discovered within the commercially produced Sema3E and the detailed process of determining that the original effects attributed to Sema3E were in fact caused by the contamination, thus ending the project prepublication.

Introduction

Platelets play a crucial role normal hemostasis in response to injury, but are also instrumental in forming thrombi that precipitate both myocardial infarctions and ischemic cerebrovascular accidents[1]. Once thought of as simply anucleate particles that plug holes in the vasculature, platelets are now known to undergo intricate cellular processes, including extensive cytoskeletal rearrangement necessary for the

formation of stable thrombi that contribute to endothelial healing and wound repair[2]. In response to vascular injury, platelets interact with collagen, von Willebrand factor (vWF) and other components of the subendothelial matrix via specific receptor-ligand interactions[3]. Once the cells adhere, platelet $\alpha_{IIb}\beta_3$ integrins undergo a conformational change that allows stable adhesion to the extracellular matrix and further activates the platelets. The activated platelets generate thromboxane A_2 (TxA_2) and release an array of factors including fibrinogen and adenosine diphosphate (ADP) that promote activation of surrounding platelets[3]. Activated platelets in the area of injury then begin to form aggregates by binding to the platelets initially activated by the exposed subendothelial matrix. These aggregates are formed through cross-linking of fibrinogen molecules between platelets, leading to formation of a hemostatic plug or thrombus[3,4].

The cytoskeletal changes required for this sequence of events in platelet activation are reminiscent of those involved in axon guidance and endothelial cell migration during development. Similarities among these cells beg the question as to whether cytoskeletal rearrangements of platelets are regulated by the same mechanisms that direct axon guidance and vascular development. The idea that molecules once thought to be primarily involved in directing axon growth are also involved in the development and function of other tissues is a rapidly emerging field[5-8]. Each of the four classes of molecules originally thought to function primarily in axon guidance (slits, netrins, semaphorins and ephrins) have been implicated in vascular and cardiac development and more recently in immune system function[6,9].

Semaphorins are one of the largest families of conserved guidance cues and participate in a plethora of biological processes from neural and cardiovascular development to immune cell function[5,9-11]. Semaphorins are expressed in many tissues, including the vasculature[11], and are characterized by the presence of a conserved ~500 amino-acid semaphorin (Sema) domain[12]. They are present in both membrane bound and secreted forms and signal primarily through the plexin family of receptors. With the exception of Sema3E and Sema4A, which bind to PlexinD1, semaphorins bind to plexins with the help of a neuropilin (NRP1 or NRP2) coreceptor[12-14]. Plexin receptors also possess a sema domain, and plexin-semaphorin binding occurs through binding of the sema domain on semaphorins to the sema domain on their plexin receptors[12].

In addition to the sema domain, plexins contain a segmented GTPase-activating protein (GAP) domain and a GTPase binding domain[12]. Upon binding to its specific semaphorin ligand, plexins activate their intrinsic GAP activity, which inactivates the small GTPase R-Ras. Active R-Ras is necessary to maintain integrins in an active form; inactivating R-Ras leads to detachment of integrins from their ECM substrates[15,16]. At the same time, plexins activate the small GTPase RhoA, which promotes increased actomyosin contractility[12,17]. It has also been suggested that upon activation, plexins sequester active Rac at the membrane, preventing PAK1 phosphorylation and subsequent actin polymerization[18,19]. In neurons, the combination of these signaling events promotes the collapse of the growth cones (Figure 3.1)[12].

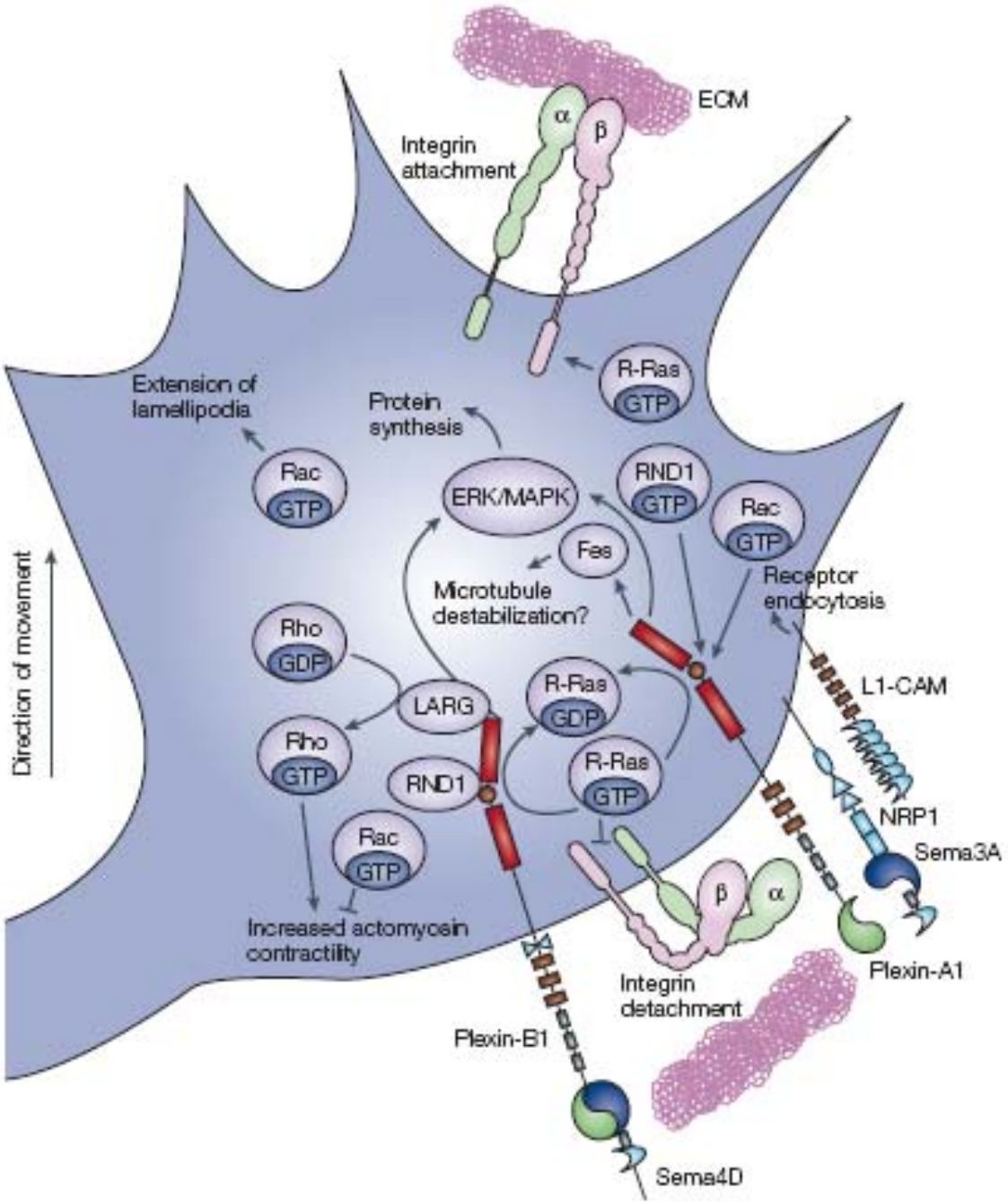

Figure 3.1. Semaphorin signaling through plexins initiates a number of signaling pathways. Actomyosin contractility is increased through RhoA activation by leukemia-associated Rho-GEF (LARG) and by blocking Rac signaling through p21-activated kinase (PAK; not shown). Stimulation of the plexin GAP (GTPase-activating protein) activity decreases active R-Ras, which limits integrin-mediated attachment. Modified from Kruger et al., Nature Reviews, 2005.

The importance of cytoskeletal modifications in platelet activation and the mechanisms involved in neural guidance cue function suggest that neural guidance cues may be very important in regulation of platelet activation.

Results

Platelet activation and thrombus formation are highly dependent on a series of cytoskeletal changes within the platelet. In order to assess the possibility that these processes might be regulated by neural guidance cues, we performed a screen to determine the effect of neural guidance cues on platelet spreading. We used ligands from three of the four major guidance cue families (slits, netrins, and semaphorins) and assessed their effect on platelet spreading on fibrinogen (Figure 3.2a-f). It has previously been reported that Sema3A can inhibit platelet function[20]; our data suggests that multiple members of the semaphorin family but not the slit or netrin families can inhibit platelet spreading (Figure 3.2). Interestingly, our screen found that Sema3E was able to inhibit platelet spreading and was at least an order of magnitude more potent than the previously published Sema3A. Furthermore, if Sema3E is washed from platelets, they recovered the ability to spread similar to untreated platelets. For these reasons, we chose to focus our efforts on exploring the role of Sema3E in platelet activation.

Unlike many of the other semaphorins that require a neuropilin co-receptor, Sema3E signals directly through PlexinD1[14]. We found that platelets contain mRNA encoding PlexinD1 and that PlexinD1 is highly expressed on the plasma membranes of human platelets (Figure 3.3a,b). In order to determine if PlexinD1 was sufficient

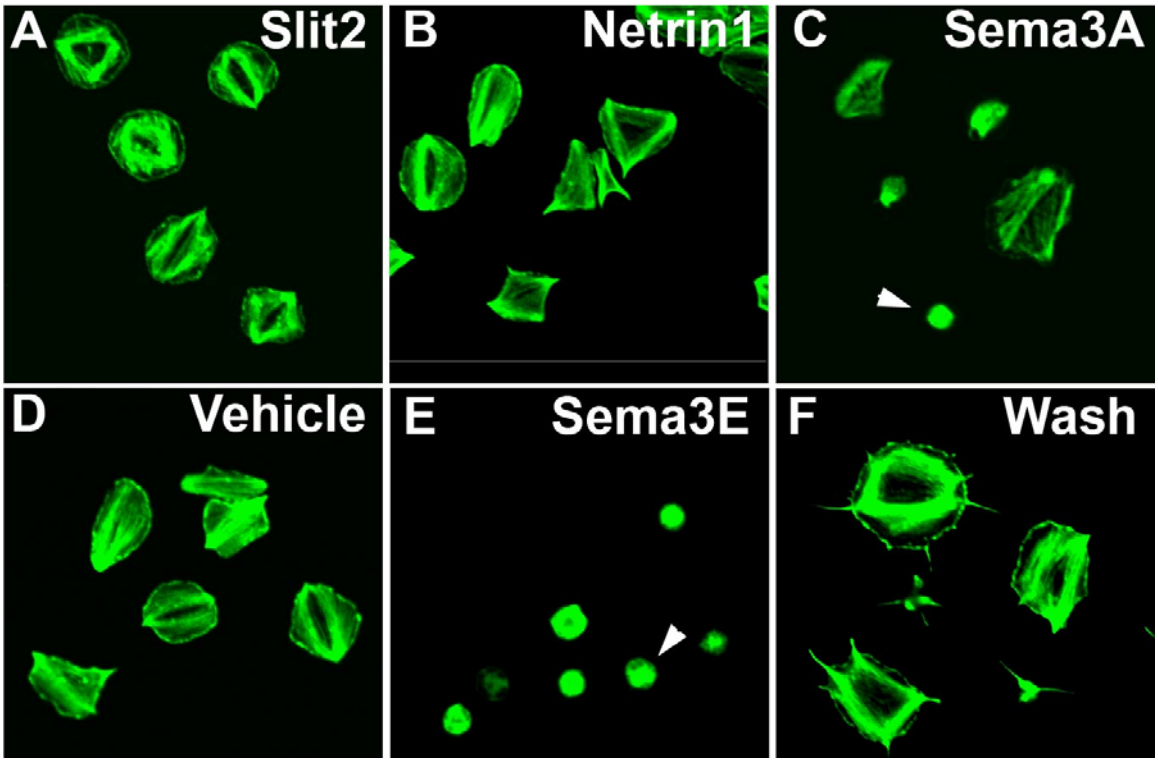

Figure 3.2. Semaphorin family members inhibit platelet spreading. Human platelets were pretreated with Slit2 (A), Netrin1 (B), Semaphorin3A (C), vehicle (D), or Semaphorin3E (E) for 10 minutes and subsequently adhered to immobilized fibrinogen in the presence of thrombin (0.05 U/ml). After 30 minutes the cells were stained with alexa 488 phalloidin. In panel F the platelets were treated similarly with the exception that after 10 minutes of adherence in the presence of Sema3E, the culture media was replaced with semaphorin 3E-deficient media and then the cells were treated with thrombin. Arrowheads indicate unspread platelets. This figure is representative of 4 independent experiments. Staining=Phalloidin

for Sema3E induced collapse, we utilized a heterologous system that does not express PlexinD1 at baseline. CHO-PLA1 cells have been stably transfected with both integrin alpha chain 2b (ITGA2B) and integrin beta 3 (ITGB3), the genes that comprise the platelet specific integrin $\alpha_{IIb}\beta_3$[21]. When plated on immobilized fibrinogen, CHO-PLA1 cells spread similar to platelets and are commonly used to study platelet integrin function. We transfected CHO-PLA1 cells with a plasmid containing hPLXND1 or a control plasmid and treated these cells with Sema3E. CHO-PLA1 cells that expressed PlexinD1 as assayed by immunofluorescent cell staining collapsed in the presence of Sema3E, but CHO-PLA1 cells that were negative for PlexinD1 remained spread (Figure 3.3c,d). These data suggest that PlexinD1 is sufficient for the collapsing activity of Sema3E seen in platelets. The expression of both Sema3E and Sema4A – a membrane bound semaphorin that also signals exclusively through PlexinD1 – has been reported on the vascular endothelium, strongly suggesting that endogenous PlexinD1 signaling occurs *in vivo*[11]. We have confirmed these expression results using reverse transcriptase-PCR on primary human umbilical vein endothelial cells (HUVEC, data not shown).

In order to determine where in the platelet activation sequence Sema3E acts, we also measured the effects of Sema3E on platelet adhesion and granule secretion. Sema3E inhibited platelet adhesion to immobilized fibrinogen, collagen, and laminin, though the effects were most prominent on fibrinogen (Figure 3.4a and data not shown). Two surrogate markers for granule secretion were assayed. First we measured the production of soluble RANTES in response to thrombin; RANTES is a T-Cell chemotactic cytokine stored in the α granules of platelets that are

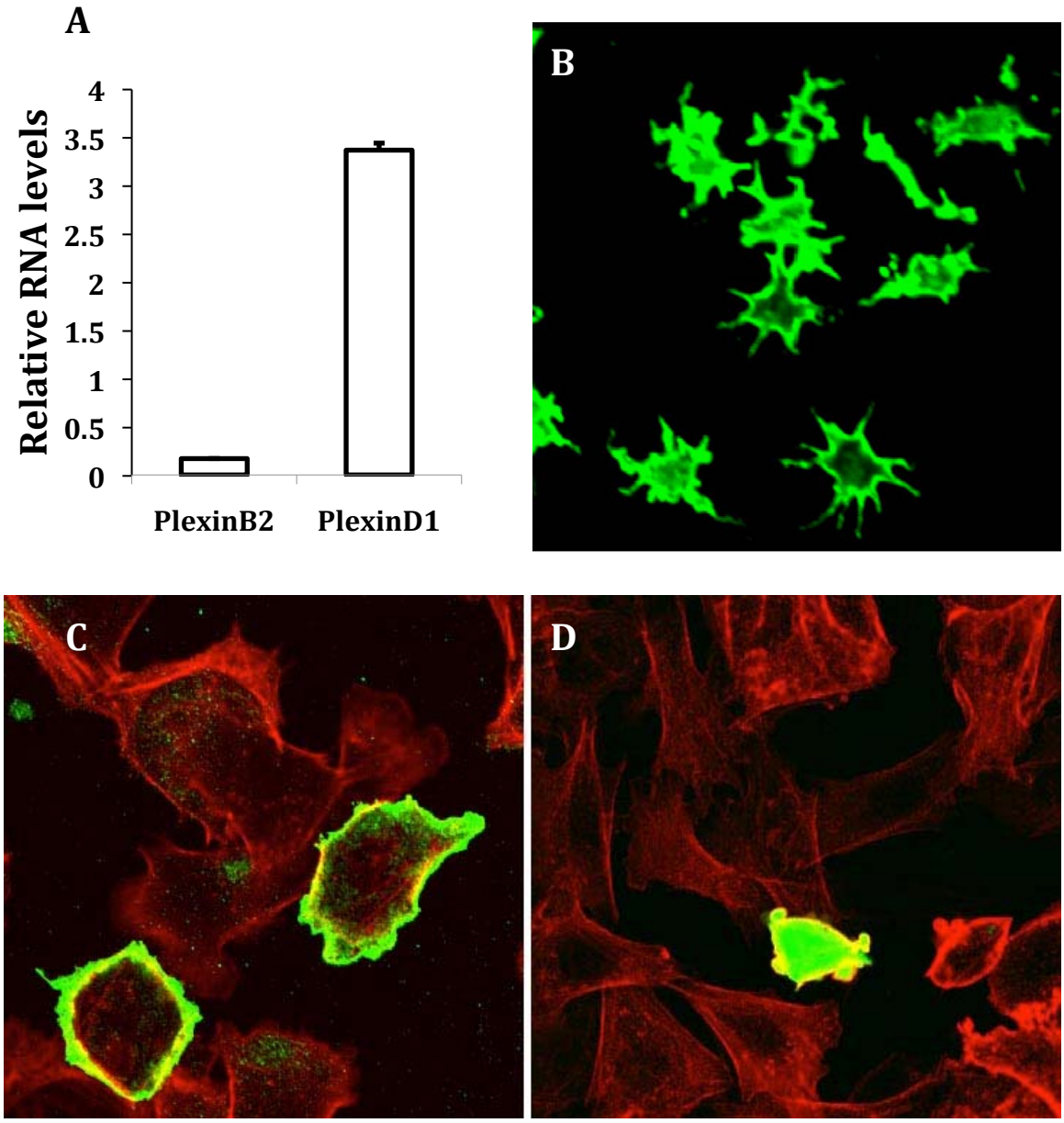

Figure 3.3. PlexinD1 is expressed in platelets and is sufficient to mediate Sema3E's collapsing effects on a heterologous cell line. PlexinD1 mRNA transcription relative to GAPDH, PlexinB2 has lower expression by comparison (A). Plexin is expressed at the surface of platelets (B). CHO cells stably expressing $\alpha_{IIb}\beta_3$ integrin were transiently transfected with PlexinD1 (Green) and plated on immobilized fibrinogen in the absence (C) or presence (D) of Sema3E. Staining=Phalloidin anti-PlexinD1

released upon platelet activation. Sema3E inhibited the secretion of RANTES in a dose-dependent manner (Figure 3.4b). We also assayed granule release of p-selectin from the platelet granules to the platelet membrane using flow cytometry for membrane bound p-selectin (CD62P). We found that Sema3E inhibited surface expression of CD62P in response to a number of agonists including Thrombin, ADP, Convulxin and collagen (Figure 3.4c and data not shown). In addition to preventing platelet adhesion, spreading, and granule secretion, Sema3E also inhibited thrombin-induced platelet aggregation (Figure 3.4d), suggesting that Sema3E is inhibiting a process central to each of these steps in platelet activation.

Given that Sema3E inhibits each step of platelet activation, many of which rely on the activation of the platelet specific $\alpha_{IIb}\beta_3$ integrin, and semaphorins are known to inhibit integrin function in neurons and endothelial cells[12,13], we examined the effect of Sema3E on activation of platelet $\alpha_{IIb}\beta_3$ integrin. Thrombin causes platelet $\alpha_{IIb}\beta_3$ integrin to undergo a conformational change from an inactive form to the active form that binds fibrinogen. Sema3E treatment of platelets inhibits the activation of $\alpha_{IIb}\beta_3$ integrin by thrombin, but more impressively, if Sema3E is applied after thrombin activation, Sema3E reverses the activation of $\alpha_{IIb}\beta_3$ in platelets, thus reversing the activation of the platelet (Figure 3.5a).

Rap1b is a small GTPase in the Ras family that is highly expressed in platelets and is necessary for maintaining $\alpha_{IIb}\beta_3$ integrin in an active conformation[22,23]. There have been no studies linking PlexinD1 to Rap1, but PlexinD1 has been shown to act as a GTPase activating protein (GAP) towards another member of the Ras family, R-Ras. For this reason, we hypothesized that

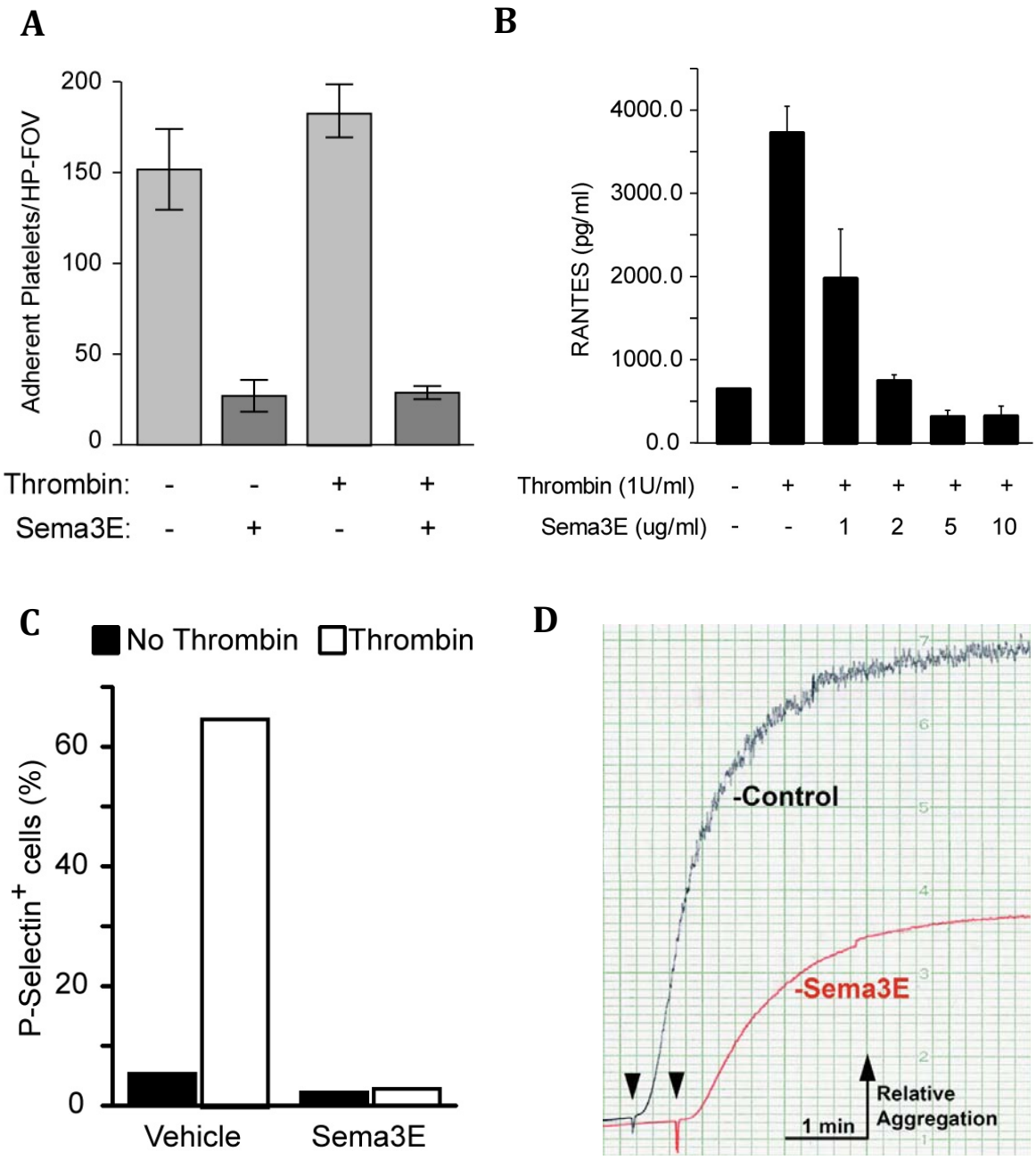

Figure 3.4. Sema3E inhibits platelet adhesion, granule secretion and aggregation. Platelet adhesion to immobilized fibrinogen in the presence or absence of thrombin treated with Sema3E or mock control (A). ELISA for RANTES secretion from activated platelets with dose response of Sema3E (B). Surface expression of P-selectin as a marker of granule release in the presence or absence of thrombin treated with Sema3E or Mock (Vehicle) control (C). Platelet aggregation in response to thrombin (arrow points) in the presence of Sema3E or mock control (D).

Sema3E may be inhibiting $\alpha_{IIb}\beta_3$ integrin by activating PlexinD1 which may act as a Rap1b GAP, thus inactivating Rap1b and subsequently inactivating $\alpha_{IIb}\beta_3$ integrin. Platelets were treated with thrombin in the presence or absence of Sema3E and active Rap1b was assayed over time using a Rap1b pull down assay that specifically recognizes GTP bound (active) Rap1b. Thrombin caused a predictable increase in GTP-bound Rap1b, and Sema3E inhibited this activation, suggesting that this may be the mechanism for Sema3E's inhibition of $\alpha_{IIb}\beta_3$ integrin and platelet activation (Figure 3.5b). To confirm these results, we tested a Rap1b specific inhibitor, GGTI-298, for it's ability to inhibit platelet function. GGTI-298 was able to inhibit both platelet spreading and $\alpha_{IIb}\beta_3$ integrin activation similar to Sema3E (Figure 3.5c,d).

Sema3Es potent ability to inhibit platelets *in vitro* suggested that it might be able to inhibit platelet function *in vivo*. In order to test this hypothesis, we utilized a ferric chloride ($FeCl_3$) thrombosis model. Localized administration of ferric chloride to the carotid artery causes local endothelial damage and subsequent platelet activation and thrombosis. Ferric chloride was administered to the right proximal carotid artery of mice and Doppler ultrasound was used to measure blood flow through the artery distal to the injury. Using 2.4% $FeCl_3$, we reproducibly induced complete occlusion of the carotid artery; however, when Sema3E was administered to the mice IV two minutes prior to $FeCl_3$ treatment of the carotid artery, this occlusion was almost completely inhibited. Time to occlusion was increased over three fold with Sema3E treatment (Figure 3.6a). Additionally, studies using *in vivo* fluorescence microscopy confirmed that Sema3E could inhibit the activation of platelets in mice (Figure 3.6b).

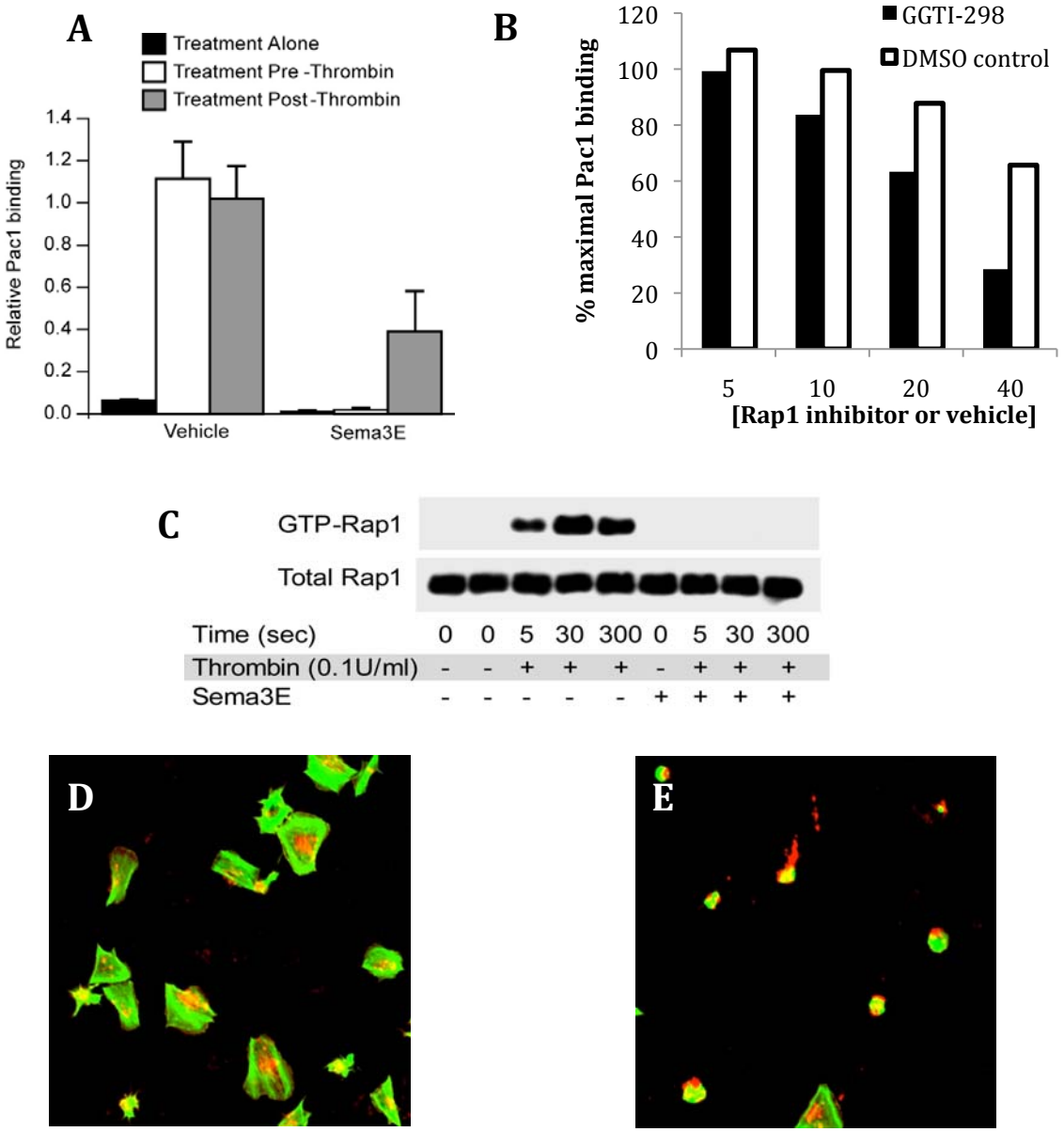

Figure 3.5. Sema3E inhibits $\alpha_{IIb}\beta_3$ integrin by inhibiting Rap1b activation. Sema3E is able to prevent and reverse binding of activation specific $\alpha_{IIb}\beta_3$ integrin antibody Pac1 (A). Rap1 inhibitor GGTI-298 inhibits Pac1 binding (B). Sema3E inhibits the activation of Rap1b by reducing GTP-Rap1b (C). Platelet spreading in response to DMSO control (D) or Rap1 inhibitor GGTI-298 (E). Staining=Phalloidin WGA.

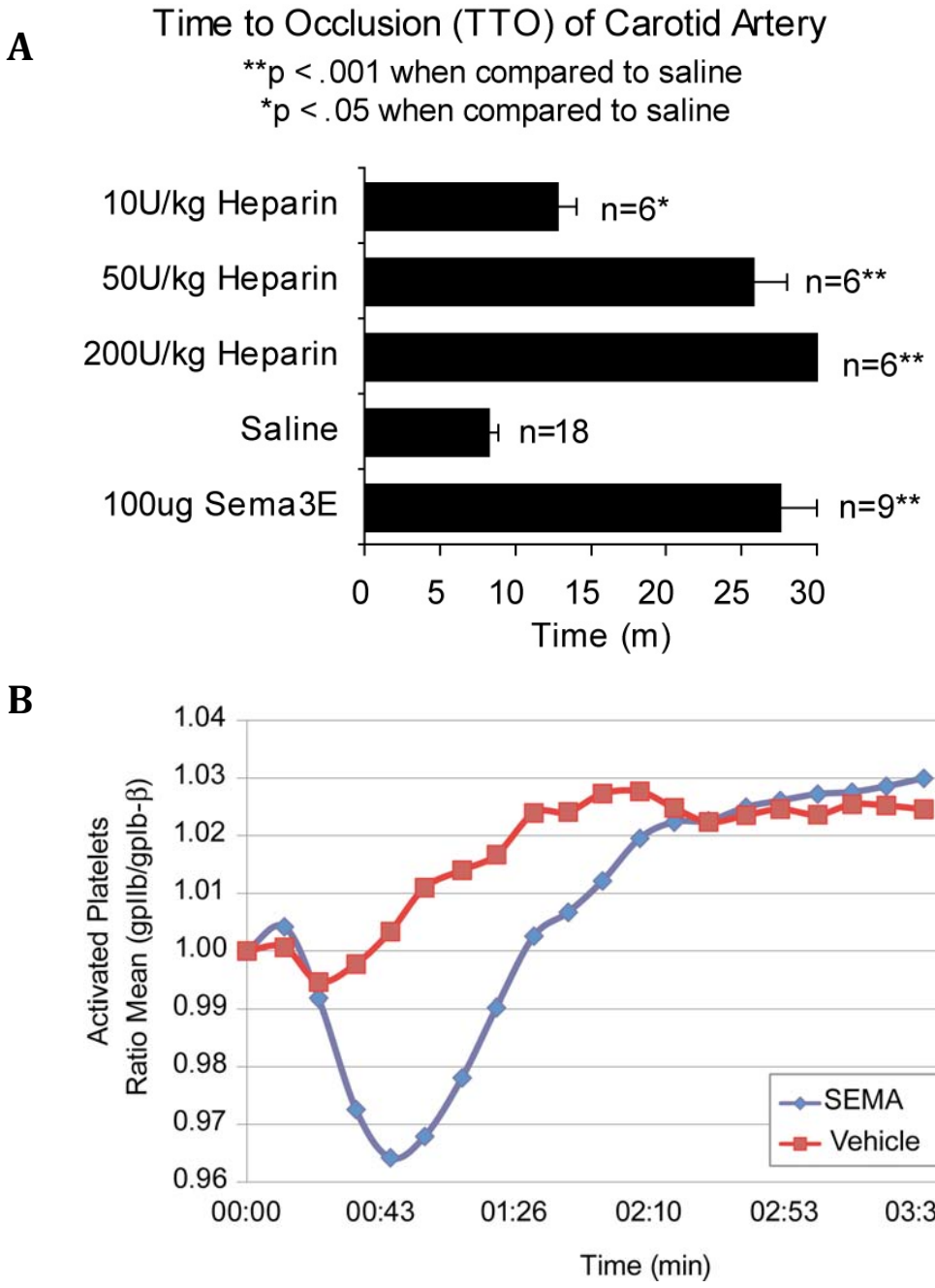

Figure 3.6. Sema3E inhibits *in vivo* thrombosis and *in vivo* platelet activation. Sema3E inhibits ferric chloride induced carotid artery thrombosis similar to a known antithrombotic, heparin (A). Sema3E inhibits *in vivo* platelet activation as measured by *in vitro* fluorescence microscopy (B).

The culmination of these data introduce a neural guidance cue with potent anti-platelet activity, working though known platelet specific mechanisms, that is both reversible and active in an *in vivo* model of thrombosis, thus suggesting an ideal therapeutic candidate. In order to solidify these results it became imperative that we conclusively establish the receptor for Sema3E and produce Sema3E in our own hands to ensure the phenotype is specific and in no way attributable to superfluous elements of a commercially produced reagent.

PlexinD1 is sufficient for the collapsing effects of Sema3E in a heterologous cell system, but it is unclear if PlexinD1 is necessary for Sema3E's effect in platelets. To address this question, we created mice deficient in PlexinD1 exclusively in the megakaryocyte and platelet lineage. Because PLXND1 deficient mice are lethal by postnatal day 1, we specifically targeted PLXND1 knockout to platelets by use of platelet-specific Cre recombinase (PLXND1$^{flox/flox}$;PF4-Cre, denoted PlxnD1^{PltKO}). PLXND1^{PltKO} mice were viable and survived till weaning in expected Mendelian ratios suggesting no lethality in the platelet specific knockout. If Plexin were necessary for Sema3E's effect on platelets, PlxnD1^{PltKO} platelets would not be inhibited by Sema3E. We tested the effects of Sema3E in platelets isolated from PlxnD1^{PltKO} mice by assaying platelet spreading, granule release, and integrin activation. Surprisingly, Sema3E was able to collapse PlxnD1^{PltKO} platelets, inhibit granule release, and inhibit activation of $\alpha_{IIb}\beta_3$ integrin (Data not shown and Figure 3.7a). Furthermore, platelets isolated from PlxnD1^{PltKO} mice or wild type littermate controls showed no difference in dose-dependent response to Sema3E (Figure 3.7a). Quantitative reverse transcriptase polymerase chain reaction (RT-PCR) was used to

determine PlexinD1 transcription in each mouse genotype and confirmed that PlexinD1 levels were markedly decreased in PlxnD1^{PltKO} platelets (Figure 3.7b). These data suggest that PlexinD1 is not necessary for Sema3E's effect on platelets, which is contrary to the current view of semaphorin-plexin biology[14].

Despite these surprising and confusing results, we prepared to treat PlxnD1^{PltKO} mice with Sema3E in the ferric chloride-induced thrombosis model. These studies would require large quantities of Sema3E, so we constructed a plasmid to express human Sema3E for purification from HEK 293T cells. A SEMA3E expressing plasmid was obtained from David Ginty[14] and was modified to contain an eight histamine residue tag and to be highly expressed in a secreted form from HEK 293T cells (Figure 3.8a). Sema3E was purified from the conditioned media of 8his-SEMA3E transfected HEK-293T cells. This conditioned media was then concentrated using size exclusion filters and the His-Sema3E was purified using nickel purification followed by size exclusion chromatography. His-Sema3E along with a control isolated in the same fashion from cells transfected with an empty plasmid lacking the SEMA3E gene (mock) were then tested for platelet inhibitory activity. Surprisingly, both His-Sema3E and mock treatment inhibited platelet activation as measured by surface P-selectin expression and activation of $\alpha_{IIb}\beta_3$ integrin (data not shown and Figure 3.8b). This result was unexpected and led us to suspect contamination in the His-Sema3E and mock preparations. Size exclusion during purification, however, should have removed most proteins and small molecules from the His-Sema3E. Retrospective analysis of our His-Sema3E purifications revealed a trend of platelet inhibitory activity correlated with the

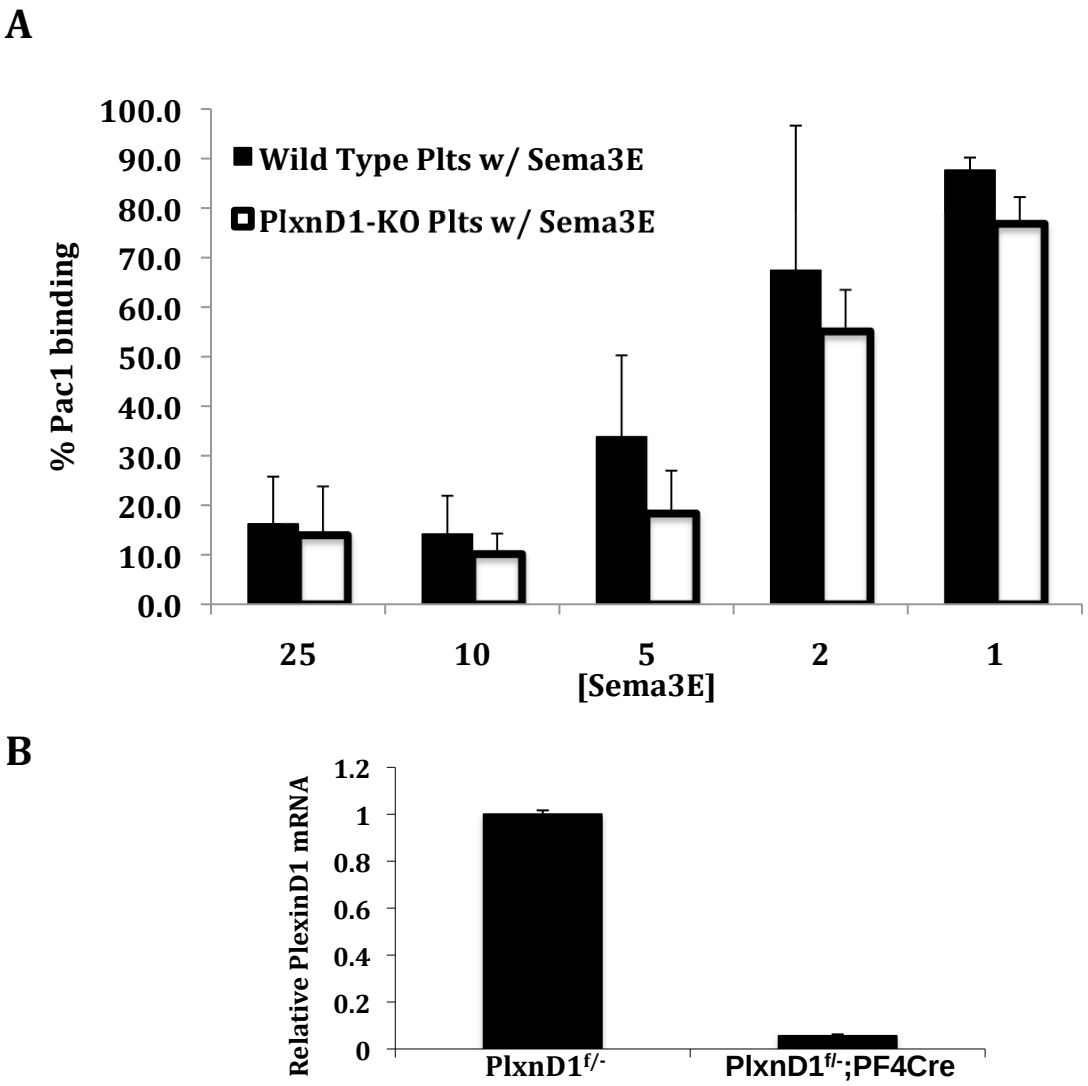

Figure 3.7. Platelets from PlxnD1$^{flox/flox}$;Pf4Cre mice are PlexinD1 deficient but still respond to Sema3E. Sema3E inhibits platelets isolated from PlxnD1^{PltKO} mice similarly to platelets isolated from wild type mice (A). PlxnD1^{PltKO} platelets have markedly reduced expression of PlexinD1 mRNA relative to 18s rRNA (B).

presence of the detergent Tween-20 in the wash buffers for protein purification. Original preparations of His-Sema3E that did not utilize Tween-20 showed no platelet inhibitory activity. The Sema3E used in our initial experiments was purchased from R&D Systems and was reported to contain 0.05% Tween-20. These data led us to hypothesize that Tween-20 was necessary for Sema3E to maintain proper protein folding and activity. Adding Tween-20 to the wash buffers during our His-Sema3E preparations reestablished platelet inhibitory activity. These observations led us to ask if it was possible that Tween-20 was causing the platelet inhibitory actions we were observing with His-Sema3E.

Tween-20 was tested in platelet collapsing assays, and we found that Tween-20 was able to collapse platelets at concentrations as low as 0.002%, near the concentration anticipated in R&D Systems produced Sema3E diluted into platelets with growth media (Figure 3.8c). Tween-20 has been reported to form micelles that appear between 35 and 200kDa depending on the method of analysis[24,25]. Using size exclusion chromatography, we determined that Tween-20 was enhanced in fractions equivalent to ~180kDa proteins, the precise molecular weight of dimerized His-Sema3E (Figure 3.9a-c). These data implied that despite our efforts to remove the detergent along with any other contaminants from the His-Sema3E, we were enhancing the Tween-20 concentration, suggesting that we may be producing functional His-Sema3E without the use of Tween-20 but that His-Sema3E does not inhibit platelet activity. Sema3E is known to inhibit spreading of endothelial cells, which naturally express PlexinD1 [26]. We tested His-Sema3E, purified with and without the use of Tween-20, for the ability to collapse HUVECs that naturally

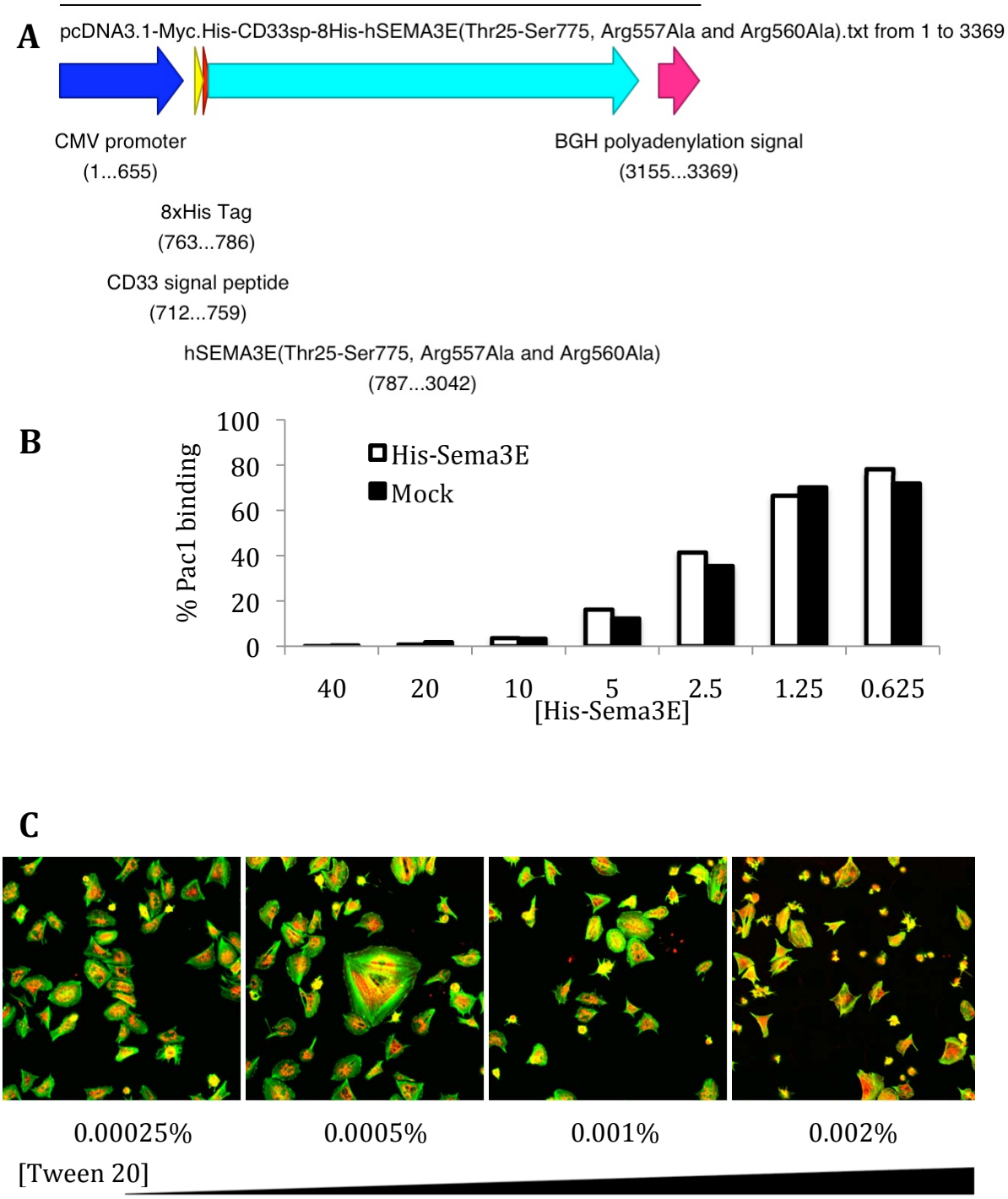

Figure 3.8. Tween-20 but not His-Sema3E inhibits platelet activation. Construction of His-tagged human Sema3E to be expressed in HEK 293T cells (A). Both His-Sema3E and Mock control inhibit activation of platelet $\alpha_{IIb}\beta_3$ integrin (B). Tween-20 is able to collapse platelets similar to previous results with Sema3E (C). Staining=Phalloidin Mitotracker

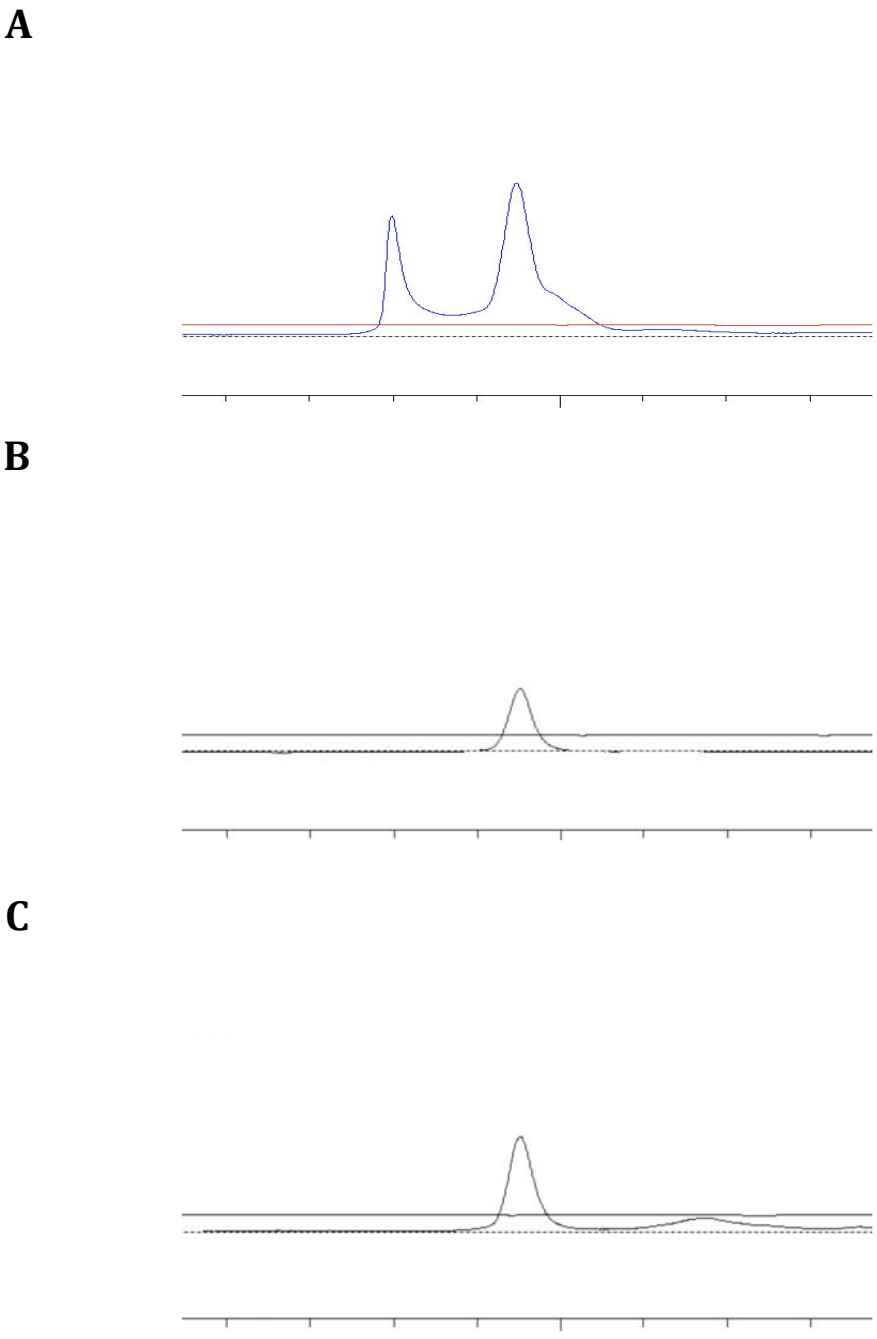

Figure 3.9. Tween-20 micelles are purified with His-Sema3E in size exclusion chromatography (SEC). Purified His-Sema3E in SEC migrates as a dimer and is eluted at approximately fraction 54. Protein aggregates are seen in fractions 34-42 (A). Mock preparation that should contain no protein demonstrates something eluting at the same fraction as dimerized His-Sema3E (B). 0.05% Tween-20 on SEC elutes at the same fraction as dimerized His-Sema3E (C).

express PlexinD1. We found that His-Sema3E but not mock preparations could collapse HUVEC regardless of the presence of Tween-20, but only the preparations containing Tween-20 (His-Sema3E or mock) could collapse platelets (Figure 3.10). To further test these findings, we used antibody depletion to remove Sema3E from R&D Systems protein preparations. R&D Systems Sema3E that had been depleted using antibodies directed against Sema3E continued to inhibit platelet spreading and activation of $\alpha_{IIb}\beta_3$ integrin, indicating that Sema3E was not responsible for the platelet inhibitory activities observed in previously described experiments, and that the platelet inhibitory activity lay with the Tween-20 in the buffer of the Sema3E (Figure 3.11).

Discussion

Platelets have long been a model for the study of axon biology due to their lack of nuclei and ease of procurement, and the cytoskeletal rearrangements that take place in platelet spreading share many of the same mechanisms as those in axon guidance. Specifically, both cells rely on integrin activation and actin dynamics to change cell shape in order to function. These similarities led us to hypothesize that neural guidance cues could inform us about platelet biology and potentially offer insights into anti-platelet therapies. The expression of PlexinD1 on platelet membranes, a cell with limited ability to regulate gene expression, was strong evidence in favor of this hypothesis, suggesting that there must be a biological purpose for this receptor. Additionally, other neural guidance cues, including Semaphorin 4D and ephrins, have been characterized in platelets and shown to

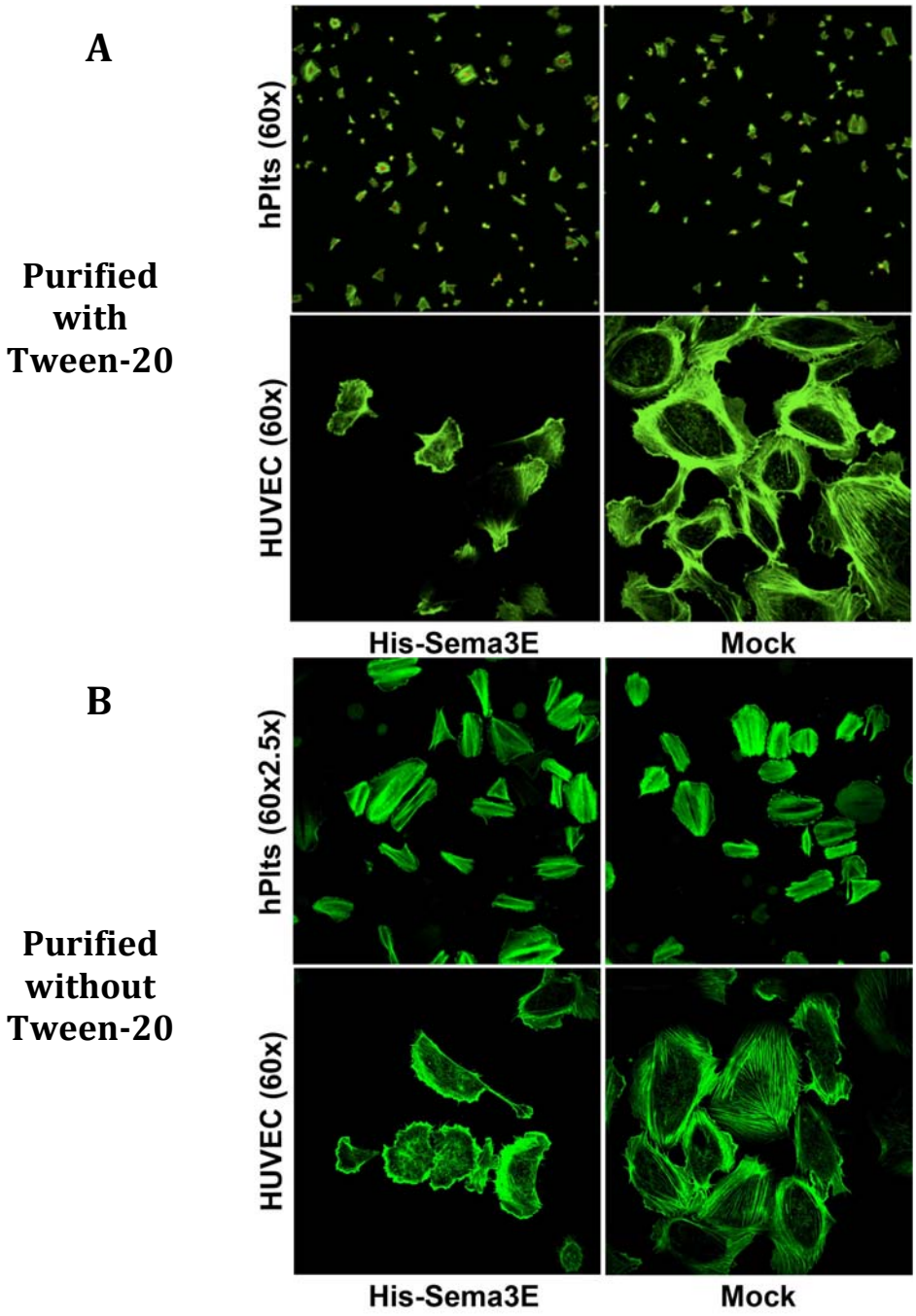

Figure 3.10. Platelet collapse activity is correlated with presence of Tween-20, not with His-Sema3E. Platelets and HUVEC treated with His-Sema3E or mock purified in the presence of Tween-20 (A). Platelets and HUVEC treated with His-Sema3E or mock purified in the absence of Tween-20 (B).

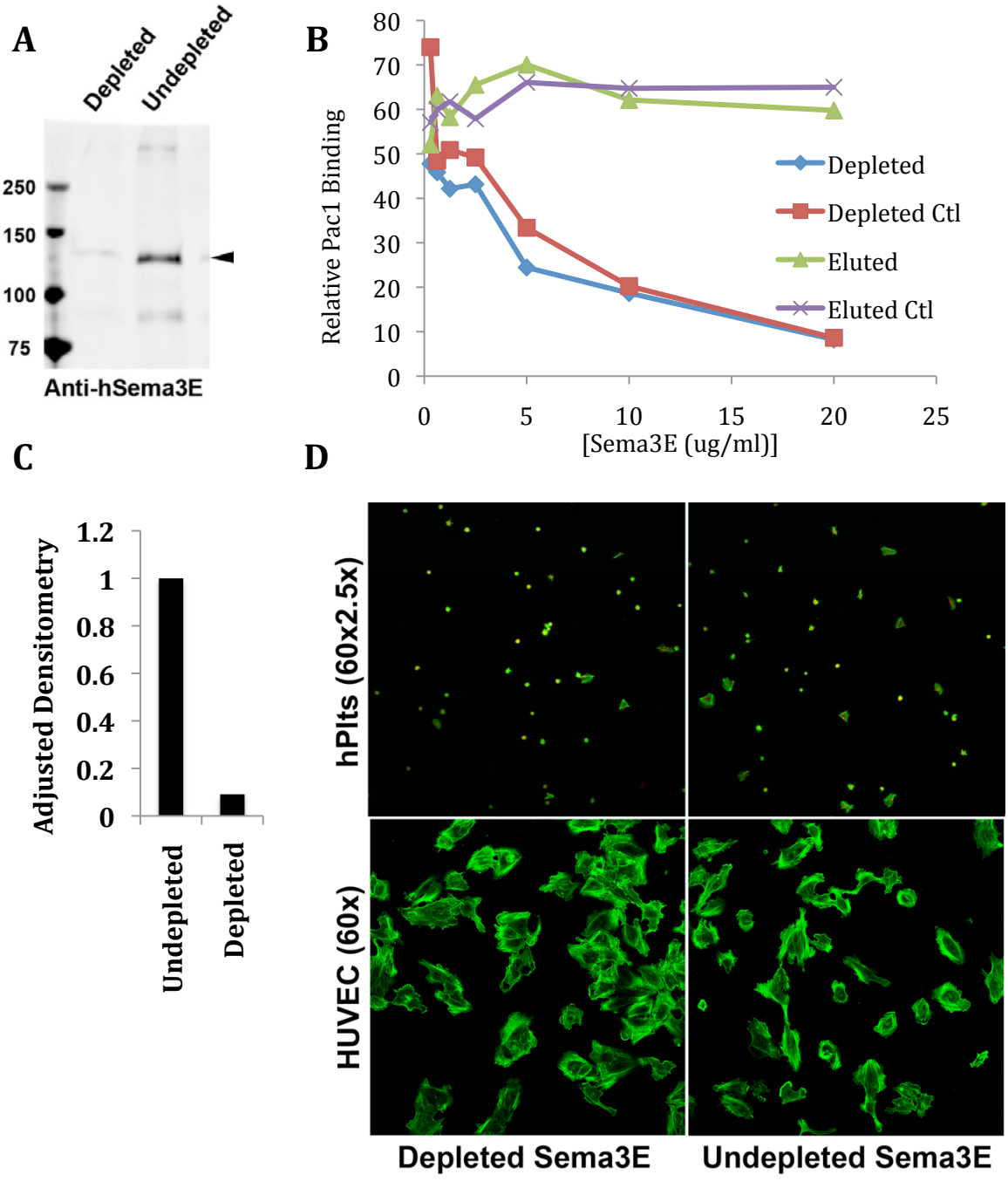

Figure 3.11. Depleted Sema3E inhibits platelets but not HUVEC. Western Blot showing Sema3E was depleted using an anti-Sema3E antibody (A). $\alpha_{IIb}\beta_3$ integrin activation with depleted Sema3E (B). Quantification of deleted Sema3E, arrowhead denotes expected Sema3E dimer (C). Platelet and HUVEC spreading with depleted or undepleted Sema3E (D).

modulate platelet cytoskeletons much like they modulate the developing axon structure[27,28]. Additionally, there have been reports that Semaphorin 3A inhibits platelet function similar to our results with Semaphorin 3E[20]. These data strongly supported our hypothesis that Sema3E, signaling through PlexinD1, could be an endogenous mechanism to inhibit platelet activation and promote platelet quiescence. However, vigilant performance of strict, arduous controls and careful, incisive data analysis led us to conclude that Sema3E's platelet inhibitory activity was due to contamination from a detergent in buffer.

Given our results, the Semaphorin 3A report, and indeed all reports characterizing a compound with anti-platelet activity, need to be carefully re-evaluated. After our discovery that Tween-20 inhibited platelet function, we did a second, more exhaustive screen on the commercially available Semaphorins and their effects on platelet activation. We found a perfect correlation between semaphorins that were produced using Tween-20 with their ability to inhibit platelets (data not shown). The concentration of Tween-20 reported by the manufacturer was always 0.05%, which when diluted into experimental conditions would usually result in a concentration of 0.001%-0.005% Tween-20. This concentration is below the critical concentration required to form micelles (CMC=0.007%)[24]; however, our independent mass spectrometry studies suggested that Tween-20 concentrations in the commercial protein preps were as high as 25 times that reported on certificates of analysis provided by R&D systems. These discrepancies are likely due to size-based purification within the commercial preparation process, probably either molecular weight cut off filters or size exclusion chromatography. In either case,

0.05% Tween-20 is greater than the CMC for Tween-20, which would cause the Tween-20 to segregate with the semaphorin, thus concentrating it in a similar fashion.

These data have wide reaching implications into the field of platelet biology, especially on published work related to guidance cue inhibition of platelets, as we have demonstrated the sensitivity of this primary cell type to detergents and other materials commonly used in research. Future studies into platelet inhibition for the purposes of antithrombotic therapy will require increased scrutiny to ensure that antithrombotic effects are indeed specific and in no way attributable to the sensitivity of the platelet. Our data, which identified the specific contaminant and demonstrated the sufficiency of that contaminant to cause a multitude of reversible anti-platelet effects have led us to discontinue further research into the effect of neural guidance cues on platelet function for the time being.

Methods

Human platelet isolation. Human blood was drawn into acid-citrate-dextrose (ACD) (7 ml ACD/42 ml of blood) and was centrifuged (200*g* for 20 min) to obtain platelet-rich plasma (PRP). PRP was recentrifuged (500*g* for 20 min) in the presence of 100 nM prostacyclin (PGE-1). The supernatant was discarded and 50 ml of Pipes/saline/glucose (PSG; 5 mM Pipes, 145 mM NaCl, 4 mM KCl, 50mM Na_2HPO_4, 1 mM $MgCl_2$–6 H2O, and 5.5 mM glucose), containing 100 nM of PGE-1, was used to resuspend the platelet pellet. The platelet suspension was centrifuged (500 *g* for 20 min), the supernatant was discarded, and the platelet pellet was resuspended in

$Ca2^{+}$- and $Mg2^{+}$-free HBSS (Invitrogen). All studies are approved by the University of Utah's Institutional Review Board (IRB). The cells were resuspended in medium 199 (M199, Invitrogen) at 37°C for each experiment. Where indicated, the washed platelets were pretreated with Semaphorin3E (R&D Systems) (10 µg/ml) or vehicle (M199+0.1% human serum albumin) for 10 minutes at room temperature (RT) prior to start of each study.

Mouse platelet isolation. Mouse blood was drawn via carotid artery cannula into ACD (150µl/1ml blood) Blood/ACD was then diluted 1:2 with PSG and centrifuged (200*g* for 10 min) to obtain PRP. PRP was diluted again 1:2 with PSG and was recentrifuged (500*g* for 7 min) in the presence of 100 nM PGE-1. The supernatant was discarded and 2 ml of PSG containing 100 nM of PGE-1 was used to resuspend the platelet pellet. The platelet suspension was centrifuged (500 *g* for 7 min), the supernatant was discarded, and the platelet pellet was resuspended in M199.

Platelet adhesion and spreading. 8-well borosilicate chamber slides (Nalge Nunc International, Rochester, NY) were coated with 100ug/ml fibrinogen, 50µg/ml collagen, or 50µg/ml laminin overnight at 4° followed by blocking with 0.5% human serum albumin for 30 minutes at 37°. Chamber slides were washed 3x with HBSS. Platelets (2×10^{7}) in M199 were incubated with 10 µg/mL hSema3A/Fc, hSema3E, mSema3E/Fc mSema3F/Fc, or hIgG (R&D Systems) for 10 minutes at room temperature, and then they were placed on the coated chamber slides for 30 minutes at 37°, 5% CO_2 in the presence or absence of 0.05U/ml Thrombin or 20µg/ml ADP. Platelets were fixed for 20 minutes with 2% PFA and washed three

times with HBSS. Morphologic study of adhered platelets was performed by staining platelets with Alexa Fluor 488-phalloidin and 544-WGA followed by imaging using confocal microscopy. Adhesion assays were performed by counting platelets in 5 high powered fields. For wash experiments, Sema3E treated platelets were seeded on fibrinogen coated chamber slides and allowed to spread for 10 minutes. Then Sema3E containing media was removed, cells were washed once with M199, and M199 containing 0.05U/ml thrombin was added to platelets. Platelets were then allowed to spread for 30 minutes.

Platelet contraction. Platelet contraction studies were performed like platelet spreading studies with the exception that platelets were allowed to adhere in the presence of thrombin for 10 minutes before Sema3E was added. Platelets were then allowed to adhere/contract for 20 more minutes at 37°.

Immunocytochemistry. CHO-PLA1 cells transiently transfected with hPlexinD1, or platelets were allowed to spread on fibrinogen coated chamber slides as above. Fixed cells were blocked with 1% bovine serum albumin (BSA) and stained with Alexa Fluor 544-Phalloidin (Molecular Probes, Eugene, OR) and goat anti-plexinD1 (R&D systems, Minneapolis, MN) for 1 hour at room temperature (RT) followed by Alexa Fluor 488 donkey anti-goat 488-IgG (Molecular Probes, Eugene, OR) for 1 hour at RT. Cells were imaged using confocal microscopy.

RANTES ELISA. Washed human platelets were treated with specified concentrations of Sema3E for 10 minutes at RT followed by 0.05U/ml Thrombin for 10 minutes. Platelets were then centrifuged at 500*g* for 10 minutes, and supernatants were removed and used for RANTES ELISA according to the

manufacturer's protocol (human Rantes DuoSet Elisa, R&D systems, Minneapolis, MN).

Granular secretion as detected by membrane expression of P-selectin. Washed human platelets were treated with Sema3E or vehicle as described above followed by various platelet agonists for 15 minutes in the presence of FITC-CD62P antibody. Membrane P-selectin expression was immediately monitored using flow cytometry.

Platelet aggregation. Platelet aggregation was monitored using a platelet aggregometer at 37°C with a stirring rate of 1000 rpm. Sema3E or vehicle treated platelets were suspended in M199 at 10^9/ml and aggregation was initiated by addition of 0.05U/ml thrombin.

Activation of $\alpha_{IIb}\beta_3$ by various agonists. Activation state of $\alpha_{IIb}\beta_3$ was monitored by binding of ligand-mimetic antibodies. 10^6 platelets in M199 were preincubated with Sema3E for 10 minutes, followed by incubation with agonists and FITC-conjugated PAC-1 (BD Biosciences, Franklin Lakes, NJ) for human platelets or PE-JonA (Emfret, Eibelstadt, Germany) for mouse platelets for 15 minutes at room temperature. Then, platelets were analyzed immediately by flow cytometry.

Purification of His-Sema3E. The NaCl and Tween-20 were added to the conditioned media from transient transfection of HEK293T or stable transfection of HEK293 FS with hSema3E 8xHis (KARFAR) to the final concentration of 0.5M NaCl and 0.05% Tween-20 before loaded to HisTrap™ FF (GE Healthcare Lifescience) The column was washed with 5 column volume of 500mM NaCl, 0.54mM KCl, 0.86mM Na_2HPO_4, 0.29mM KH_2PO_4, 75mM imidazole, and 0.05% Tween-20 at a

flowrate of 1ml/min using Biologic DuoFlow (Bio-Rad). Sema3E was eluted from HisTrap™ FF with the gradient of 75-300mM imidazole over 10ml of buffer described above. The Eluted protein was dialyzed with PBS (137mM NaCl, 2.7mM KCl, 4.3mM Na_2HPO_4, 1.47mM KH_2PO_4) and reduced to 1ml using Amicon Ultra™ 30K MWCO (molecular weight cut off). The eluted protein was further purified with sizing column Superdex™200 10/300GL (GE Healthcare Lifescience) equilibrated with 500mM NaCl, 0.54mM KCl, 0.86mM Na_2HPO_4, 0.29mM KH_2PO_4. The Sema3E fractions were identified by SDS-PAGE with reduce and nonreduced condition and westernblot with anti Sema3E antibody (R&D System).

Ferric chloride thrombosis model. Mice were anesthetized with intraperitoneal injection of Avertin (0.3ml of 2.5%) and anesthesia was maintained by using inhalation of 2% isoflurane in an isoflurane vaporizer. The skin on top of the throat is removed and the fascia bluntly dissected to isolate the left jugular vein. A cannula is then inserted into and immobilized to the left jugular vein for administration of Sema3E or saline. The right common carotid artery was then exposed. Carotid blood flow was monitored using ultrasound biomicroscopy (UBS, Visualsonic Vevo 660) with a 40 MHz transducer and image-guided 23 MHz spectral pulsed-wave (PW) Doppler. Heart rate, blood flow velocities, and blood flow volumes were determined from pulsed Doppler waveforms. During scanning, mouse body temperature was maintained within normal range. Following baseline carotid blood flow readings, mice were injected with 200µl of specified control or inhibitor 2 minutes prior to $FeCl_3$ treatment. Thrombosis was then induced by applying 2 pieces of filter paper (1x2 mm) saturated with various concentrations of $FeCl_3$. The

pieces of filter paper were placed on opposite sides of the carotid artery in contact with the adventitial surface of the artery. The $FeCl_3$ saturated filter paper was removed after 3 minutes and the area was washed 3x with 1ml saline irrigation. Blood flow was then monitored every minute from 5-15 minutes, then at 5-minute intervals until 30 minutes after $FeCl_3$ application.

Intravital fluorescence microscopy. Antibodies to murine CD41 were labeled with Alexa Fluor-660 or -647 using the Alexa Fluor Protein Labeling kit (Molecular Probes, Eugene, OR) in accordance with the manufacturer's instructions. Mice were anesthetized with intraperitoneal injection of 125 mg/kg ketamine, 12.5 mg/kg xylazine, and 250 µg/kg atropine sulfate. Anesthesia was maintained with 5 mg/kg pentobarbital as required through a jugular vein cannula. The cremaster muscle was exteriorized, connective tissue was removed, and an incision was made to allow the muscle to be affixed as a single sheet over a glass slide. During preparation and throughout the experiment the muscle preparation was hydrated with buffer (135 mM NaCl, 4.7 mM KCl, 2.7 mM $CaCl_2$, 18 mM $NaHCO_3$, pH 7.4). Labeled anti-CD41 antibody (0.1 µg/g bodyweight) was infused through the jugular cannula 10 minutes before beginning induction of the first thrombus. Between 1 and 3 arterioles were visible in each cremaster muscle preparation. Arterioles with undisrupted flow were chosen (estimated shear rate between 800 and 1600 s^{-1}) and a number of thrombi were studied tracking up each vessel against the direction of blood flow. Endothelial injury was induced using a pulsed nitrogen dye laser at 440 nm that was focused onto the blood vessel wall through the microscope optics. Widefield fluorescence (660 nm excitation wavelength, 60 ms) and brightfield (40 ms) images were collected

alternately for up to 3 minutes after injury formation. Thrombi were visualized using an Olympus AX-70 fluorescence microscope (Olympus, Melville, NY) with a 60x water immersion objective lens (numeric aperture 0.9) and recorded using a Cooke SensiCam digital camera (Cooke, Auburn Hills, MI). Images were taken in rapid-repeating sequence to visualize platelets (excitation wavelength 660 nm, 20 ms) and fibrin (excitation wavelength 488 nm, 15 ms) followed by a brightfield image (20 ms). Data were collected and analyzed using the SlideBook imaging software (Intelligent Imaging Innovations, Denver, CO), and thrombus area and integrated thrombus fluorescence were measured over time.

References

1. Davi, G. & Patrono, C. Platelet activation and atherothrombosis. *N Engl J Med* **357**, 2482-2494 (2007).

2. Jirouskova, M., Shet, A.S. & Johnson, G.J. A guide to murine platelet structure, function, assays, and genetic alterations. *J Thromb Haemost* **5**, 661-669 (2007).

3. Meadows, T.A. & Bhatt, D.L. Clinical aspects of platelet inhibitors and thrombus formation. *Circ Res* **100**, 1261-1275 (2007).

4. Troxler, M., Dickinson, K. & Homer-Vanniasinkam, S. Platelet function and antiplatelet therapy. *Br J Surg* **94**, 674-682 (2007).

5. Torres-Vazquez, J., *et al.* Semaphorin-plexin signaling guides patterning of the developing vasculature. *Dev Cell* **7**, 117-123 (2004).

6. Wilson, B.D., *et al.* Netrins promote developmental and therapeutic angiogenesis. *Science* **313**, 640-644 (2006).

7. Park, K.W., *et al.* Robo4 is a vascular-specific receptor that inhibits endothelial migration. *Dev Biol* **261**, 251-267 (2003).

8. Hafner, C., *et al.* Ephrin-B reverse signaling induces expression of wound healing associated genes in IEC-6 intestinal epithelial cells. *World J Gastroenterol* **11**, 4511-4518 (2005).

9. Suzuki, K., *et al.* Semaphorin 7A initiates T-cell-mediated inflammatory responses through alpha1beta1 integrin. *Nature* **446**, 680-684 (2007).

10. Gitler, A.D., Lu, M.M. & Epstein, J.A. PlexinD1 and semaphorin signaling are required in endothelial cells for cardiovascular development. *Dev Cell* **7**, 107-116 (2004).

11. Toyofuku, T., *et al.* Semaphorin-4A, an activator for T-cell-mediated immunity, suppresses angiogenesis via Plexin-D1. *Embo J* **26**, 1373-1384 (2007).

12. Kruger, R.P., Aurandt, J. & Guan, K.L. Semaphorins command cells to move. *Nat Rev Mol Cell Biol* **6**, 789-800 (2005).

13. Tran, T.S., Kolodkin, A.L. & Bharadwaj, R. Semaphorin regulation of cellular morphology. *Annu Rev Cell Dev Biol* **23**, 263-292 (2007).

14. Gu, C., *et al.* Semaphorin 3E and plexin-D1 control vascular pattern independently of neuropilins. *Science* **307**, 265-268 (2005).

15. Keely, P.J., Rusyn, E.V., Cox, A.D. & Parise, L.V. R-Ras signals through specific integrin alpha cytoplasmic domains to promote migration and invasion of breast epithelial cells. *J Cell Biol* **145**, 1077-1088 (1999).

16. Sethi, T., Ginsberg, M.H., Downward, J. & Hughes, P.E. The small GTP-binding protein R-Ras can influence integrin activation by antagonizing a Ras/Raf-initiated integrin suppression pathway. *Mol Biol Cell* **10**, 1799-1809 (1999).

17. Basile, J.R., Barac, A., Zhu, T., Guan, K.L. & Gutkind, J.S. Class IV semaphorins promote angiogenesis by stimulating Rho-initiated pathways through plexin-B. *Cancer Res* **64**, 5212-5224 (2004).

18. Hu, H., Marton, T.F. & Goodman, C.S. Plexin B mediates axon guidance in Drosophila by simultaneously inhibiting active Rac and enhancing RhoA signaling. *Neuron* **32**, 39-51 (2001).

19. Vikis, H.G., Li, W., He, Z. & Guan, K.L. The semaphorin receptor plexin-B1 specifically interacts with active Rac in a ligand-dependent manner. *Proc Natl Acad Sci U S A* **97**, 12457-12462 (2000).

20. Kashiwagi, H., *et al.* Negative regulation of platelet function by a secreted cell repulsive protein, semaphorin 3A. *Blood* **106**, 913-921 (2005).

21. Vijayan, K.V., Goldschmidt-Clermont, P.J., Roos, C. & Bray, P.F. The Pl(A2) polymorphism of integrin beta(3) enhances outside-in signaling and adhesive functions. *J Clin Invest* **105**, 793-802 (2000).

22. Franke, B., *et al.* Sequential regulation of the small GTPase Rap1 in human platelets. *Mol Cell Biol* **20**, 779-785 (2000).

23. Bertoni, A., *et al.* Relationships between Rap1b, affinity modulation of integrin alpha IIbbeta 3, and the actin cytoskeleton. *J Biol Chem* **277**, 25715-25721 (2002).

24. Mahler, H.C., Printz, M., Kopf, R., Schuller, R. & Muller, R. Behaviour of polysorbate 20 during dialysis, concentration and filtration using membrane separation techniques. *J Pharm Sci* **97**, 764-774 (2008).

25. Dissanayake, V.U., Gee, N.S., Brown, J.P. & Woodruff, G.N. Spermine modulation of specific [3H]-gabapentin binding to the detergent-solubilized porcine cerebral cortex alpha 2 delta calcium channel subunit. *Br J Pharmacol* **120**, 833-840 (1997).

26. Yukawa, K., *et al.* Sema4A induces cell morphological changes through B-type plexin-mediated signaling. *Int J Mol Med* **25**, 225-230.

27. Zhu, L., *et al.* Regulated surface expression and shedding support a dual role for semaphorin 4D in platelet responses to vascular injury. *Proc Natl Acad Sci U S A* **104**, 1621-1626 (2007).

28. Prevost, N., Woulfe, D., Tanaka, T. & Brass, L.F. Interactions between Eph kinases and ephrins provide a mechanism to support platelet aggregation once cell-to-cell contact has occurred. *Proc Natl Acad Sci U S A* **99**, 9219-9224 (2002).

CHAPTER 4

PROTEASOMAL INHIBITION CAUSES THROMBOCYTOPENIA THROUGH HYPERACTIVATION OF RHOA

Introduction

Thrombocytopenia, or low platelet counts, is often a complication of many other medical conditions, and results in a dangerous situation in which a person has an inability to manage bleeding adequately. The causes of thrombocytopenia are multifactorial, ranging from autoimmune diseases (e.g., immune thrombycytopenic purpura) to chemotherapy, major trauma, and surgery. However, the physiologic response to any thrombocytopenia is the increased production of new platelets from megakaryocyte progenitors in the bone marrow. Megakaryocytes are rare, polyploid myeloid cells that arise from hematopoietic stem cells and are the precursor cells that eventually differentiate into platelets[1]. The production of these anucleate platelets marks the final stage of megakaryocyte development; an intricate reorganization of the cytoskeleton eventually results in the production of thousands of platelets from a single megakaryocyte in a process termed thrombopoiesis[2,3].

Thrombopoiesis begins with cellular enlargement along with DNA replication through multiple rounds of endomitosis. The megakaryocyte increases its cytosolic content, including ribosomes and other organelles, and replicates its DNA.

However, unlike typical mitosis, endomitosis is arrested during anaphase B when the mitotic spindles fail to separate and cytokinesis is bypassed. The megakaryocyte goes through many rounds of endomitosis until it reaches a size of nearly 100μm and has a DNA content ranging from 4N to 128N[2]. Among the enriched cytoplasmic contents are proteins necessary for platelet function, including vWF, P-selectin, and $\alpha_{IIb}\beta_3$ integrin; the megakaryocyte packages these proteins appropriately into granules or the membrane. In addition to DNA and cytoplasmic structures, the megakaryocyte will also develop an expansive membrane network termed the Demarcation Membrane System (DMS). This membrane network is connected to the plasma membrane and serves as a membrane reserve for production of proplatelets, the immediate precursor to platelets.

Proplatelet formation initiates with the process of pseudopodial elongation from the large polyploid megakaryocyte. These pseudopods elongate and branch to form many proplatelet-like extensions from the megakaryocyte until the entire cytoplasmic content of the megakaryocyte is involved in an extensive network of (Figure 4.1). At this point, the multilobulated nucleus is extruded from the proplatelet network and degraded. Though the exact events that precipitate the release of individual platelets are still unknown, it is thought that these proplatelets invade the venous sinusoids of the bone marrow, where blood flow shear stress causes individual or pairs of platelets to be released from the proplatelet network into the circulation[3]. It is unclear exactly how much time is required *in vivo* for thrombopoiesis, from cellular expansion to the release of proplatelets into the circulation, but *in vitro* systems that mimic this process require 13-17 days[3].

Figure 4.1. “Overview of megakaryocyte production of platelets. As megakaryocytes transition from immature cells (**A**) to released platelets (**E**), a systematic series of events occurs. (**B**) The cells first undergo nuclear endomitosis, organelle synthesis, and dramatic cytoplasmic maturation and expansion, while a microtubule array, emanating from centrosomes, is established. (**C**) Prior to the onset of proplatelet formation, centrosomes disassemble and microtubules translocate to the cell cortex. Proplatelet formation commences with the development of thick pseudopods. (**D**) Sliding of overlapping microtubules drives proplatelet elongation as organelles are tracked into proplatelet ends, where nascent platelets assemble. Proplatelet formation continues to expand throughout the cell while bending and branching amplify existing proplatelet ends. (**E**) The entire megakaryocyte cytoplasm is converted into a mass of proplatelets, which are released from the cell. The nucleus is eventually extruded from the mass of proplatelets, and individual platelets are released from proplatelet ends.” -Adapted from Patel SR, Hartwig JH, and Italiano JE, *Journal of Clinical Investigation*, 2005.

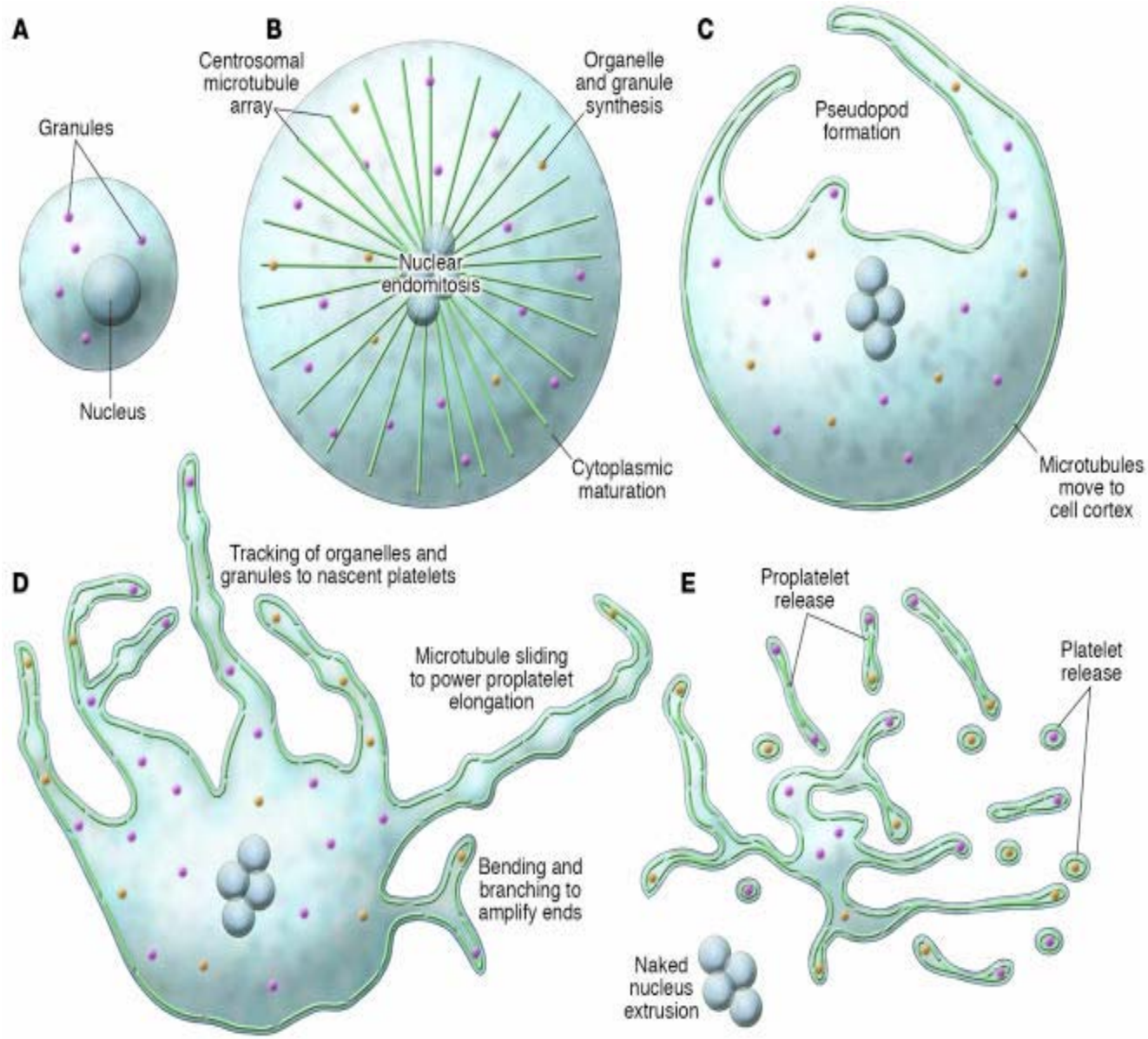
A
Granules
Nucleus
B
Centrosomal microtubule array
Organelle and granule synthesis
Nuclear endomitosis
Cytoplasmic maturation
C
Pseudopod formation
Microtubules move to cell cortex
D
Tracking of organelles and granules to nascent platelets
Microtubule sliding to power proplatelet elongation
Bending and branching to amplify ends
E
Proplatelet release
Platelet release
Naked nucleus extrusion

The entire process of thrombopoiesis, including differentiation of hematopoietic stem cells into immature megakaryocytes, is dependent on thrombopoietin[4]. Thrombopoietin is constitutively produced in the liver and bone marrow stroma and released into the circulation at relatively constant levels regardless of platelet count. It binds primarily to the thrombopoietin receptor c-Mpl, expressed on platelets, megakaryocytes and hematopoietic stem cells. Platelet binding of thrombopoietin acts as a sink, soaking up the thrombopoiesis-inducing cytokine and preventing it from reaching stem cells or megakaryocytes. When bleeding occurs or platelets are otherwise depleted, more thrombopoietin is available to bind to hematopoietic stem cells and megakaryocytes in the bone marrow, thus spurring platelet production for a return to normal platelet numbers[4].

Proper regulation of thrombopoeisis and continued production of platelets is essential for hemostasis. Platelets have a lifespan of approximately 10 days and normal platelet counts in humans are $150x10^9$ to $400x10^9$/liter[4]. Maintaining such high numbers of such a short-lived cell means that it would only take 2 to 3 days of halted platelet production for a person to fall into thrombocytopenia. One common mechanism of thrombocytopenia is chemotherapy treatment. Chemotherapy drugs frequently cause thrombocytopenia in patients, which may result in bleeding or potentially a reduction in chemotherapy dosing in order to avoid thrombocytopenia[5]. Thrombocytopenia of chemotherapy is often attributed to cytotoxic effects of the cell cycle-active agents on megakaryocytes and hematopoietic stem cells[6]. Megakaryocytes that are no longer going through the cell cycle can still produce platelets, but megakaryocyte differentiation often takes many days following

chemotherapy cessation. Therefore, delayed but prolonged periods of thrombocytopenia can be expected following treatments[7].

Bortezomib, a chemotherapeutic primarily used in the treatment of multiple myeloma, also causes thrombocytopenia, but with kinetics much different from other chemotherapeutics[8-10]. Bortezomib causes thrombocytopenia within a few days of therapy initiation, but the thrombocytopenia resolves within 2-3 days following completion of the treatment. Moreover, platelet numbers actually rise above their pretherapy levels after completion of the treatment, suggesting a very different mechanism of thrombocytopenia from the cell cycle inhibition of other chemotherapeutics.

Bortezomib is the first approved drug in its class and its mechanism of action is through reversible yet specific inhibition of the chymotryptic activity of the proteasome[10]. The proteasome is a 2.5MDa complex of at least 66 proteins organized into a 19S regulatory particle and a 20S core particle whose primary function in the cell is to degrade proteins that are either misfolded or no longer needed[11]. The proteasome degrades proteins into 7-8 amino acid peptides through enzymatic digestive actions similar to those of trypsin, chymotrypsin, and caspases. These amino acids can then be further broken down and recycled for new protein synthesis. Misfolded or short-lived proteins are targeted to the proteasome through the actions of a pathway known as the ubiquitin-proteasome pathway, by which a series of proteins termed ubiquitin ligases covalently link multiple monomers of ubiquitin to the protein to be degraded. This poly-ubiquitin chain is then recognized by the proteasome regulatory subunit and the protein is targeted for destruction[12].

Very little is known about the specific functions of the ubiquitin-proteasome pathway in megakaryocytes and platelets, though the presence of proteasomal function in megakaryocytes and platelets suggests that we can extrapolate what we know of the proteasome in other cells[13]. A few major platelet-specific molecules are regulated at least in part by the proteasome, including pro-α_{IIb} integrin and the thrombopoietin receptor, c-Mpl[14,15]. Failure to degrade either of these proteins is unlikely to explain the thrombocytopenia associated with bortezomib therapy because both are known to be upregulated during thrombopoiesis[1].

The kinetics of bortezomib-induced thrombocytopenia suggest that inhibition of the proteasome may be temporarily stalling thrombopoiesis. This temporary stall in platelet production in the absence of major cytotoxicity to the megakaryocytes and hematopoietic stem cells primes the system for increased circulating thrombopoietin levels, which then drastically increase platelet production as soon as bortezomib is withdrawn[7]. This pattern of rapid therapy induced thrombocytopenia followed by rapid platelet recovery following treatment cycles is unique to bortezomib and thus offers a unique opportunity to determine the role of the proteasome in thrombopoiesis. Better understanding of this process will both advance our understanding of mechanisms regulating thrombopoiesis and provide potential therapeutic targets for regulation of platelet production.

Results

In the clinic, patients treated with bortezomib rapidly develop thrombocytopenia within 4 days of initiation of treatment[7]. We first aimed to

determine if mice were susceptible to the same kinetics of thrombocytopenia following bortezomib treatment. Mice were administered a single dose of 2mg/kg body weight of bortezomib and platelet counts were followed for 6 days. We observed an early onset thrombocytopenia beginning within 24 hours of treatment that rapidly recovered by 72 hours (Figure 4.2a). The thrombocytopenia temporally correlated with proteasomal inhibition in circulating platelets suggesting that proteasomal inhibition was responsible for the kinetics of the thrombocytopenia (Figure 4.2b). Thrombocytopenia is primarily caused by one of two mechanisms: reduced platelet production or increased platelet destruction. To determine which mechanism was at work in bortezomib-induced thrombocytopenia, we injected platelet-specific antibodies IV along with bortezomib and monitored total platelet numbers and the percent of platelets bound to the antibody. Because free circulating antibody of non-host origin will be cleared rapidly, only platelets present in the circulation at the time of injection will be labeled. We determined that platelets from mice treated with bortezomib had a half life of 70.5hrs (95% C.I.=64-77hrs), nearly identical to mice treated with DMSO control (64.7hrs, 95% C.I.= 59-70hrs Figure 4.2c); notably, these platelet half-lives are very similar to those reported by others[16]. Moreover, the unlabeled platelet population indicated that platelet production in bortezomib treated mice is markedly reduced when compared with control mice suggesting a defect of platelet production rather than elevated platelet destruction (Figure 4.2d).

Previous studies have suggested that bortezomib may increase platelet activation *in vitro*, which would potentially lead to increased platelet destruction or

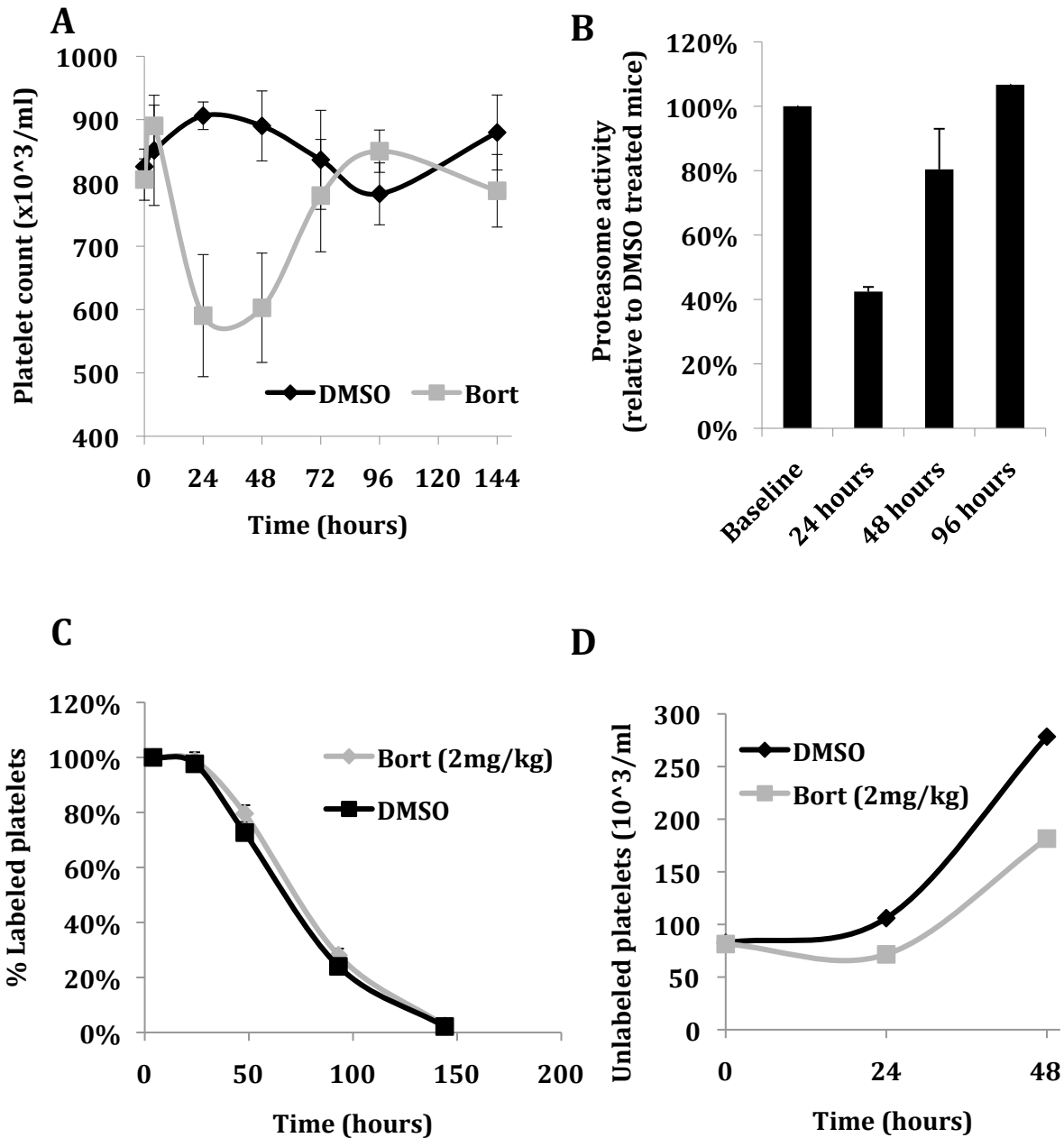

Figure 4.2. Bortezomib-induced thrombocytopenia is due to reduced platelet production rather than increased platelet destruction. Bortezomib causes rapid onset-rapid recovery thrombocytopenia in mice (A). Proteasome activity is inhibited after *in vivo* bortezomib treatment (B). Platelet half-life is unchanged in bortezomib treated mice (C). Platelet production is reduced in bortezomib treated mice (D).

sequestration in tissues[17]. To ensure destruction or sequestration was not contributing to bortezomib-induced thrombocytopenia, we isolated platelets from mice treated with bortezomib or DMSO control and assessed their response to activation. We found no difference in activation between bortezomib and DMSO-treated platelets by either granule release and surface presentation of P-selectin or $\alpha_{IIb}\beta_3$ integrin activation in response to multiple agonists (Figure 4.3a-b). We also tested the activation of human platelets in response to agonists from three major signaling pathways – thrombin, ADP, and thromboxane – after bortezomib treatment *in vitro*. We found no difference in surface P-selectin expression or activation of $\alpha_{IIb}\beta_3$ integrin in human platelets treated with bortezomib compared to DMSO control (Figures 4.4a,b). To confirm that we were adequately inhibiting of the proteasome, we measured levels of polyubiquitinated proteins in the treated platelets; we found that the proteasome was indeed inhibited by bortezomib, resulting in a subsequent buildup of polyubiquitinated proteins (Figure 4.5a,b). To further test platelet function, we also assayed the effect of bortezomib on platelet spreading on fibrinogen in the presence or absence of thrombin; bortezomib had no effect on platelet spreading on fibrinogen (Figure 4.5c). These data suggest that bortezomib-treated platelets are not hyperactive *ex vivo* in mice or humans and are in agreement with published studies reporting that patients on bortezomib are less likely to develop thromboembolic events than patients on other chemotherapeutics[18]. Furthermore, these data suggest that bortezomib has no effect on markers of platelet activation and likely therefore must be acting on the megakaryocyte.

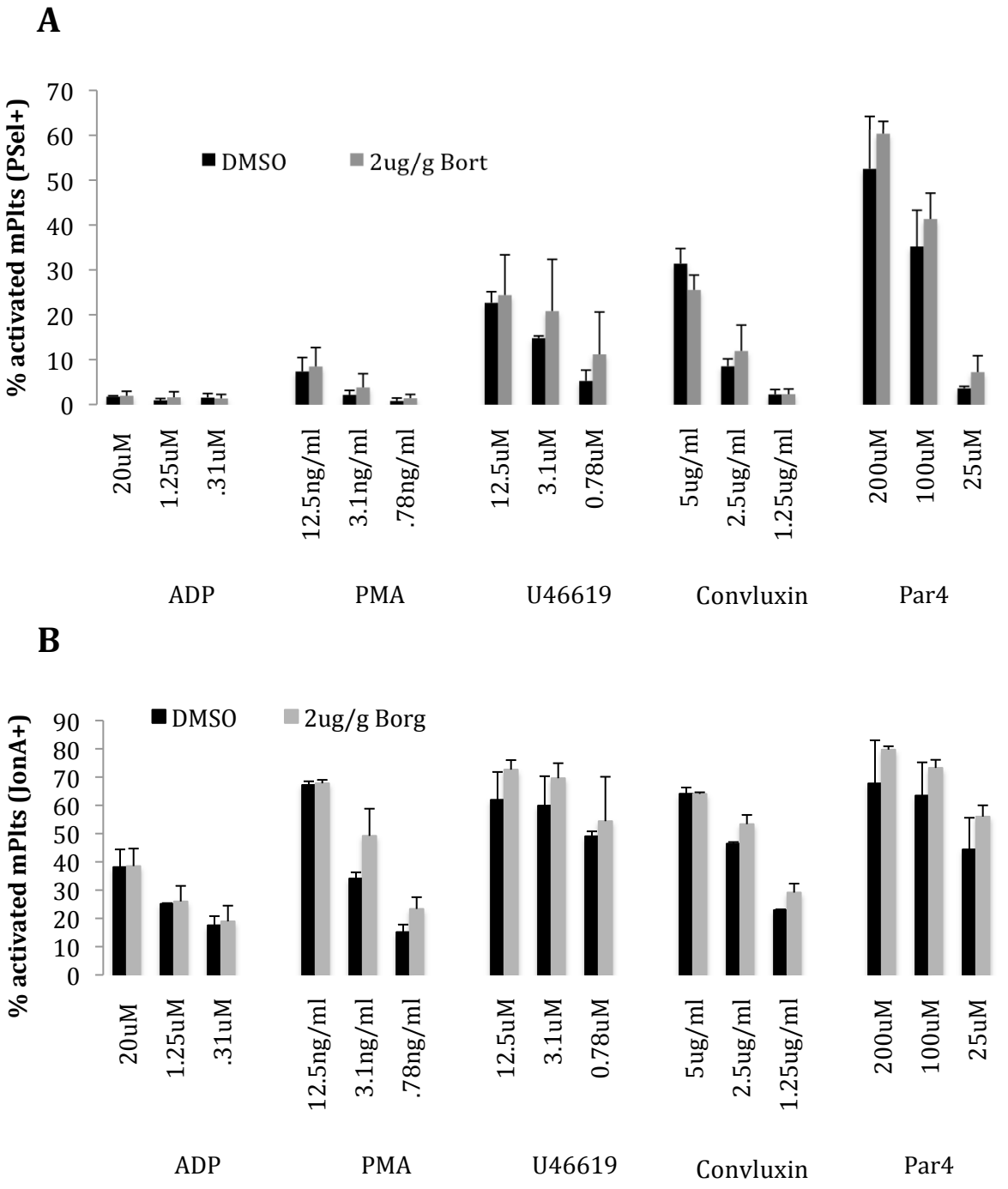

Figure 4.3. Murine platelet activation from bortezomib treated mice. Platelet granule secretion as measured by P-selectin translocation to the membrane is unaltered in platelets from bortezomib treated mice (A). Platelet $\alpha_{IIb}\beta_3$ integrin activation as measured by binding of ligand-mimetic antibody JonA is unaltered platelets from bortezomib treated mice (B).

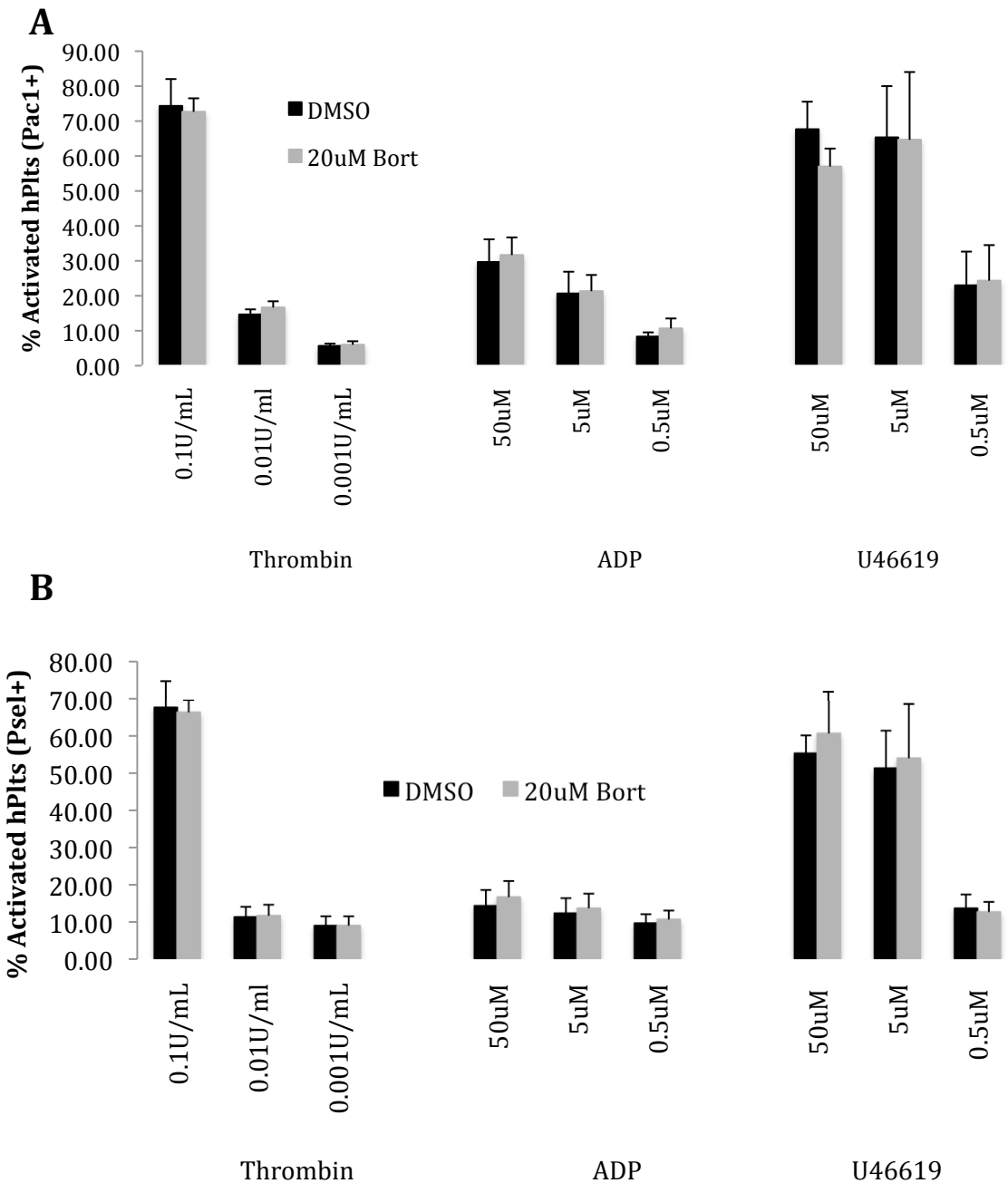

Figure 4.4. Human platelet activation. Platelet granule secretion as measured by P-selectin translocation to the membrane is unaltered in human platelets treated with bortezomib (A). Platelet $\alpha_{IIb}\beta_3$ integrin activation as measured by binding of ligand-mimetic antibody Pac1 is unaltered human platelets (B).

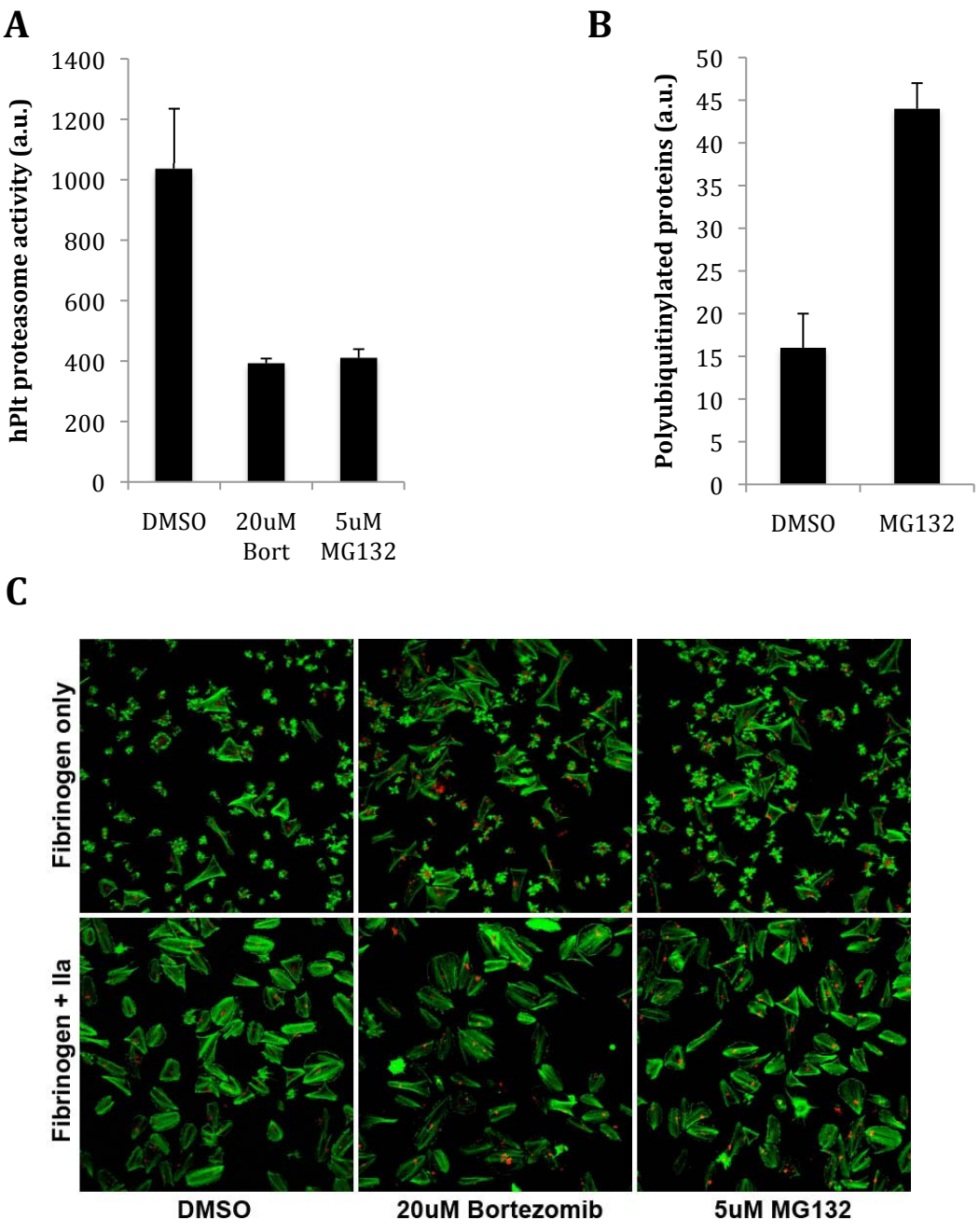

Figure 4.5. Bortezomib inhibits the proteasome in human platelets but does not alter platelet spreading. Bortezomib and MG132 inhibit the proteasome in human platelets (A). Proteasomal inhibition causes a build up of ubiquitinylated proteins in human platelets (B). Neither bortezomib nor MG132 alter platelet spreading on fibrinogen (C). a.u.= arbitrary units. Staining + Phalloidin and WGA

To study the effects of bortezomib on megakaryocytes, we developed a system to culture human megakaryocytes *in vitro*. $CD34^+$ hematopoietic stem cells were isolated from human fetal umbilical cord blood and differentiated into megakaryocytes using a cytokine cocktail of interleukin 3 (IL-3), stem cell factor (SCF), and thrombopoietin (TPO). These cells have been shown to undergo thrombopoiesis over the course of 11-13 days, including the formation of proplatelets and the release of platelet-like particles when exposed to a fibrinogen matrix[19]. These $CD34^+$-derived megakaryocytes possess all the necessary components of the ubiquitin-proteasome pathway, and proteasomal activity can be blocked in these cells using bortezomib or the proteasome inhibitor MG-132 (Figure 4.6a). We assayed the effects of bortezomib on end stage thrombopoiesis in $CD34^+$-megakaryocytes. Megakaryocytes plated on fibrinogen and exposed to DMSO control for 6-12 hours formed proplatelet extensions, just like untreated megakaryocytes (Figure 4.6b,c). In stark contrast, megakaryocytes plated on fibrinogen and treated with bortezomib failed to produce proplatelets, and instead appeared fully spread (Figure 4.6d). To ensure the phenotype was specific to inhibition of the proteasome, we also treated megakaryocytes with two other proteasome inhibitors, MG-132 and lactacystin. Both proteasome inhibitors phenocopied the megakaryocyte spreading seen with bortezomib, confirming that this phenotype is a result of proteasomal inhibition (Figure 4.6e,f).

Because we observed this phenotype when terminal thrombopoiesis was occurring on fibrinogen, we next asked if bortezomib-induced megakaryocyte spreading was dependent on $\alpha_{IIb}\beta_3$ integrin, the integrin necessary for binding to

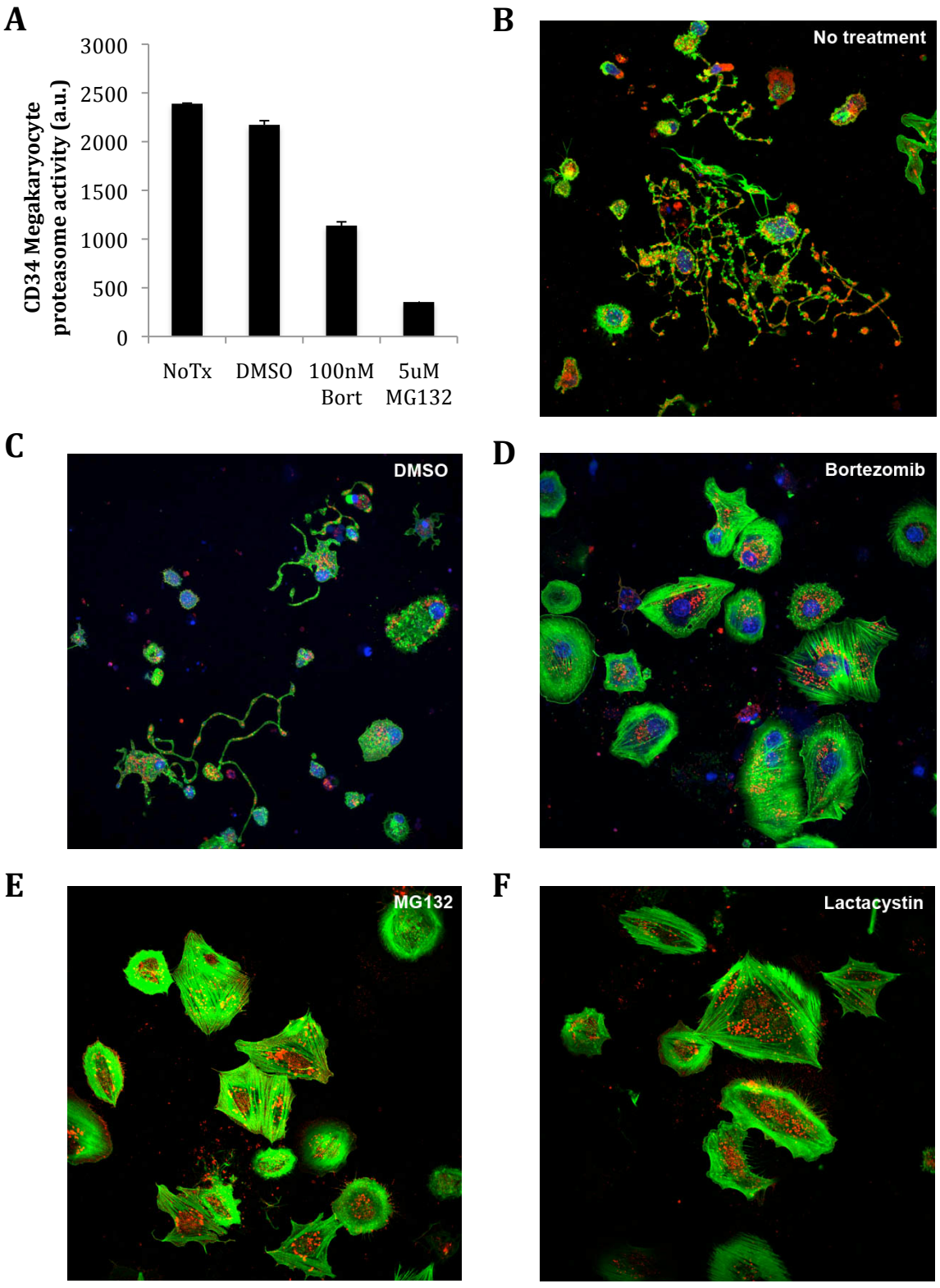

Figure 4.6. Proteasomal inhibition prevents proplatelet formation. Proteasome activity is inhibited in CD34⁺ megakaryocytes (A). Proplatelet formation in CD34⁺ megakaryocytes treated with no additional treatment (B), DMSO (C), Bortezomib (D), MG132 (E), or Lactacystin (F). Staining=Phalloidin, WGA and TO-PRO-3

fibrinogen. We plated megakaryocytes on fibrinogen, fibronectin, collagen, laminin and poly-L-lysine. Both bortezomib and MG-132 induced megakaryocyte spreading on all matrices; however, these effects were most prominent and only statistically significant on fibrinogen and fibronectin, both of which are bound by $\alpha_{IIb}\beta_3$ (Figure 4.7a).

$\alpha_{IIb}\beta_3$ integrin is the most prominent integrin combination expressed on megakaryocytes and platelets, and increased expression and/or activation due to decreased proteasomal activity could explain the megakaryocytes spreading phenotype. To determine whether $\alpha_{IIb}\beta_3$ integrin function was upregulated, we measured the expression of α_{IIb} integrin by western blot. Megakaryocytes treated with bortezomib did not have increased expression of α_{IIb} integrin (Figure 4.7b). Flow cytometric studies also showed that there was no increased expression of α_{IIb} or β_3 integrin on the surface of megakaryocytes (data not shown). These data are congruent with published reports demonstrating that while the proteasome regulates destruction of pro-α_{IIb} integrin, it does not regulate $\alpha_{IIb}\beta_3$ integrin expression[14]. Next we sought to determine if $\alpha_{IIb}\beta_3$ had increased activation after bortezomib treatment. We measured the binding of megakaryocytes to Pac1, an antibody that binds only to activated $\alpha_{IIb}\beta_3$, and to soluble fibrinogen. There was no difference in binding to either Pac1 or soluble fibrinogen between bortezomib and DMSO-treated megakaryocytes, indicating that the mechanism for bortezomib-induced megakaryocyte spreading is not due to increased expression or activation of $\alpha_{IIb}\beta_3$ integrin (Figure 4.7c,d).

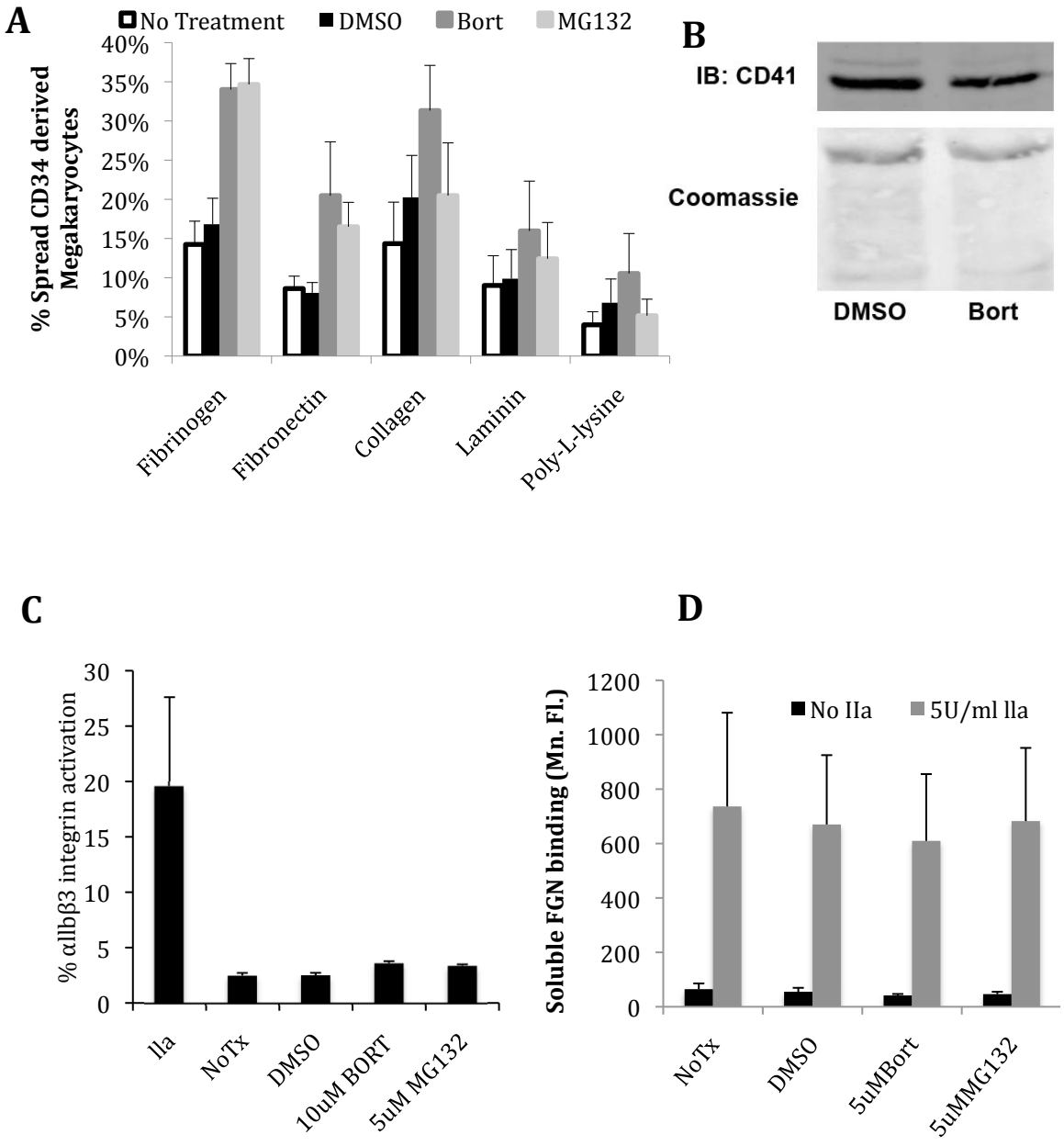

Figure 4.7. Proteasome inhibited megakaryocytes spread more on fibrinogen but do not have elevated CD41 or hyperactive $\alpha_{IIb}\beta_3$ integrin. Megakaryocyte spreading on various indicated matrices (A). Megakaryocyte expression of CD41 as assayed by Western blot (B). Megakaryocyte $\alpha_{IIb}\beta_3$ integrin activation as assayed by Pac1 binding (C). Soluble fibrinogen binding to megakaryocytes treated as indicated (D). IB=Immuno Blot, Mn.Fl.=mean fluorescence

The drastic spreading phenotype of megakaryocytes treated with proteasome inhibitors is strikingly reminiscent of the spreading of activated endothelial cells or platelets. In both cases, the small GTPase RhoA activation is necessary for spreading[20]. We found that RhoA expression was increased in megakaryocytes treated with bortezomib, consistent with other proteasomally inhibited cells (Figure 4.8a)[21-23]. Additionally, we found that RhoA was also activated to a greater extent in megakaryocytes treated with bortezomib (Figure 4.8b).

Inactivation of RhoA has been shown to be required for the production of proplatelets, and the combination of increased expression and hyperactivation of RhoA in proteasome-inhibited megakaryoctyes suggests that RhoA activity may be responsible for megakaryocyte spreading and failure to produce proplatelets[20]. Inhibition of RhoA (using C3 transferase) or its downstream kinase ROCK (using Y-27632) were both able to inhibit bortezomib-induced megakaryocyte spreading, though the ROCK inhibitor was much more potent than the RhoA inhibitor (Figure 4.9a). Furthermore, the ROCK inhibitor rescued the proplatelet production function of bortezomib-treated megakaryocytes (Figure 4.9b). These data demonstrate that enhanced RhoA signaling is responsible for bortezomib-induced failure of proplatelet production and thus likely plays a major role in bortezomib-induced thrombocytopenia.

Discussion

Thrombocytopenia is a common adverse effect of many chemotherapeutic regimens. In the case of bortezomib, one of the only effective treatments for

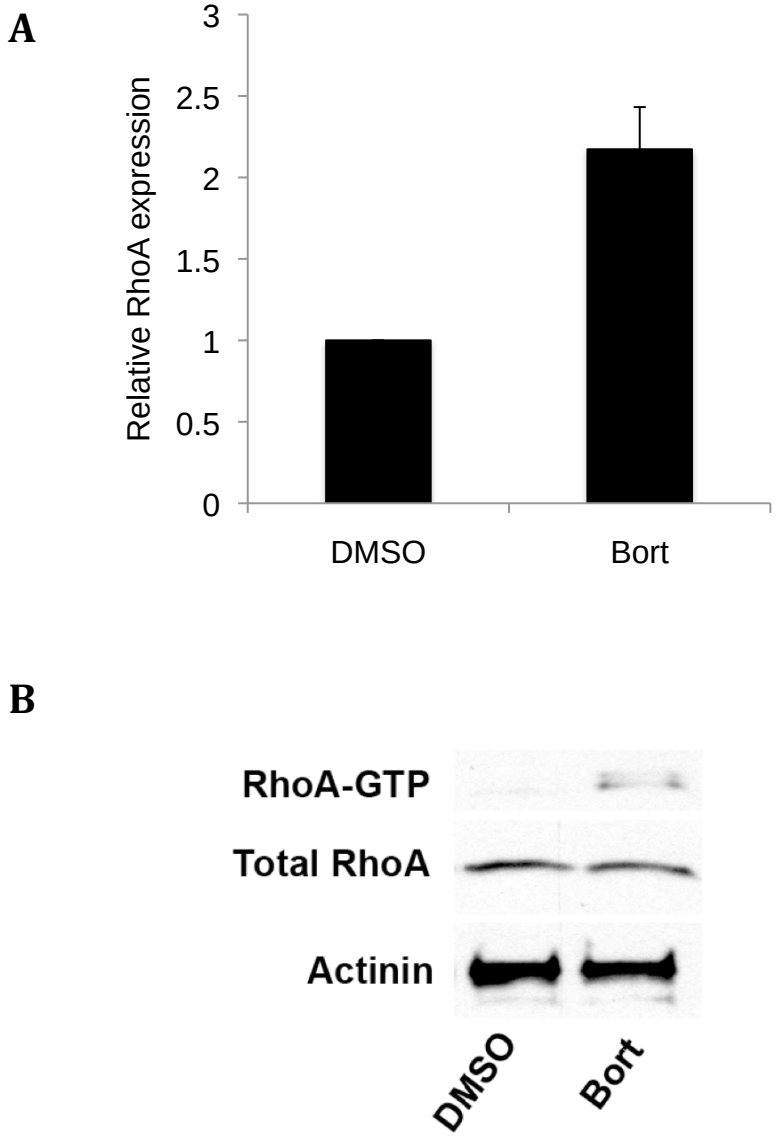

Figure 4.8. RhoA is elevated in bortezomib-treated megakaryocytes. Graphic representation of densitometry of western blots for RhoA in DMSO and bortezomib treated megakaryocytes (A). RhoA-GTP pull down on megakaryocytes treated with DMSO or bortezomib (B).

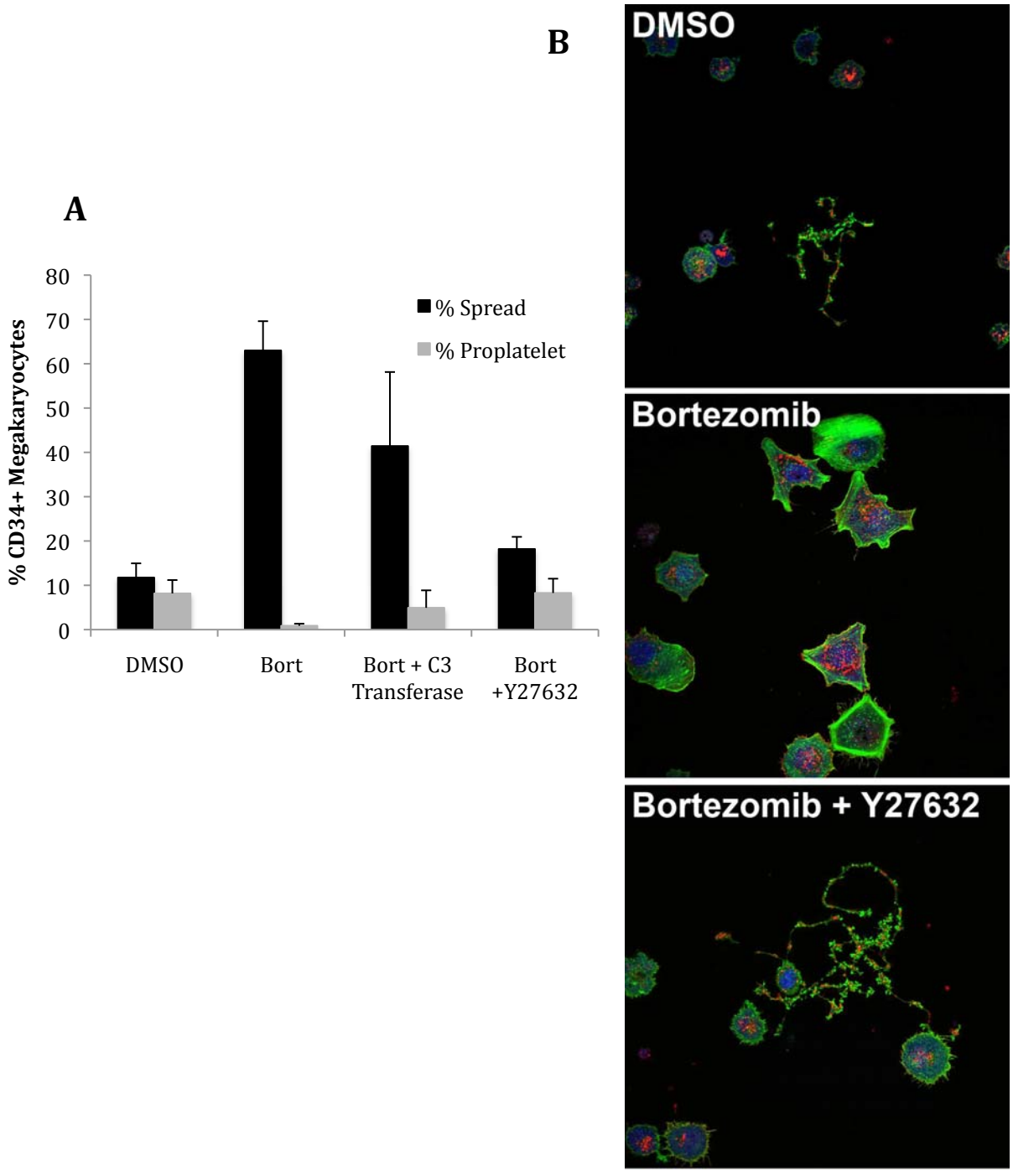

Figure 4.9. Inhibition of the RhoA signaling pathway restores the ability of $CD34^{+}$ megakaryocytes to form proplatelets. Graph demonstrating Inhibition of RhoA (using C3 Transferase) or ROCK (using Y27632) inhibits megakaryocyte spreading and restores production of proplatelets (A). Megakaryocytes treated with-from top to bottom-DMSO, bortezomib or bortezomib + Y27632 (B).

refractory multiple myeloma, thrombocytopenia is dose-limiting and the most common reason that patients are withdrawn from life-saving treatment[8,9]. Most chemotherapy-induced thrombocytopenias are a direct result of cytotoxicity to hematopoietic stem cells. However, the kinetics of bortezomib-induced thrombocytopenia suggest an alternate mechanism, most likely linked to proplatelet budding[7]. We have demonstrated that bortezomib-induced thrombocytopenia is due to decreased platelet production, not increased platelet destruction. We have also shown that proteasomal inhibition has no effect on the activation state of circulating platelets. Until now, the mechanism of bortezomib-induced thrombocytopenia has been unknown. It has been hypothesized that bortezomib-induced thrombocytopenia is a result of diminished NF-κB-dependent transcription through decreased proteasomal destruction of the inhibitor of NF-κB (I-κB), which binds to and inhibits NF-κB[7]. The evidence for this hypothesis, however, is lacking; while megakaryocytes and platelets posses NF-κB, there has been no evidence that NF-κB is required for proplatelet development[24]. Moreover, inhibitors of NF-κB cause platelet and megakaryocyte collapse while proteasomal inhibitors have no effect on platelets and causes megakaryocytes to spread[25] (Figures 4.3c,4.4d-f). Though there is good evidence to suggest that bortezomib may function as a chemotherapeutic through inhibiting NF-κB function in tumor cells[26], these results do not necessarily translate to bortezomib function in megakaryocytes.

Here we show that bortezomib inhibits proplatelet production from megakaryocytes *in vitro* and that this inhibition results in megakaryocyte spreading similar to thrombin treatment of megakaryocytes or platelets. Others have witnessed

a similar megakaryocyte spreading phenotype in the presence of constitutively active RhoA[20]. We show that proteasomally inhibited megakaryocytes have elevated levels of RhoA and that a higher proportion of RhoA is in the active, GTP-bound form. GTP-RhoA is rapidly targeted for the proteasome via its E3 Ubiquitin ligase Smurf1 and deficiency of Smurf1 leads to a buildup of GTP-RhoA and subsequent activation of ROCK and downstream signaling[21]. This could explain the buildup of RhoA and more specifically GTP-RhoA in megakaryocytes treated with proteasome inhibitors. We used inhibitors for both RhoA and ROCK to rescue bortezomib-induced megakaryocyte spreading. Interestingly, inhibition of ROCK and to some extent, inhibition of RhoA not only prevented bortezomib treated megakaryocytes from spreading but also restored their ability to produce proplatelets. These data strongly suggest that the megakaryocyte phenotype caused by proteasomal inhibition is mediated by enhanced RhoA signaling.

These studies offer the first real insight into the requirement of the proteasome for thrombopoiesis. In addition to this work, it is known that Cyclin B is proteasomally regulated, and that rapid degradation of Cyclin B is involved in megakaryocyte endomitosis[27], but it would also be of interest to know the function of the proteasome in other aspects of thrombopoiesis including granule trafficking and platelet release. Proteasome inhibitors are under investigation for a multitude of malignant disorders and their use as chemotherapeutics is likely to rise drastically in the near future. Because of this it will be important to understand the mechanisms of proteasome inhibitor-induced thrombocytopenias in hopes of preventing these thrombocytopenias in order to maximize chemotherapeutic effects.

Future studies in this field would involve finding a suitable Rho pathway inhibitor that could be used as an adjunct to bortezomib therapy. RhoA is known to function at the cell membrane and requires a geranylgeranyl lipid modification to localize to the cell membrane. This lipid is a byproduct of cholesterol synthesis, therefore suggesting that statin drugs may be a potential candidate for rescuring bortezomib-induced thrombocytopenia. Statins are especially attractive because they are an already approved drug and are among the best-tolerated drugs in all of pharmacopeia. Clearly, the ability of statins to inhibit megakaryocyte spreading and restore proplatelet formation in the face of proteasomal inhibition would first have to be tested *in vitro* before moving on to animal or human trials.

Methods

Human platelet isolation. Human blood was drawn into acid-citrate-dextrose (ACD) (7 ml ACD/42 ml of blood) and was centrifuged (200*g* for 20 minutes) to obtain platelet-rich plasma (PRP). PRP was recentrifuged (500*g* for 20 minutes) in the presence of 100 nM PGE-1. The supernatant was discarded and 50 ml of Pipes/saline/glucose (PSG; 5 mM Pipes, 145 mM NaCl, 4 mM KCl, 50mM Na_2HPO_4, 1 mM $MgCl_2$–6 H2O, and 5.5 mM glucose), containing 100 nM of PGE-1, was used to resuspend the platelet pellet. The platelet suspension was centrifuged (500 *g* for 20 minutes), the supernatant was discarded, and the platelet pellet was resuspended in $Ca2^+$- and $Mg2^+$-free HBSS. All studies are approved by the University of Utah's Institutional Review Board (IRB). The cells were resuspended in medium 199 (M199) at 37°C for each experiment.

Mouse platelet isolation. Mouse blood was drawn via carotid artery cannula into ACD (150µl/1ml blood) Blood/ACD was then diluted 1:2 with PSG and centerfuged (200g for 10 minutes) to obtain PRP. PRP diluted again 1:2 with PSG and was recentrifuged (500*g* for 7 minutes) in the presence of 100 nM PGE-1. The supernatant was discarded and 2 ml of PSG containing 100 nM of PGE-1, was used to resuspend the platelet pellet. The platelet suspension was centrifuged (500 *g* for 7 minutes), the supernatant was discarded, and the platelet pellet was resuspended in $Ca2^{+}$- and $Mg2^{+}$-free HBSS.

Differentiation of $CD34^{+}$ hematopoietic stem cells. Umbilical cord blood samples from normal full-term human newborns were obtained after informed consent by the mothers (IRB# 11919). Whole blood was diluted in half with 0.9% saline and placed on Ficoll-Paque^{TM} PLUS (Amersham Biosciences, Uppsal, Sweden) to separate the mononuclear cells by centrifugation. Hematopoietic progenitors were purified from the mononuclear interphase with magnetic beads that were directly conjugated to anti-$CD34^{+}$ (Miltenyi Biotec Inc., Auburn, CA). After a 30-minute incubation period, $CD34^{+}$ cells were isolated from the mononuclear suspension using an Auto-MACS cell separator (Miltenyi).

The $CD34^{+}$ cells were resuspended in 2.5 mls of X Vivo-20 culture medium (BioWhittaker, Walkersville, MD) that contained 50 ng/ml of thrombopoietin (Chemicon International, Inc., Temecula, CA), 40 ng/ml of human stem cell factor (Biosource, Camarillo, CA), and 10 ng/ml of interleukin-3 (IL-3; R&D systems, Minneapolis, MN). The cell suspension was transferred to bacterial tissue culture plates to prevent adherence. The liquid cultures were maintained at $37^{o}C$ in a

humidified 5% CO_2 atmosphere and the cells were replenished with fresh growth factors and culture medium every 2-3 days. IL-3 was removed from the culture medium on day 7. At day 13, the cells were placed on immobilized human fibrinogen (100 mg/ml;Calbiochem-Novabiochem Corporation, San Diego, CA) coated surfaces to generate megakaryocytes that possess proplatelet extensions.

Mouse studies. C57BL/6 mice were injected I.V. on Day 0 with 0.1ug/g body weight Dylight 488 mouse platelet labeling antibody (Emfret Analytics) and 2ug/g body weight bortezomib in 100ul 10% DMSO in 0.9% saline or DMSO control. 30μL blood samples were then taken via tail stick, each day for the remainder of the experiment. 5μL whole blood was added to 44ul HBSS and 1μL phycoerythrin conjugated anti-mouse CD41 antibody (BD Biosciences) and taken for analysis using a FacScan (Becton Dickinson, Franklin Lakes, NJ). The remainder of the whole blood sample was subjected to complete blood count and differential using a Hevavet 950 (Drew Scientific, Waterbury, CT).

Platelet adhesion and spreading. 8 well borocilicate chamber slides (Nalge Nunc International, Rochester, NY) were coated with 100ug/ml fibrinogen, 50μg/ml collagen, or 50μg/ml laminin overnight at 4° followed by blocking with 0.5% human serum albumin for 30 minutes at 37°. Chamber slides were washed 3x with HBSS. Platelets (2×10^7) in M199 were placed on the coated chamber slides for 30 minutes at 37°, 5% CO_2 in the presence or absence of 0.05U/ml Thrombin or 20μg/ml ADP. Platelets were fixed for 20 minutes with 2% PFA and washed three times with HBSS. Morphologic study of adhered platelets was performed by staining platelets

with Alexa 488-phaloidin and 544-WGA followed by imaging using confocal microscopy. Platelets were then allowed to spread for 30 minutes.

Immunocytochemistry. Cells were fixed with 4% paraformaldehyde for 20 minutes at room temperature followed by permiabilization in 0.1% Triton-X 100 for 5 minutes. Fixed and permiabilized cells were stained with alexa fluor 488 Phaloidin and Alexa fluor 555 wheat germ agglutinin (WGA) and To-pro-3 iodide (all Molecular Probes, Eugene, OR). Cells wee imaged using an FV300 Olympus IX81 microscope (Melville, NY).

Activation of αIIbβ3 by various agonists. Activation state of IIbβ3 was monitored by binding of a ligand-mimetic antibodies. 1 x 10^6 platelets in M199 were treated with agonis concentrations indicated along with FITC-conjugated PAC-1 (BD Biosciences, Franklin Lakes, NJ) for human platelets or PE-JonA (Emfret, Eibelstadt, Germany) for mouse platelets for 15 minutes at room temperature. Then, platelets were analyzed immediately using a FacScan (Becton Dickinson, Franklin Lakes, NJ).

GTPase activation assays. Activity of RHOA, was measured using activation assay kits (Upstate) according to manufacturer's instructions. Briefly, transfected cells were scraped into Mg2+ lysis buffer supplemented with protease inhibitors (Roche) and phosphatase inhibitors (Sigma). A small portion of the lysate was retained as total cell lysate and the rest was incubated with the assay reagent. GTP-bound forms were eluted from the assay reagent using Laemmli sample buffer and analyzed by western blotting. The total cell lysate was analyzed by western for total GTPase.

References

1. Pang, L., Weiss, M.J. & Poncz, M. Megakaryocyte biology and related disorders. *J Clin Invest* 115, 3332-3338 (2005).

2. Patel, S.R., Hartwig, J.H. & Italiano, J.E., Jr. The biogenesis of platelets from megakaryocyte proplatelets. *J Clin Invest* 115, 3348-3354 (2005).

3. Thon, J.N.*, et al.* Cytoskeletal mechanics of proplatelet maturation and platelet release. *J Cell Biol* 191, 861-874 (2010).

4. Kaushansky, K. The molecular mechanisms that control thrombopoiesis. *J Clin Invest* 115, 3339-3347 (2005).

5. Zuckerman, K.S. Hematopoietic abnormalities in patients with cancer. *Cancer Control* 5, 6-11 (1998).

6. Kaufman, R.M.A., K.C. *Hematologic complications and blood bank support*, (Decker, Hamilton, ON, Canada, 2003).

7. Lonial, S.*, et al.* Risk factors and kinetics of thrombocytopenia associated with bortezomib for relapsed, refractory multiple myeloma. *Blood* 106, 3777-3784 (2005).

8. Richardson, P.G.*, et al.* A phase 2 study of bortezomib in relapsed, refractory myeloma. *N Engl J Med* 348, 2609-2617 (2003).

9. Jagannath, S.*, et al.* A phase 2 study of two doses of bortezomib in relapsed or refractory myeloma. *Br J Haematol* 127, 165-172 (2004).

10. Adams, J.*, et al.* Proteasome inhibitors: a novel class of potent and effective antitumor agents. *Cancer Res* 59, 2615-2622 (1999).

11. Xie, Y. Structure, assembly and homeostatic regulation of the 26S proteasome. *J Mol Cell Biol* 2, 308-317.

12. Naujokat, C. & Saric, T. Concise review: role and function of the ubiquitin-proteasome system in mammalian stem and progenitor cells. *Stem Cells* 25, 2408-2418 (2007).

13. Yukawa, M.*, et al.* Proteasome and its novel endogeneous activator in human platelets. *Biochem Biophys Res Commun* 178, 256-262 (1991).

14. Mitchell, W.B., Li, J., French, D.L. & Coller, B.S. alphaIIbbeta3 biogenesis is controlled by engagement of alphaIIb in the calnexin cycle via the N15-linked glycan. *Blood* 107, 2713-2719 (2006).

15. Saur, S.J., Sangkhae, V., Geddis, A.E., Kaushansky, K. & Hitchcock, I.S. Ubiquitination and degradation of the thrombopoietin receptor c-Mpl. *Blood* 115, 1254-1263.

16. Heilmann, E.*, et al.* Biotinylated platelets: a new approach to the measurement of platelet life span. *Br J Haematol* 85, 729-735 (1993).

17. Avcu, F., Ural, A.U., Cetin, T. & Nevruz, O. Effects of bortezomib on platelet aggregation and ATP release in human platelets, in vitro. *Thromb Res* 121, 567-571 (2008).

18. Lonial, S.*, et al.* Characterisation of haematological profiles and low risk of thromboembolic events with bortezomib in patients with relapsed multiple myeloma. *Br J Haematol* 143, 222-229 (2008).

19. Foulks, J.M.*, et al.* PAF-acetylhydrolase expressed during megakaryocyte differentiation inactivates PAF-like lipids. *Blood* 113, 6699-6706 (2009).

20. Chang, Y.*, et al.* Proplatelet formation is regulated by the Rho/ROCK pathway. *Blood* 109, 4229-4236 (2007).

21. Boyer, L.*, et al.* CNF1-induced ubiquitylation and proteasome destruction of activated RhoA is impaired in Smurf1-/- cells. *Mol Biol Cell* 17, 2489-2497 (2006).

22. Von Zee, C.L. & Stubbs, E.B., Jr. Geranylgeranylation facilitates proteasomal degradation of rho G-proteins in human trabecular meshwork cells. *Invest Ophthalmol Vis Sci* 52, 1676-1683.

23. Guilluy, C.*, et al.* Transglutaminase-dependent RhoA activation and depletion by serotonin in vascular smooth muscle cells. *J Biol Chem* 282, 2918-2928 (2007).

24. Liu, F., Morris, S., Epps, J. & Carroll, R. Demonstration of an activation regulated NF-kappaB/I-kappaBalpha complex in human platelets. *Thromb Res* 106, 199. (2002).

25. Spinelli, S.L.*, et al.* Platelets and megakaryocytes contain functional nuclear factor-kappaB. *Arterioscler Thromb Vasc Biol* 30, 591-598.

26. Hideshima, T.*, et al.* NF-kappa B as a therapeutic target in multiple myeloma. *J Biol Chem* 277, 16639-16647 (2002).

27. Zhang, Y., Wang, Z., Liu, D.X., Pagano, M. & Ravid, K. Ubiquitin-dependent degradation of cyclin B is accelerated in polyploid megakaryocytes. *J Biol Chem* 273, 1387-1392 (1998).

CHAPTER 5

CONCLUDING REMARKS

Platelets play a crucial role in hemostasis and throughout evolution they may have been the most important defense against accidental death available in mammals. However, as times change and we are less likely to die of massive hemorrhage, and diet and lifestyle changes alter the micro and macro environments within our body, platelets take on a different role. They become the enemy in diseases such as thromboembolic disorders, myocardial infarction[1], cerebrovascular accidents[2], atherosclerosis[3], arthritis[4,5], acute respiratory distress syndrome[6] and malignancy[7]. Because platelets were originally thought to be nothing more than cellular fragments that plug up holes in the vascular system, research on these fascinating little cells lagged behind much of the rest of biological sciences. We now know that platelets undergo complex cellular processes including translation[8], RNA splicing[9], and division[10], in addition to activation in the face of hemorrhage or inflammation. The processes involved in platelet production and activation are tightly regulated by cytoskeletal alterations, and modulating these cytoskeletal alterations is of keen interest in modulating platelet function or production therapeutically.

The data presented in this dissertation lend additional insight into these cytoskeletal processes and how to study them. Neural guidance cues (Slits, Netrins, Ephrins and Semaphorins) were originally distinguished for their ability to alter the migration patterns of axon growth cones, but we now know that these cues also alter the migration patterns and activities of the developing vasculature and other systems as well. Because of the highly cytomorphic properties of platelets and the similarities in the cytoskeletal changes between platelet, endothelial cell, and axonal growth cones, we hypothesized that platelets too may be regulated by the same extracellular cues as migrating neurons and endothelial cells. Indeed, ephrins are well known for their ability to stabilize thrombus formation through enhancing outside-in platelet integrin signaling[11]. Additionally, Semaphorin 4D is also known to be elevated in platelet activation, and mice lacking Semaphorin4D have an impaired ability to develop stable thrombi[12]. However, only one neural guidance cue, Semaphorin 3A, has been shown to inhibit platelet cytoskeletal function[13], but in the wake of my studies, even this knowledge must be called into question. My result, that effects attributed to semaphorin 3E were actually caused by detergent contamination, underscores the fragility of platelets but also demonstrates how a non-specific molecule such as a detergent can reversibly inhibit platelet cytoskeletal rearrangements. Though these studies did not lead to the next anti-thrombotic therapeutic as one might have hoped, they did teach us a great deal about how platelets react and more specifically about how to view other potential targets under study as anti-thrombotics. These studies also underscore the necessity for *in vivo* studies and the use of gene-targeted small animal models to demonstrate the

specificity of a protein target under question. Only when these models are used and multiple approaches to pathway inhibition have proven successful *in vivo* can there be a start to speculation on the clinical applicability of a candidate anti-platelet target.

After these discoveries, I turned my expertise with platelet function and biology towards a different clinical problem; bortezomib, a newly approved chemotherapeutic agent used to treat multiple myeloma, results in a dose-limiting thrombocytopenia. Here I show that bortezomib-induced thrombocytopenia is caused by aberrant activation of the RhoA GTPase signaling pathway, preventing the formation of new platelets from megakaryocytes[14]. Though others may have possibly come to know this through another route, I was able to make this connection because of previous studies in the lab which demonstrated the importance of endothelial RhoA signaling in the pathogenesis of cerebral cavernous malformations (CCMs)[15,16]. The similarities of bortezomib-treated megakaryocytes and endothelial cells deficient in CCM2 allowed me to more quickly dissect the mechanism by which bortezomib inhibits platelet production *in vitro* and rescue that phenotype with inhibition of RhoA or ROCK. I now hope to use these findings to ameliorate bortezomib-induced thrombocytopenia *in vivo*, using statins or the ROCK inhibitor fasudil, both of which are used safely in patients for other indications.

References

1. Wong, C.K. & White, H.D. Antithrombotic therapy in ST-segment elevation myocardial infarction. *Expert Opin Pharmacother* **12**, 213-223.

2. Lazzaro, M.A., Malhotra, K. & Mohammad, Y.M. The role of antithrombotics in secondary stroke prevention. *Semin Neurol* **30**, 492-500.

3. Nurden, A.T. Platelets, inflammation and tissue regeneration. *Thromb Haemost* **105 Suppl 1**, S13-33.

4. Boilard, E.*, et al.* Platelets amplify inflammation in arthritis via collagen-dependent microparticle production. *Science* **327**, 580-583 (2010).

5. Zimmerman, G.A. & Weyrich, A.S. Immunology. Arsonists in rheumatoid arthritis. *Science* **327**, 528-529 (2010).

6. Katz, J.N., Kolappa, K.P. & Becker, R.C. Beyond thrombosis: the versatile platelet in critical illness. *Chest* **139**, 658-668.

7. Gay, L.J. & Felding-Habermann, B. Contribution of platelets to tumour metastasis. *Nat Rev Cancer* **11**, 123-134.

8. Weyrich, A.S., Lindemann, S., Tolley, N.D., Kraiss, L.W., Dixon, D.A., Mahoney, T.M., Prescott, S.M., McIntyre, T.M., Zimmerman, G.A. Change in protein phenotype without a nucleus: translational control in platelets. *Seminars in Thrombosis and Hemostasis* **30**, 493-500 (2004).

9. Denis, M.M.*, et al.* Escaping the nuclear confines: signal-dependent pre-mRNA splicing in anucleate platelets. *Cell* **122**, 379-391 (2005).

10. Schwertz, H.*, et al.* Anucleate platelets generate progeny. *Blood* **115**, 3801-3809 (2010).

11. Prevost, N.*, et al.* Eph kinases and ephrins support thrombus growth and stability by regulating integrin outside-in signaling in platelets. *Proc Natl Acad Sci U S A* **102**, 9820-9825 (2005).

12. Wannemacher, K.M.*, et al.* Diminished contact-dependent reinforcement of Syk activation underlies impaired thrombus growth in mice lacking Semaphorin 4D. *Blood* **116**, 5707-5715.

13. Kashiwagi, H.*, et al.* Negative regulation of platelet function by a secreted cell repulsive protein, semaphorin 3A. *Blood* **106**, 913-921 (2005).

14. Chang, Y.*, et al.* Proplatelet formation is regulated by the Rho/ROCK pathway. *Blood* **109**, 4229-4236 (2007).

15. Whitehead, K.J.*, et al.* The cerebral cavernous malformation signaling pathway promotes vascular integrity via Rho GTPases. *Nat Med* **15**, 177-184 (2009).

16. London, N.R., Smith, M.C. & Li, D.Y. Emerging mechanisms of vascular stabilization. *J Thromb Haemost* **7 Suppl 1**, 57-60 (2009).